Target cell-type specificity of a cortico-amygdala long range synaptic connection

Présentée le 18 mars 2021

Faculté des sciences de la vie
Laboratoire de mécanismes synaptiques
Programme doctoral en neurosciences

pour l'obtention du grade de Docteur ès Sciences

par

Ayah KHUBIEH

Acceptée sur proposition du jury

Prof. C. Petersen, président du jury
Prof. R. Schneggenburger, directeur de thèse
Dr S. Krabbe, rapporteuse
Prof. R. Stoop, rapporteur
Prof. C. Sandi, rapporteuse

Acknowledgements

First and foremost, I would like to express my gratitude to my thesis supervisor, Prof. Ralf Schneggenburger. Indeed, I would probably not have reached the end of this project without his support. A few years ago, he welcomed me in his laboratory and offered me a great scientific environment for which I will be eternally grateful for. He took the time to teach me how to conduct a scientific project and always pushed me to better myself. He is a model to me in terms of scientific honesty and knowledge.

I would like to thank my thesis external examiners, Prof. Ron Stoop, and Dr. Sabine Krabbe, for taking the time to read my thesis and for the very interesting discussion during the thesis defense.

I would also like to thank Prof. Carl Petersen (president of the jury) and Prof. Carmen Sandi (internal examiner) for the valuable feedback and discussion they have offered me both during my defense, as well as multiple times during the past few years.

I would like to thank my laboratory colleagues: Shriya, Bei-Xuan, Denys, Aiste, Olexiy, Michael, Evgeniya and Barbara – thank you all for helping me in this journey and answering my questions (and I had many!). Special thanks to Heather for always being on my side for so many years and cheering me on the very last stretch. Thank you all for the good times and discussions we shared on scientific and non-scientific topics. It is truly beneficial to work with people of such diverse backgrounds and origins.

I would also like to thank old colleagues from my previous laboratory. Thank you Rodrigo, Julie, Mimi, Rajnish, Jane, Deborah, Ying, Tabea, Cristina R. and Cristina C.. You were the reason I was able to continue working despite very difficult conditions, because I loved working with all of you.

Acknowledgements

My journey to electrophysiology started after I met with Vincent Delattre. He was the first person to show me an electrophysiological recording live and I remember thinking to myself it was the most magnificent thing I had seen in my life. Neurons had always fascinated me for their electrical signals, so I thought being able to record this electrical activity from real neurons was the most amazing thing one could do.

I then had the chance to learn first-hand the patch-clamp technique with Brice, who took the time to teach me the method and allowed me to practice a few recordings by myself. Following this experience, I found myself in the laboratory of Prof. Steve Prescott, who has furthered my love for electrophysiology. My experience in his laboratory was truly valuable and it was during this time I had learned that one could be emotionally moved by science. Rodrigo Perin taught me another art, the secrets to multi-patch. Although he is the master of such an art, with his impressive 12-pipette setup, he helped me in the journey of discovering how neurons communicate with each other, or as I would call it: magic.

A PhD is not an easy journey, and I was blessed to have my friends supporting me every step of the way.

Thank you to my long time friends: Fadi, Bilal, les Badawi, les Ziadé, the Lashuels, Basma, Safia, les Khadamal, Clémence, Edouard and so many more for always keeping me down to earth, and remember that there are other things outside of science.

Thank you to all my EPFL classmates: Thomas, Camille, Jasmina, Sibylle, Nadia and Anass for always reminding me of who I was before I started this journey.

Thank you to the friends I have made during my thesis: Nour, Jane, Firat, Rita, Silvia, Grégoire, Matteo, Hiba, Sara for supporting me in the good and the bad times.

I want to thank all of you for being patient with me during the times I could not be a good friend because the PhD life was too much. I love you all.

Et maintenant, quelques derniers remerciements en Français cette fois. Je tiens d'abord à remercier des personnes qui ont rejoins mon cercle familial durant mes études de doctorat: ma belle-famille. Vous m'avez connue occupée et la tête dans mon travail, sans jamais m'en tenir rigueur. Je tiens donc à vous remercier pour l'accueil que vous m'avez fait dans votre famille et pour m'avoir soutenue dans mon parcours.

Bien sûr, un de mes piliers tout au long de ce voyage de doctorat a été ma famille. Je remercie

ma famille au Canada pour son soutien constant et la joie que vous m'avez toujours apportée. Je remercie aussi mes soeurs, qui ont supporté toutes mes plaintes et m'ont forcée à sortir de ma bulle pour aller au cinéma ou en voyage avec elles. Je remercie enfin mes parents, qui m'ont vue dans tous mes états durant ces années belles mais aussi difficiles. Néanmoins, j'ai toujours su que je pouvais compter sur vous et de nombreuses fois vous avez su répondre à mes appels à l'aide pour me donner une bonne bouffée d'air. Je vous aime.

Il y a enfin une personne que je désire remercier en dernier: mon mari, Maxime. Ce paragraphe restera modeste puisque tu sais déjà toute ma gratitude vis-à-vis de ton soutient. S'il y a bien une personne qui a pu voir de près mes moments les plus extrèmes, il s'agit bien de toi. Je te remercie de ton soutien constant, et de m'avoir constamment répété que tu crois en moi. Tu as su m'apporter du jeu et du divertissement dans mes moments les plus anxiogènes. Je t'aime de tout mon coeur.

Je sens comme si je dois ma réussite à de nombreuses personnes. Vous avez tous contribué à ce travail par votre soutiens constant. Je vous remercie. Je tiens aussi à m'excuser de tous mes manquements.

I feel I owe this success to many people. You have all contributed to this work with your constant support. I thank you. I also would like to apologize for my negligence.

Lausanne, February 17, 2021   A. K.

Résumé

Une fonction importante du cerveau est d'analyser l'information sensorielle et d'ajuster le comportement animal en fonction de l'expérience passée. Pendant un apprentissage émotionnel, les perceptions sensorielles aux effets de renforcement, aussi appelés stimuli inconditionnés (SI), influencent la perception d'un stimulus sensoriel à priori inoffensif. Le noyau latéral de l'amygdale (LA) est une région du cerveau impliquée dans l'intégration du stimulus inoffensif et inconditionné. Ce noyau représente la porte d'entrée vers le reste du circuit des structures amygdaliennes. Les structures du cerveau qui projettent l'information du SI au LA sont encore méconnues. Cependant, des études désignent l'insula postérieure (ou cortex insulaire postérieur), qui traite l'information somatosensorielle nociceptive, comme une région potentielle pour la source d'information du SI. Le réseau local de neurones dans le LA est composé de neurones excitateurs principaux (ou neurones de projection) et des interneurones inhibiteurs ; ces derniers jouent un rôle primordial dans le contrôle de l'activité locale et de la plasticité. Afin d'étudier la connexion entre l'insula postérieure et les neurones du LA, nous utilisons une méthode dite de cartographie de circuit par l'intermédiaire d'outils optogénétiques en combinaison avec des lignées de souris « Cre » qui permettent l'identification génétique de types cellulaires. Notamment, nous avons utilisé la lignée VGluT2^{Cre}, qui marque des cellules excitatrices, ainsi que les lignées VIP^{Cre} et SOM^{Cre} pour marquer deux types d'interneurones inhibiteurs. Nous avons trouvé que les neurones VGluT2^{Cre}+ reçoivent un fort signal excitateur ainsi qu'un signal inhibiteur indirect de l'insula postérieure. Le signal excitateur est suffisant pour générer un potentiel d'action, et ainsi induire une activité neuronale locale. Les interneurones VIP^{Cre}+ sont modérément excités par l'insula postérieure, et reçoivent un fort signal inhibiteur indirect. Les interneurones VIP^{Cre}+ et SOM^{Cre}+ reçoivent aussi tous deux un signal excitateur indirecte

qui résulte sans doute de l'activité locale engendrée par les neurones principaux. Enfin, les interneurones SOM^{Cre}+ reçoivent une excitation modérée ainsi qu'une inhibition indirecte de la part de l'insula postérieure, malgré un taux de connectivité élevé. Cette étude soutient l'idée de l'insula postérieure comme une possible voie par laquelle l'information du SI est transmise au LA, avec le potentiel d'activer les neurones principaux du LA. En revanche, cette étude suggère que l'effet désinhibiteur sur les neurones principaux du LA par l'intermédiaire des interneurones VIP, qui a été observé lors d'études précédentes, est le fruit de signaux afférents supplémentaires, incluant probablement un signal neuromodulateur. Au travers des enregistrements systématiques des connexions entre l'insula postérieure et les différents types cellulaire du LA, cette étude offre un accès à une meilleure compréhension des règles de connectivité locale qui gouvernent l'activité des circuits amygdaliens en réponse à un signal de source corticale éloignée.

Mots clefs : amygdale, cortex insulaire, connexion excitatrice de longue portée, transmission synaptique, optogénétique, neurones excitateurs, interneurones inhibiteurs, inhibition indirecte, désinhibition.

Abstract

An important function of the brain is to analyze sensory information, and to modulate animal behaviour according to previous experience. During processes of emotional learning, sensory percepts with a reinforcing quality, also called unconditioned stimuli (US), influence the quality of innocuous sensory stimuli. A brain structure involved in the integration of innocuous and reinforcing sensory stimuli is the lateral amygdala (LA), an input station to further amygdalar circuits. Little is known about which upstream brain regions convey US-information to the LA; however, evidence indicates that the posterior insular cortex, which processes nociceptive somatosensory information, might be a candidate. The LA microcircuit is composed of principal neurons and inhibitory interneurons; the latter play a prominent role in the control of local activity and plasticity. To investigate how the posterior insular cortex might recruit LA neurons, we used optogenetically-assisted circuit mapping in combination with genetic identification of cell types with Cre-mouse lines. Specifically, a VGluT2^{Cre} mouse line, producing a marker for excitatory neurons, and VIP^{Cre} and SOM^{Cre} mice as markers for two classes of inhibitory interneurons, were used. We found that VGluT2^{Cre}+ neurons received strong excitatory and feedforward inhibitory inputs from the posterior insular cortex. The excitatory input was sufficient to induce action potential firing, hence engaging the local circuit. VIP^{Cre}+ interneurons were moderately excited by posterior insular cortex input, and received strong feedforward inhibition. Both VIP^{Cre}+ and SOM^{Cre}+ interneurons also received feedforward, polysynaptic excitation, likely the result of the activity of local principal neurons. Finally, SOM^{Cre}+ interneurons received moderate excitatory and feedforward inhibitory input from the posterior insular cortex, and their connectivity probability was high. This study supports the notion that the posterior insular cortex can convey US-information to the LA, with the potential to strongly activate

Abstract

LA principal neurons. However, it suggests that a disinhibition of LA principal neurons through VIP interneurons, which has been observed in previous studies, might be shaped by additional afferents, possibly including neuromodulatory inputs. Through systematic recordings of input connections to defined neuron types in the LA, this study provides an entry point to the understanding of the synaptic connectivity rules that govern the activation of amygdalar circuits by incoming long-range cortical inputs.

Keywords: amygdala, insular cortex, long-range excitatory connection, synaptic transmission, optogenetics, principal neurons, inhibitory interneurons, feedforward inhibition, disinhibition.

Contents

Contents

List of Figures

List of Tables

1 | Introduction

One fundamental function of the brain is to process, store and recall sensory information originating from the environment of animals and humans, which is performed by the circuits of neurons it is composed of. The most important feature of the brain is its ability to reshape, through the rewiring of the neuronal networks. This is made possible by the dynamic property of the connections between neurons, called synapses. Many areas of the brain are dedicated to the processing of sensory information. While some of the sensory information can be innocuous, others can be of reinforcing quality with the capacity to induce plasticity, and thereby an adaptation of the behaviour.

Through evolution, animals have developed the capacity to associate external stimuli to internal sensation that will prompt the animal to perform appetitive behaviours contributing to survival, such as searching for food and reproduction. On the other hand, the animal will avoid situations that can be injury-inducing or life threatening. One type of learning which is robust, due to its importance to survival, is aversively motivated associative learning, or "fear learning". In the last two decades, neuroscientists have been interested in understanding this mechanism, which allows an animal to detect and avoid danger. A behavioural paradigm, which was used to investigate more closely the brain circuits responsible for this learning, is fear conditioning.

1.1 Fear learning

Fear conditioning is a behavioural paradigm, which is a variant of classical pavlovian conditioning, during which an animal learns to associate a neutral conditioned stimulus (CS), often as a sound, to an aversive unconditional stimulus (US), often a footshock, which induces a defensive behaviour. When the two stimuli are paired repeatedly, with the CS preceding the US, the animal learns that the CS is a cue to the US and will respond to the CS by displaying a strong defensive behaviour, typically freezing, or visceral changes such as heart rate variations (LeDoux, 2000; Fanselow and Poulos, 2005). Learning can be quantified during a recall session, during which the animal is exposed to the CS alone and the time the animal spends freezing indicates how strongly the animal associates the CS with the US (Tovote et al., 2015).

Lesion studies, during which damage to specific brain regions were linked to resulting functional deficits during the behaviour have been instrumental to finding the brain areas underlying fear conditioning. Using this method, the amygdala was established to be involved in this aversively-motivated plasticity (Swanson and Petrovich, 1998; Janak and Tye, 2015).

1.2 The amygdala

The amygdala is located in the medial temporal lobe and is composed of a dozen of nuclei which are not structurally and functionally homogeneous. In terms of structure, the amygdala can be divided in 3 groups which seem to be differentiated parts of the striatum (centromedial nuclei), the claustrum (basolateral nuclei) and the cortex (see Fig. 1.1). As for the function, the nuclei can be divided in 4 distinct groups which are involved in the frontotemporal system, the autonomic system, the main olfactory system and the accessory olfactory systems. Groups with a similar structure are not bound to share the same function, thus there is little overlap between these 2 groupings. The relevant systems in this study are the nuclei involved in the frontotemporal and autonomic systems, which belong to,

respectively, the claustrum and striatum structures (Swanson and Petrovich, 1998; Sah et al., 2003).
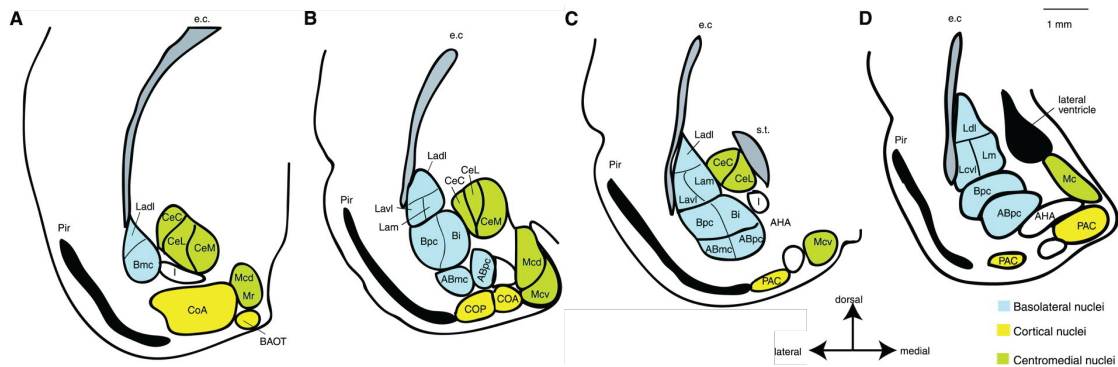
Figure 1.1 – The amygdala complex and its nuclei in the rat. Representation of the nuclei composing the amygdaloid complex in the rat in coronal sections. From (A) to (D), slices go from rostral to caudal. ABmc, accessory basal magnocellular subdivision; ABpc, accessory basal parvicellular subdivision; AHA, amygdalohippocampal area; BAOT, bed nucleus of the accessory olfactory tract; Bpc, basal nucleus magnocellular subdivision; CeC, capsular subdivision of the central amygdala; CeL, lateral subdivision of the central amygdala; CeM, medial subdivision of the central amygdala; CoA, anterior cortical nucleus; COP, posterior cortical nucleus; e.c., external capsule; I, intercalated nuclei; Ladl, lateral amygdala medial subdivision; Lam, lateral amygdala medial subdivision; Lavl, lateral amygdala ventrolateral subdivision; Mc, medial amygdala caudal subdivision; Mcd, medial amygdala dorsal subdivision; Mcv, medial amygdala ventral subdivision; Mr, medial amygdala rostral subdivision; PAC, periamygdaloid cortex; Pir, piriform cortex; s.t., stria terminalis.
Adapted from Sah et al., 2003

The two sub-areas of the amygdala which are most relevant to the fear conditioning are the basolateral complex (BLA) and the central amygdala (CEA). The BLA is composed of 3 nuclei: the lateral amygdala (LA), the basal amygdala (BA), and the basal medial amygdala (BMA). The BLA is differentiated from the claustrum and is often described as "cortex-like" given its similar composition of neurons as compared to the cortex. The CEA on the other hand, is a striatum-like structure, given that it is mainly composed of GABAergic neurons (see Sah et al., 2003 and Tovote et al., 2015 for reviews).

The connectivity between these nuclei is very extensive and explains how the information flows through the circuit. Namely, during fear conditioning, sensory information is thought to enter the amygdala through the LA. The LA, in turn, projects to most of the other nuclei, where the information will be processed in parallel, and will then converge to the CEA (Pitkänen et al., 1997). The CEA finally projects to brain areas which are critical for the behavioural expression, such as the periaqueductal gray (PAG) involved in generating freezing behaviour

(Tovote et al., 2016) and the hypothalamus involved in adapting physiological and autonomic parameters such as heart beat rate (LeDoux et al., 1988; Medina et al., 2002).

Many studies have highlighted the role of these regions in fear learning. For example, impairing the sensory input by lesioning the LA prevents fear learning during fear conditioning, but does not affect innate fear responses. This suggested that the LA is not involved in general fear, but rather in the specific association occurring during emotionally motivated learning (LeDoux et al., 1990). Additional studies using functional inactivation with muscimol infusion in the BLA showed that when performed immediately before the training, the fear learning was impaired (Muller et al., 1997), whereas a muscimol infusion right after training did not affect the learned behaviour on the next day (Wilensky et al., 1999). This suggests that the BLA is important for the acquisition of the fear memories at the moment of the pairing of both the CS and US.

Given the large amount of multimodal sensory afferents terminating in the LA (McDonald, 1998), the LA is most likely the input station of both the CS and US stimuli during fear learning. The temporal coincidence of both these signals in the neurons of the LA would contribute to a Hebbian plasticity (Blair et al., 2001). Single-unit activity recordings in the LA confirmed that many local neurons respond to both a footshock and an auditory input (Romanski et al., 1993). Although the US activated many neurons in the LA (Johansen et al., 2010b), the CS input only activated the neurons in the dorsolateral area of LA (LAdl) (Romanski et al., 1993). These findings gave rise to the idea that the LAdl is the site of convergence of the CS and US inputs (Fig. 1.2; LeDoux, 2000).

The idea of the LA being an important site of plasticity during fear learning was supported by single-unit recordings in the LA of awake mice which showed that following fear conditioning, the number of CS (tone) responsive neurons was increased (Quirk et al., 1995). Another study showed that the CS-evoked response increased in the LA of rats before they showed freezing behaviour in response to the CS, supporting that plasticity in the LA is responsible for the fear conditioning (Repa et al., 2001).

Additionally, preventing the molecular process of plasticity in the LA was shown to pre-
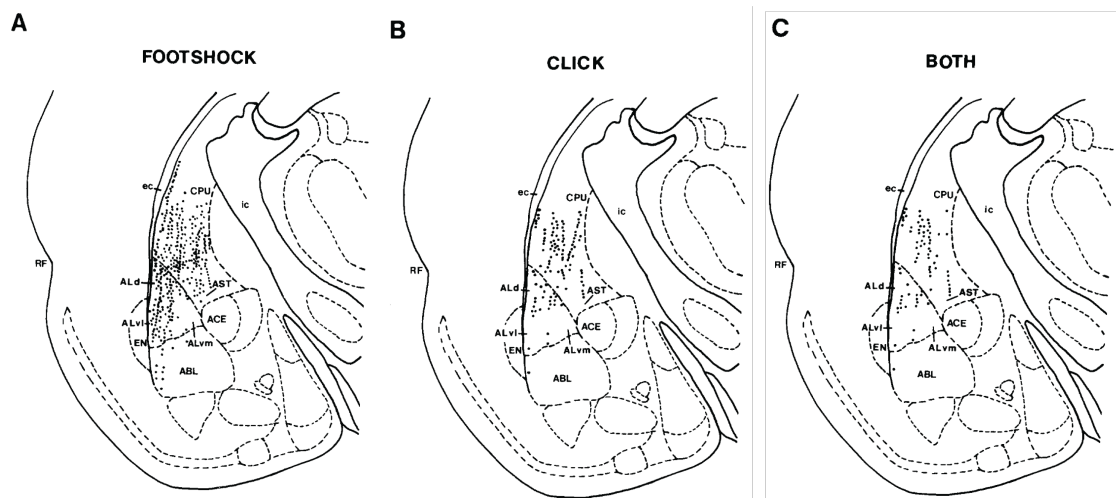
Figure 1.2 – LA units responsive to footshock and auditory clicks. **(A)** Units responsive to footshock. **(B)** Units responsive to auditory clicks. **(C)** Units responsive to both footshock and auditory clicks. ABL = basolateral amygdaloid nucleus; ACE = central amygdaloid nucleus; ALd = dorsal subdivision of the AL; ALvl = ventrolateral subdivision of the AL; ALvm = the ventromedial subdivision of the AL; AST = amygdalostriatal transition zone; CPU = posterior caudate-putamen; ec = external capsule; EN = endopiriform nucleus; ic = internal capsule; and RF = rhinal fissure.)
Reproduced from Romanski et al., 1993.

vent fear learning. For example, preventing the AMPA (α-amino-3-hydroxy-5-methyl-4-isoxazolepropionic acid) receptor recruitment in LA neurons, which is necessary in the process of long-term potentiation (LTP), reduced the strength of auditory-cued fear learning as well as LTP measurements *in vitro* upon electrical stimulation of thalamic synapses onto LA neurons (Rumpel et al., 2005). This suggested that LTP at thalamic synapses onto LA neurons underlies fear learning.

Presumably, following fear conditioning, a stronger response to the CS would recruit the circuits usually stimulated by the US, thus inducing the fear behaviour (Blair et al., 2001). A recent paper using *in vivo* calcium (Ca^{2+}) imaging showed that following fear learning, the population response of BLA neurons to a CS came to resemble the US response induced before learning (Grewe et al., 2017). As the animal learns to associate the CS with the US, expectation of the aversive stimulus grows leading to a decreased response in LA neurons to the noxious stimulus (Johansen et al., 2010b).

To understand how this plasticity occurs, it is essential to understand where the US and CS input come from and how they activate local circuits.

1.3   Long-range synaptic inputs onto the LA

The exact circuitry which leads to the activation of neurons and their plasticity in the LA is important to consider, especially which regions upstream of the amygdala are necessary or sufficient to the learning process. In auditory fear conditioning, the pathways which transmit the CS information have been extensively studied. Based on anatomical tracing studies, the putative auditory input is known to originate from two adjacent thalamic nuclei, namely the posterior intralaminar nucleus (PIN) and the medial geniculate nucleus (MGm), as well as from primary, secondary and associative auditory cortical areas (McDonald, 1998). However, lesion of either cortical or thalamic pathways did not lead to an impairment of the learning, except if both pathways were disrupted at the same time (Romanski and LeDoux, 1992). Nonetheless, when the MGm/PIN were electrically stimulated at high frequency *in vivo*, LTP of evoked potentials was induced in the LA, showing that this pathway can contribute to plasticity (Rogan and LeDoux, 1995).

As for the US pathway upstream of the LA, the exact origin of the aversive information remains unknown (Herry and Johansen, 2014). Interestingly, the US signal seems to be involved in upstream nuclei that have been classically thought to code for auditory stimuli alone. For example, it seems that the auditory MGm and PIN also respond to the US signal (Weinberger, 2011; Taylor et al., 2020; Barsy et al., 2020). Moreover, similarly to what was observed in LA principal neurons, the primary auditory cortex and the MGm increase their frequency-tuning to the CS, following CS and US pairing (Weinberger, 2007; Weinberger, 2011; Taylor et al., 2020). Other evidence suggests a role of the PAG in the aversive pathway of the US, but no direct projection to the LA was found (Johansen et al., 2010b). This suggests that PAG might instead induce the activation of LA neurons by recruiting another region which projects onto the LA, or through the activation of neuromodulatory systems (Herry and Johansen, 2014).

For many years, the investigation of the long-range inputs to LA and BA neurons in slices was performed with electrical stimulation of the external capsule (EC) and internal capsule (IC) which grossly mimic, respectively, "cortical" and "thalamic" inputs (Weisskopf et al.,

1999; Huang and Kandel, 1998). This technique allowed a better understanding of the ways plasticity might occur in the LA. For example, a study found that thalamic and cortical afferents contact distinct spines in the same dendrites, suggesting functional interactions of both these pathways within the same dendritic compartment (Humeau et al., 2005). Another *in vitro* study was able to induce hebbian plasticity in principal neurons of the LA through the paired stimulation of the IC followed by EC (Cho et al., 2012). While stimulation of EC and IC fibers might activate different cortical and thalamic afferents, there are several areas upstream of the LA, which are involved in the CS and/or US pathways, and this method fails to distinguish them. Recently, an alternative approach, which offers more precision with regard to the presynaptic origin of afferent fibers, has become available.

1.4   Optogenetically-assisted circuit mapping

A recently developed technique has contributed to identifying long-range connectivity in the rodent brain. It is a technique which allows precise temporal and regional control of the activity of different cell types or areas of the brain: optogenetically-assisted circuit mapping. This technique relies on the use of modified rhodopsins, light-dependent ion channels, to induce ion currents which can depolarize or hyperpolarize neurons. Channelrhodopsin-2 (ChR2), a blue light-gated cation channel, is an opsin found in the green alga *Chlamydomonas reinhardtii*, which can be used to depolarize cells in which it is expressed by applying blue light (Nagel et al., 2003). This depolarization can drive the neuron towards the threshold of action potential (AP) firing, even evoking an AP at short ms-range delay (Boyden et al., 2005).

One of the first studies to use optogenetics to investigate long-range projections was by Petreanu et al. (2007), who electroporated ChR2 in the barrel cortex into one hemisphere of mice and performed *in vitro* patch-clamp recordings of pyramidal neurons in the contralateral side. Applying blue light to the local tissue of the contralateral side resulted in excitatory synaptic transmission which could be recorded post-synaptically. Even though axons which expressed ChR2 were severed from their somata, they appeared to conserve their function. Thanks to this new tool, neuroscientists could now express ChR2 in a distant brain region

and easily check whether this distant region made a functional projection onto the region of interest.

To ensure that the recorded responses were from mono-synaptic connections, in a subsequent study, Petreanu et al. (2009) applied Tetrotoxin (TTX) on the slice to block AP firing of the neurons. Although one could stimulate the ChR2 with blue light, no AP could be generated or propagated through the neuron due to the presence of TTX, and so synaptic release was prevented. When 4-Aminopyridine (4-AP) was applied in combination with TTX, potassium channels, which prevented the nerve terminals from depolarizing in response to ChR2 activation, were blocked. As a result, when shining blue light, synapses of neurons expressing ChR2 depolarized the synapse, allowing synaptic release. 4-AP did not however allow poly-synaptic signaling as the input onto an interneuron for example could not lead to an AP (see Fig. 1.3). Thus the application of TTX and 4-AP has become a standard measure for assessing whether optogenetically-evoked excitatory postsynaptic currents (oEPSCs) are of mono-synaptic or poly-synaptic origin.
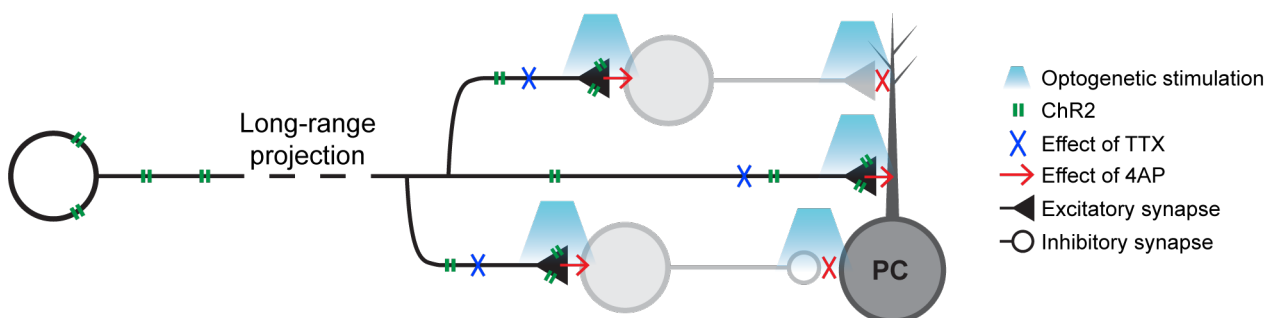
Figure 1.3 – Scheme of the effect of TTX and 4-AP. TTX prevents the induction of APs, which prevents synaptic transmission. Although light can depolarize the membrane potential of neurons, it is only when 4-AP is added that the depolarization of the neuron terminals can induce synaptic transmission. Hence, TTX and 4-AP would only allow the recording of mono-synaptic currents from long-range projection neurons.

Another significant improvement of the method was to constrain the expression of ChR2 to specific neuron types, through the use of Cre knockin and transgenic mouse lines in combination with Cre-activated viral vectors. Hence, in such experiments, the expression of ChR2 was restricted to neurons which expressed Cre and through Cre-recombination allowed the transcription of the ChR2 gene (Atasoy et al., 2008). Furthermore, the use of adeno-associated virus (AAV) could allow a localized targeting of a brain region (Kuhlman

and Huang, 2008).

Over the years, many other opsins were found in algae with different properties which could potentially be useful. Additionally, the opsins are continuously being mutated to improve their properties such as an increased sensitivity, a reduced photobleaching and higher temporal precision.

The advent of optogenetic stimulation technique also allowed neuroscientists to test hypotheses with better temporal resolution in *in vivo* experiments. For example, a study by Johansen et al. (2010b) showed that replacing the US signal with optogenetic stimulation of LA neurons, during fear conditioning, induced learning. However, the optogenetic stimulation appeared to be less efficient than the natural US, given that the freezing levels were lower during retrieval. This suggested that other processes might be necessary for the acquisition of fear memory besides the simple depolarization of LA principal neurons. In another study using optogenetics, Nabavi et al. (2014) showed that, in rats which had been previously fear conditioned, inducing long-term depression (LTD) optogenetically in auditory afferents (from the MGm and the auditory cortex) to the LA could impair fear memory. This could be recovered following a subsequent optogenetic induction of LTP at the same afferents. These studies provided additional evidence that plasticity in the LA is indeed necessary for fear conditioning.

During this project, I decided to take advantage of optogenetically-assisted circuit mapping techniques, to investigate a long-range projection using Chronos, an opsin from the *Stigeoclonium helveticum* algae which has faster kinetics than ChR2 and an increased light-sensitivity (Klapoetke et al., 2014).

1.5 Neuron types in the LA and feedforward inhibition circuits

As mentioned previously, the BLA is often described as "cortical-like" although it does not have a layered organization or parallel pyramidal neuron dendrites. However, its cellular composition is equivalent to what is found in the cortex: around 80% of the neurons are

excitatory neurons, and around 20% are inhibitory interneurons (McDonald, 1992). Different studies have investigated BLA neurons and confirmed their similarities with cortical neurons in their electrophysiological behaviour as well as morphology (Washburn and Moises, 1992).

In terms of electrophysiological behaviour, the majority of principal neurons appear to respond to depolarizing currents with a burst followed by a slowing of spike discharge, called accommodation (Washburn and Moises, 1992; Sosulina et al., 2006). Other types were late-spiking or didn't show an initial burst (Rainnie et al., 1993; Washburn and Moises, 1992). In terms of morphology, principal neurons were found to be similar to cortical pyramidal and spiny stellate cells (Rainnie et al., 1993; Washburn and Moises, 1992; Sosulina et al., 2006).

Although the BLA doesn't have a layer organization such as the cortex, the amygdala appears to have a hierarchical organization, with precise connections between selective sub-nuclei, ensuring the information travels through the nuclei in a specific order (Pitkänen et al., 1997). The LA itself is divided into 3 sub-nuclei: the LAdl, the ventrolateral LA and the medial LA (see Fig. 1.1). The LAdl forms unidirectional projections to the other 2 sub-nuclei which distribute the information to other nuclei of the amygdala, which was shown with anatomical (Pitkänen et al., 1997) as well as electrophysological methods (Samson and Paré, 2006).

Interestingly, on the public database of the Allen Brain Institute, we found *in situ* hybridization (ISH) images from *Slc17a6*, the gene which codes for the Vesicular Glutamate Transporter 2 (VGluT2), that seemed to indicate that the neurons in the dorsal tip of the LAdl express VGluT2 (Fig. 1.4). The fact that this population of neurons seemed to specifically express this transporter which otherwise is mainly utilized by thalamic neurons and a few nuclei in the brain was intriguing (Fremeau et al., 2004b). Thus, we were interested in targeting the VGluT2^{Cre}+ neuron population and comparing them to the other principal neurons in the LA, hypothesizing that this difference in molecular marker might be linked to their specific function and position in the LAdl.

Regarding the inhibitory interneuron types found in the BLA, they seem to be in general similar to the ones found in the cortex: parvalbumin-expressing interneurons (PV-INs) which, as in the cortex, target the perisomatic and distal dendritic region of principal neurons

Figure 1.4 – Localization of VGluT2 expressing neurons. Image of *In situ* hybridization of VGluT2 from the Allen Brain Institute. The overlay is from Paxinos and Franklin, 2012 (Bregma -1.22 mm). AIP, agranular insular cortex, posterior part; ASt, amygdalostriatal transition area; BLA, basolateral amygdaloid nucleus, anterior part; CeC, central amygdaloid nucleus, capsular part; CeL, central amygdaloid nucleus, lateral division; CeM, central amygdaloid nucleus, medial division; CPu, caudate putamen; DEn, dorsal endopiriform claustrum; DI, dysgranular insular cortex; GI, granular insular cortex; LaDL, lateral amygdaloid nucleus, dorsolateral part; Pir, piriform cortex; VEn, ventral endopiriform claustrum.

(Muller et al., 2006), somatostatin-expressing interneurons (SOM-INs) which mainly target distal dendrites and dendritic spines of principal neurons (Muller et al., 2007), and vasoactive intestinal peptide-expressing interneurons (VIP-INs) which target distal dendrites somewhat more than the perisomatic compartments of principal neurons (Muller et al., 2003).

Despite grouping the interneurons according to the molecular markers mentioned above, these interneuron groups do not seem to be homogeneous. For example, Woodruff and Sah (2007) showed that PV-INs in the BLA could be divided into four subtypes according to their different AP-firing properties, as well as their differential patterns of connectivity. Similarly, using VIP[Cre] mice, Rhomberg et al. (2018) showed that based on anatomy, molecular markers and electrophysiological behaviour, VIP-INs in the BLA can be further divided into three sub-groups. Recently, Guthman et al. (2020) observed that SOM-INs in the BLA could be divided into 2 sub-populations, with one of these sub-populations exhibiting fast-spiking

properties and functionally mediating feedforward inhibition in BLA upon optogenetic stimulation of lateral entorhinal cortex inputs.

Given that interneurons in the LA are also innervated by cortical and thalamic afferents (Szinyei et al., 2000), it is expected that they can be recruited by distal regions to control local activity of neurons. For example, an *in vitro* slice study found that in the mouse LA, dopamine induced a suppression of feedforward inhibition, which in turn allowed LTP to be induced at thalamic afferent synapses onto LA principal neurons (Bissière et al., 2003). It also appears that interneurons can control the induction of LTP at cortical afferent synapses with LA principal neurons through presynaptic inhibition preventing the generalization of fear through non-associative potentiation (Shaban et al., 2006). Additionally, an *in vivo* study found that tetanic stimulation induced a potentiation of the excitatory postsynaptic current (EPSC) in the "cortical" pathway on interneurons, which in turn potentiated the disynaptic feedforward inhibition (Mahanty and Sah, 1998).

Lucas et al. (2016), using optogenetically-assisted circuit mapping, showed that *in vitro* optogenetic stimulation of MGm afferents evoked EPSCs in the majority of PV^{Cre}+ neurons in the LA, but not in the BA. When the temporal association cortex afferents were optogenetically stimulated, they evoked EPSCs in the majority of PV-INs in both the LA and BA. Following fear conditioning, Lucas et al. (2016) found that cortical input to PV-INs in the LA showed signs of LTD. Furthermore, there was a reduced γ-aminobutyric acid (GABA) release from PV-INs specifically for synapses onto principal neurons in the LA. These findings suggested that auditory-cued fear learning can induce overall weakening of the feedforward inhibition that auditory thalamic and cortical inputs exert on LA principal neurons.

In the BLA, Guthman et al. (2020) found that electrical stimulation of the lateral entorhinal cortex (LEC) *in vitro* elicited an excitatory input onto principal neurons as well as a feedforward inhibitory signal. They observed that a SOM^{Cre}+ neuron subtype, which displayed a fast-spiking phenotype and was activated by LEC stimulation, was likely responsible for the feedforward inhibition onto principal neurons. PV^{Cre}+ neurons, which were strongly activated by local principal neurons, were more likely to be involved in feedback inhibition. Due to technical limitations with the use of horizontal slices, the distinction between BA

and LA could not be done; however, these results might be specific to the BA given that LEC mainly outputs to the BA. This shows that the feedforward inhibitory process in the LA and BA might be different, or could be input-specific (Lucas et al., 2016; Guthman et al., 2020).

In a recent study in GAD67-GFP mice, Polepalli et al. (2020) showed that optogenetic stimulation of the auditory cortex or thalamus induced an excitatory postsynaptic potential (EPSP) in the majority of interneurons in the LA, showing a high connectivity rate. 20% of LA interneurons were driven to threshold with stimulation of either auditory cortical or thalamic afferents. As a result, they could also observe feedforward inhibition evoked in LA interneurons. This suggests that interneurons can have an additional control over the principal neuron activity through disinhibition, the process of releasing principal neurons from an inhibitory control.

1.6 Disinhibition as a circuit motif for associative plasticity

Disinhibition was shown to prevent inhibition and thereby to modify the information processing of excitatory (principal) neurons, such as increasing their response gain, which can modulate the induction of plasticity at excitatory synapses onto principal neurons (Wilson et al., 2012; Atallah et al., 2012; Letzkus et al., 2015). In the cortex, VIP-INs are often described as responsible for disinhibition given that they preferentially target other interneurons (Pi et al., 2013), making them potential candidates for the disinhibition in the amygdala.

Wolff et al. (2014), in *in vivo* recordings of PV-INs and SOM-INs, showed that during the footshock stimulation applied in fear learning protocols, the activity of PV-INs is reduced (Fig. 1.5.B). On the other hand, their forced optogenetic activation during the footshock impairs learning, while their optogenetic silencing during the US improved the fear learning. On the contrary, during the CS, some PV-INs appeared to be excited which led to an inhibition of SOM-IN, which in turn caused a disinhibition of the principal neuron dendrites, despite the perisomatic inhibition (Fig. 1.5.A). The activation of PV-INs by auditory stimuli was later supported by an *in vitro* study by Lucas et al. (2016). Possibly due to the limitations of *in vivo* precise targeting, Wolff et al. (2014) did not differentiate between the LA and BA.

However, this study proved that different sensory inputs can lead to differential activation of interneurons, which in turn can control the activity of principal neurons. This shows the importance to consider how each region upstream of the LA would recruit the local circuit.
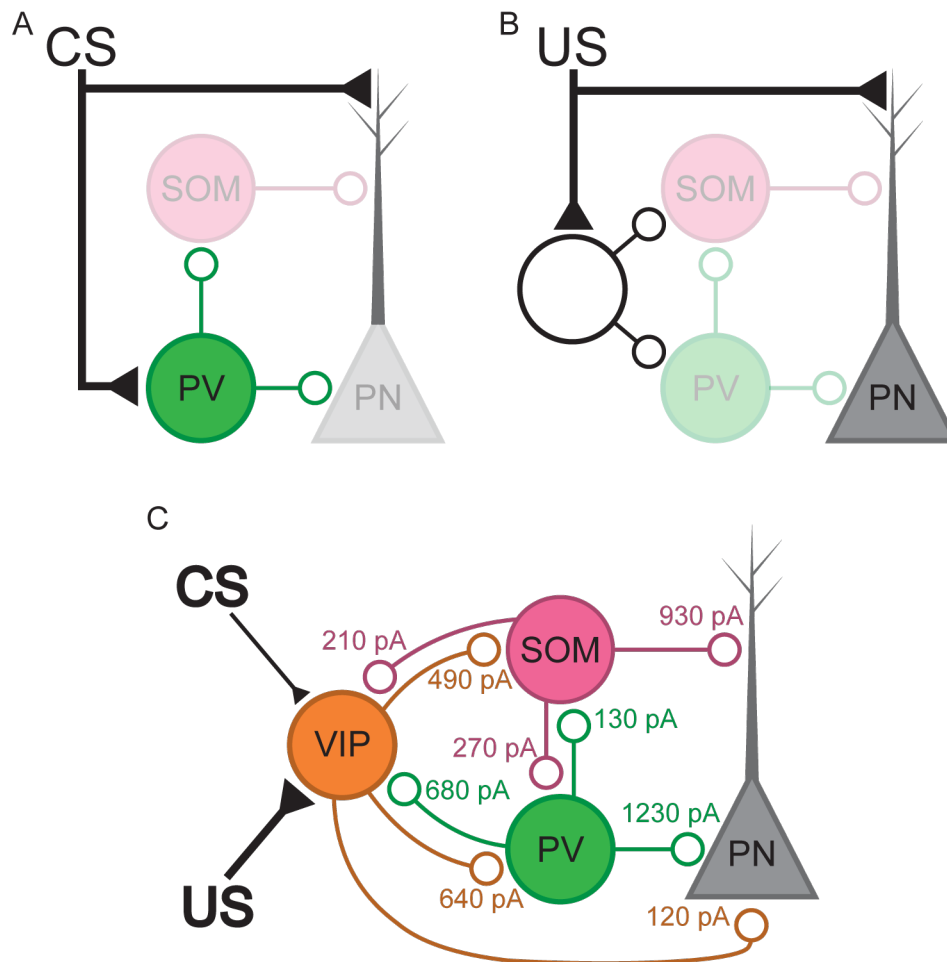
Figure 1.5 – Connectivity of interneurons reported in the BLA... (A) Scheme of the effect of the CS on the BLA microcircuit. The CS input activated PV-INs, which inhibit SOM-INs and disinhibit the dendrite of the principal neuron (PN). As reported by Wolff et al., 2014, adapted from Krabbe et al., 2018. (B) Scheme of the effect of the US on the BLA microcircuit. The US input induces the inhibition of PV-INs and SOM-INs which disinhibit the dendrite and soma of the PN, allowing the US to activate the PN. As reported by Wolff et al., 2014, adapted from Krabbe et al., 2018. (C) Scheme of the effect of the US and CS on VIP-INs as reported by Krabbe et al., 2019. Values of the intensities of connections between the neurons of the LA microcircuit as reported by Krabbe et al., 2019 referring to light stimulation of 10 ms at a holding potential of -60 mV with an E_{Cl} = -5 mV.

Krabbe et al. (2019), in a study combining *in vivo* miniscope Ca^{2+} imaging and optogenetic manipulations, reported that most BLA VIP-INs were activated during the US and mildly activated during the CS. Interestingly, when Krabbe et al. investigated the brain regions which projected to VIP^{Cre}+ neurons using a rabies-virus mediated backlabelling approach, they found that VIP-INs and PV-INs had common input regions, with notably a differential input depending on the location of the target neurons in the BA or LA. For example, the rabbies approach in VIP^{Cre}+ and PV^{Cre}+ neurons in LA showed many backlabelled cells in the auditory cortex, whereas in the BA they showed a strong ventral hippocampus or rhinal cortex input. Although the interneurons appeared to be interconnected, the strongest inhibition was from SOM^{Cre}+ and PV^{Cre}+ neurons onto principal neurons, showing the importance of the disinhibition (see Fig. 1.5.C). Because *in vivo* optogenetic silencing of VIP-INs during the US reduced the response of principal neurons and impaired learning (Krabbe et al., 2019), this suggests that VIP-INs drive a disinhibition of BLA principal neurons during the footshock.

1.7   Thesis aims

So far, US-induced signalling in the LA has been studied in awake animals or through afferents electrical stimulations (such as the external capsule which excites all cortical inputs indistinctly). The region which is the source of the nociceptive information to the LA during fear conditioning is still debated. A candidate for the nociceptive input onto the LA is the posterior insular cortex (pInsCx). This region is known to process somatosensory inputs (Rodgers et al., 2008), and was shown to be involved in pain coding in functional magnetic resonance imaging experiments in humans (Brooks et al., 2005). Additionally, projection studies in monkeys, cats and rats suggest that the pInsCx projects to the LA (McDonald, 1998). Tracing experiments from our laboratory confirmed that pInsCx neurons project to the LA. Similarly, optogenetic stimulation and electrophysiological recordings of CamKIIa^{Cre}+ neurons in the LA suggest a functional input from the pInsCx to the LA (Palchaudhuri, *unpublished*).

Because the interneurons can modulate the principal neurons gain or even plasticity, it is important to consider the effect of long-range input on all the cell-types composing the local circuit. The main goal of this PhD thesis was to investigate the inputs to LA neurons originating from the pInsCx to better understand how this putative nociceptive input recruits various genetically-identified neuron types of the LA, including VGluT2$^{\text{Cre}}$+, SOM$^{\text{Cre}}$+ and VIP$^{\text{Cre}}$+ neurons. This was done by using a combination of Cre mouse lines, for genetic identification of the cell-types of interest, and optogenetic stimulation of long-range inputs to record the response of different LA neurons following stimulation of pInsCx afferents.

2 | Materials and Methods

2.1 Animals

All the experiments on laboratory mice described in this thesis were performed in accordance with authorizations VD3274 and VD3518 delivered by the Service of Consumption and Veterinary Affairs of the Canton of Vaud.

The strains of mice used in these experiments were backcrossed with the C57BL/6J to maintain a uniform genetic background. Here is a list of these strains:

- VGluT2$^{\text{Cre}}$ (Slc17a6$^{\text{tm2(cre)Lowl}}$/J; Jackson Laboratory #016963; see Vong et al., 2011)
- VIP$^{\text{Cre}}$ (Vip$^{\text{tm1(cre)Zjh}}$/J; Jackson Laboratory #010908; see Taniguchi et al., 2011)
- SOM$^{\text{Cre}}$ (Sst$^{\text{tm2.1(cre)Zjh}}$/J; Jackson Laboratory #013044; see Taniguchi et al., 2011)
- R26_LSL_tdTomato Cre-dependent reporter (B6.Cg-Gt(ROSA)26Sor$^{\text{tm9(CAG-tdTomato)Hze}}$/J; Jackson Laboratory #007909; see Madisen et al., 2010)
- R26_LSL_H2B_mCherry Cre-dependent reporter (B6;129S-Gt(ROSA)26Sor$^{\text{tm1.1Ksvo}}$/J; Jackson Laboratory #023139; see Peron et al., 2015).

Some of these strains were bred together to take advantage of the Cre/*loxP* recombination so the offspring can have fluorescence expression in the targeted cell lines. The mouse line R26_LSL_H2B_mCherry was kindly provided by Prof. Carl Petersen (EPFL) and allowed for a nucleus restricted fluorescence expression.

All the mice used for histology or electrophysiological experiments were virgin males with no prior contact to female mice, group-housed in a controlled environment with 12/12h light/dark cycle and unlimited access to food and water. To ensure enrichment, the cages contained a cardboard tunnel, a plastic Igloo® shelter for mice (Bio-Serv, USA) and nesting material.

2.2 Viral injections

2.2.1 Viral vectors and injection coordinates

Virus suspension of AAV8:hsyn:Chronos-GFP (200 nL; $6.5\text{x}10^{12}$ vg/mL; UNC vector core) was bilaterally injected into the pInsCx to perform optogenetically-assisted circuit mapping. This method allowed us to stimulate the pInsCx afferents in a remote region with blue light (wavelength 470 nm) to mimic pInsCx input. See coordinates of injections in Table 2.1.

To visualize the targetted cells in the mouse brain, if the strain of the mouse did not include a Cre-dependent reporter, virus suspension of AAV8:CAG:DIO:tdTomato (200 nL; $6.5\text{x}10^{12}$ vg/mL; UNC vector core) was injected in bilateral LA using the coordinates reported in the Table 2.1.

	Coordinates relative to Bregma in [mm]		
Target region	Medio-lateral	Anterior-posterior	Dorso-ventral
pInsCx	± 4.25	$- 0.96$	$- 3.85$
LA	± 3.43	$- 1.18$	$- 4.45$

Table 2.1 – Stereotaxic coordinates relative to Bregma in [mm] used to target specific regions of the mouse brain.

2.2.2 Surgery and virus injection

Viral injection surgeries were performed on male mice aged between 6 and 8 weeks. At least 24h prior to the surgeries, the mice were separated into individual cages and were single-housed until the end of the experiments. As the mice were transferred, pain-relief

drug (paracetamol) was mixed with the water (1 mg/mL) in order to allow the mice to get accustomed to the new taste of the water before the surgery.

Surgeries were performed in a specialized, biosafety level 2 (P2) surgery room following the precautions and safety guidelines for handling the virus suspension and potentially contaminated materials. On the day of the surgery, mice were first anaesthetized with isoflurane gas flow of 3% in O_2. Once they were anaesthetized, the mice were weighed and then secured onto the stereotaxic instrument (Kopf Instruments, model 940, USA) using a tooth bar and non-rupture ear bars (Zygoma Ear cups, Kopf Model 921). This way the head could be fixed, but remained adjustable during the procedure of injection in order to align the brain.

In this setup, the mouth and nose of the mouse were covered with a rubber mask and connected to a continuous flow of 1.5 L/min of 1.5% of isoflurane in O_2. To ensure the well-being of the animal, a feedback loop warming system (Homeothermic Blanket Control unit, Harvard Apparatus, USA) was used to maintain the temperature of the animal at 37°C despite the anaesthesia, the eyes were also protected using ophtalmic ointment (Vita-POS®) and the breathing of the animal was visually monitored throughout the surgery.

The fur on the top of the head was shaved and around 30-50 µL of a mix of anaesthetics, composed of lidocain (1mg/mL), epinephrine (0.625 µg/mL) and bupivacaine (1.25 mg/mL) diluted in saline, was injected subcutaneously. After a few minutes, the skin was covered with Betadine® solution before being cut with small scissors. Bulldog forceps were then used to maintain the skin opened in order to access the skull below with a good visibility.

After locating the Bregma, the brain was aligned in all angles using a pipette mounted at the end of the stereotaxic arm and a binocular microscope (Stemi DV4, Carl Zeiss, Germany) to measure offsets. Once the brain was aligned, small craniotomies were performed using a drilling handpiece (Ram Power 35, Ram Products Inc., USA) to make small craniotomies with a dental bore (H1.204.005, Komet dental, Germany) above the desired locations for the injections (see coordinates in Table 2.1).

Alignment of the brain was re-checked after drilling and adjustements were made if needed.

Injection pipettes were back-filled with the desired virus suspension (see section 2.2.1) and placed above the target medio-lateral and anterior-posterior coordinates. Pipettes were then slowly lowered in the brain until the desired dorso-ventral position while ensuring the pipettes did not bend due to the dura matter at the surface of the brain. Once at the right coordinates, 200 nL of virus suspension was slowly injected at a speed of 80 nL/min using a hand-controlled hydraulic micromanipulator (MO-10, Narishige, Japan).

When the injections were completed, the bulldog forceps were removed and the skin humidified with sterile saline. The skin opening was then sutured (coated Vicryl® resorbable suture, Ethicon, USA). At the end, Betadine® cream or Betadine® solution was applied onto the sutured wound to ensure a good healing.

Mice were left in the P2 surgery room for 6 days following surgery, during which the health of the mice (weight, wound healing process and well-being behavioural hallmarks) was monitored according to the veterinary authorization requirements. After this period, if the mice had properly recovered (no loss of weight or infection), they were transferred to a new cage and moved to a storage room. The mice were kept in the storage room for at least 2-3 weeks before they were used for experiments.

2.3   Electrophysiology

2.3.1   Brain slicing

Electrophysiological recordings were performed on animals older than 9 weeks of age, but preferably younger than 10 weeks of age. Mice were deeply anaesthetized with 3% isoflurane in O_2 and decapitated. The following steps were all performed in ice-cold "slicing" solution (see composition in Table 2.2) which was adjusted to the pH 7.4 with HCl titration. This solution was saturated by continuous bubbling with carbogen gas (95% O_2 / 5% CO_2).

The brain was extracted from the skull and the posterior part of the brain was cut with a scalpel in order to obtain a flat surface. The brain was then glued on its flat surface onto

| | Concentrations in [mM] | | |
Chemicals components	Slicing solution	Recovery solution	Recording solution
NMDG	110		
NaCl		92	125
KCl	2.5	2.5	2.5
NaH$_2$PO$_4$	1.2	1.2	1.2
NaHCO$_3$	25	25	25
HEPES	20	20	
Glucose	25	25	10
Sodium ascorbate	5	5	5
Thiourea	2	2	2
Sodium pyruvate	3	3	3
MgCl$_2$	10	2	1
CaCl$_2$2H$_2$O	0.5	2	2

Table 2.2 – Extracellular solutions recipes. Three solutions were prepared for the electrophysiology experiments, their recipes are described in this table. Concentrations are in [mM].

the specimen plate which was magnetically attached to the buffer tray filled with slicing solution. The brain was oriented such that the anterior part was directed towards the ceiling and the cortical pia on the dorsal part opposed the blade. Using a Leica VT1200S slicer (Leica Microsystems, Wetzlar, Germany), 300 µm-thick-slices were cut with a PTFE-coated blade (Ted Pella Inc., USA) once the posterior nerve of the anterior commissure could be seen. For each slice, hemispheres were separated and moved to a storage chamber filled with slicing solution and located in a water bath at a temperature of 34°C under continuous oxygenation with carbogen gas.

After 7 min, the slices were then transferred in another storage chamber, located in the same water bath, but containing a "recovery" solution (see composition in Table 2.2). After transferring the last slice to the recovery solution, the water bath was turned off so the temperature could slowly return to room temperature.

2.3.2 *Ex vivo* electrophysiology

For the recording, slices were placed into the recording chamber and secured using a grid made of nylon thread. The recording chamber had a constant flow of oxygenated (with

carbogen gas) "recording" solution (see composition in Table 2.2).

The patch-clamp setup was equipped with an upright microscope (BX51WI, Olympus, Japan) equipped with an EMCCD camera (iXon[EM]+897, Andor Technology, Ireland). Electrophysiological recordings were done using a 60x / 0.9 NA water-immersion objective (LUMPlanFl, Olympus) and fluorescence was imaged using a monochromator (Polychrome V, TILL Photonics, Germany). Using a pulled borosilicate glass pipette of resistance 4 to 8 MΩ, filled with intracellular solution, whole-cell patch clamp recordings were made at room temperature (21-23°C) with an EPC9/2 patch-clamp amplifier (HEKA Elektronik, Germany), under the control of the associated software PATCHMASTER (HEKA Elektronik).

Chemicals components	Concentrations in [mM]	
	Cesium solution	Potassium solution
K-gluconate		145
Cs-gluconate	145	
KCl		8
TEA-Cl	8	
HEPES	10	10
EGTA	0.5	0.5
Na$_2$-phosphocreatine	5	3
Mg-ATP	4	4
Na-GTP	0.3	0.3

Table 2.3 – Intracellular solutions recipes. Two solutions were prepared for the electrophysiology experiments, their recipes are described in this table. Concentrations are in [mM].

Depending on the type of experiment, one of two types of intracellular solutions was used, one with potassium-gluconate, and the other with cesium-gluconate (see compositions in Table 2.3). Both solutions had an osmolarity around 300 mOsm and 310 mOsm, respectively, and their pH were adjusted to 7.2. Some of the stock aliquots of the intracellular solutions were concentrated 2x in order to allow the addition of 0.5 to 2% Neurobiotin (Vector Laboratories, USA) in some recordings, to later stain the recorded cells (see staining procedure in the next section). Given the chloride concentration differences between the intracellular and extracellular solutions, the reversal potential of chloride during recordings is estimated to be around -71.8 mV.

For activation of Chronos, light pulses were delivered by a high-power LED (CREE XP-E2, royal blue, 480 nm, Cree Inc., USA) with a maximal measured power at the focal plane of 8 mW/mm^2. The LED was controlled with a driver (BLS-1000-2, Mightex Systems, Canada) activated with an analog signal from the amplifier, which allowed calibrated scaling of the LED intensity. All light pulses lasted for 1 ms.

In a few experiments, in order to verify the type of currents recorded, drugs were added to the extracellular solution. The drugs include:

- Gabazine (Biotrend, Germany) which is an antagonist at GABA$_A$ receptors
- 2,3-dioxo-6-nitro-7-sulfamoyl-benzo[f]quinoxaline (NBQX; Biotrend, Germany) which is an antagonist of the AMPA receptor
- TTX (Biotrend, Germany) which is a sodium channel blocker
- 4-AP (Sigma-Aldrich, USA), which is a selective blocker of some voltage-activated potassium channels.

2.3.3   Slice processing

At the end of each experiment, the slices which had been cut between the anterior commissure and the posterior amygdala were moved to 24-well plates. They were then covered with 4% paraformaldehyde (PFA) for at least 30 min at room temperature on a shaker and then either rinsed or kept overnight at 4°C in PFA. The PFA was then washed out with phosphate-buffered saline (PBS), for 5 min on a shaker, three times, after which the slices were stored in the fridge until staining or mounting.

Slices in which a recording had been performed using Neurobiotin in the intracellular solution were then moved to another well-plate to undergo a staining protocol. Two solutions were prepared for the staining, composed of different concentrations of Triton X-100 (Sigma), Bovine serum albumin (BSA; fraction V, Sigma) and horse serum (see composition in Table 2.4). At first the PBS in which they were covered was rinsed out and they were covered with Solution A . The slices were then left on a shaker for at least 2 hours. Then Solution A

was replaced with Solution B to which Streptavidin-Alexa 647 (Lifetechnologies, USA) was added at 1:1000 dilution. Then the slices were left overnight at 4°C on a shaker. The next day, the slices were rinsed with PBS and stored in the fridge until mounting.

	Concentrations in PBS	
	Solution A	Solution B
Triton X-100	0.3%	0.15%
BSA	0.2%	0.2%
Horse Serum	5%	2%

Table 2.4 – Solutions used for cell-fills staining. Content of the two solutions used to stain the cell-fills.

2.3.4 Slice mounting and imaging

The slices to be mounted were first washed three times for 5 min with PBS. Then while submerging a microscope slide (Superfrost® Plus slides, Thermo Scientific, USA) in diluted PBS, using a brush, slices were moved from the well-plates to the slide and placed with the patched side facing up. Once all the slices were placed on the microscope slide, excess liquid was removed using a filter paper and left to dry for at least 3 hours.

Once the slices appeared to have dried, mounting medium solution with DAPI (Fluoroshield mounting medium, Sigma-Aldrich) was spread on the slices and a coverslip (Menzel-Gläser, Thermo Scientific) was placed to cover all the slices. After waiting 15 min for the medium to dry, nailpolish was applied on the sides of the coverslip to seal the openings and prevent further appearance of bubbles. Once dried, slides were stored in the 4°C storage.

Microscope slides were later imaged with a slide scanner VS120 (Olympus) with a 10x/0.4 NA objective. Given that the samples were thick, the focus of the microscope was manually set to the surface of the slice on multiple ROIs for each slice.

The images from the microscope were later compared with the brain atlas from Paxinos and Franklin (the 4th edition; 2012). If needed, the microscope images were superimposed with atlas overlays using Adobe Illustrator software (Adobe, USA). This allowed to verify the injection sites and identify the regions which were patched.

When Neurobiotin was used, microscope images allowed to verify whether a staining had successfully worked. If this was to be the case, these slices were later imaged using a confocal microscope (SP8, Leica Microsystems) to extract a detailed z-stack of the filled cells.

2.4 Histology

2.4.1 Perfusion

The perfusion procedure was done in mice older than 10-weeks of age.

A mouse was first injected intra-peritoneally with pentobarbital (150 µg per gram body weight) and placed back into its cage. Once the mouse stopped moving and after verifying it had become insensitive to toe pinching, a cardioperfusion was done with around 35 mL of 4% PFA in PBS. Afterwards, the brain, which should appear blood-free was removed from the skull and stored in around 15 mL of 4% PFA in PBS overnight at 4°C. The next day, the brain was moved to 30% sucrose for at least 2 days in 4°C. Once the brain no longer floated at the surface of the sucrose, the brain was stored at -80°C until the slicing.

2.4.2 Brain slicing

Brain slicing was performed on the HM 450 sliding microtome (Thermo Scientific). While the platform was set to cool down to -40°C, the brain was placed on its posterior side in Cryomatrix$^{\text{TM}}$ embedding resin (Thermo Scientific) to fix it for the slicing procedure. If necessary, the platform was adjusted in order to have the brain straight with the olfactory bulb facing the ceiling. At this stage, a sharp blade was used to mark a region of the right hemisphere (usually in M1) to be able to differentiate the hemispheres in the slices.

Using the sliding blade, thick slices were cut until the posterior nerve of the anterior commissure could be seen, at which stage slices were collected either all or every second 35 or 40 µm-thick-slices until the end of the amygdala. Slices were stored in 24-well plates at 4°C

until I could either perform immunohistochemistry (IHC) on them or mount them.

2.4.3 Immunohistochemistry protocol

In the first attempts to perform IHC on brain slices to stain CamKIIa positive neurons, the background fluorescence prevented from differentiating CamKIIa+ neurons (believed to be caused by the use of anti-mouse antibody and by an insufficient tissue penetration of the antibody). A protocol was designed to improve penetration of the tissue and gave better images. This protocol is detailed below.

First, slices were washed with PBS 3 times for 5 min on a shaker. Then the PBS was replaced with a blocking solution composed of: PBS with 0.3% Triton X-100 and 1% BSA. The slices were left on a shaker at room temperature for at least 2 hours. Then the blocking solution was removed and replaced with a primary antibody solution containing: PBS with 0.1% Triton X-100, 1%BSA and 1:500 dilution of anti-CamKIIa mouse mAb clone 6G9 (Cayman Chemical, USA). The slices were left to incubate in this solution on a shaker overnight at 4°C. The next day, the slices were washed 3 times with PBST (PBS with a low concentration of Tween) and then left on a shaker for around 1 hour to wash in PBS containing 0.1% Triton X-100. Then the solution was washed out and slices were incubated for around 5 hours at room temperature in a secondary antibody solution containing: PBS with 0.1% Triton X-100, 1% BSA and 1:1000 dilution of donkey anti-mouse conjugated to Alexa-647 antibody (Lifetechnologies). Finally, the slices were washed 3 times for 5 min on a shaker with PBST, and then once in PBS.

At this point, the slices were either mounted or they were stored at 4°C in PBS until they could be mounted.

2.4.4 Histology slice mounting and imaging

The procedure described here is very similar to the one described in section 2.3.4. First, the slices were first washed 3 times for 5 minutes on a shaker with PBS. Then the slices were

transported from the 24-well plate to the microscope slide using a paint brush and placed in the same orientation (based on the right hemisphere marking). Given that the slices were much thinner, they dried a lot faster than thick slices and so excess solution was simply removed from the sides of the slide using a tissue.

Once the slices had dried, they were covered with water for around 5 seconds and then 125 μL of mounting medium (DAPI Fluoromount-G®, SouthernBiotech, USA) was placed on the side of the slide and spread over the tissue samples by placing the coverslip on top of the slices. The mounting medium being hydrophilic, the procedure helped remove air from the slices before the medium was added. Once the coverslip had been placed, the mounting medium was left to dry for around 2 hours before being stored at 4°C.

Similarly to the electrophysiological slices, the microscope slides were imaged using the same slide scanner with a 10x objective. Later on, if needed, some slices could be imaged with a confocal microscope in order to have higher resolution images. Images were acquired using a widefield microscope (DM5500, Leica Microsystems) or a confocal (SP8, Leica Microsystems)

2.5   Analysis

During electrophysiological recordings, series resistance was constantly monitored and recordings in which the value exceeded 25 MΩ or changed more than 20% were excluded from the analysis. Additionally, if during recordings the leak current to clamp the neuron at a potential of -70 mV became larger than -100 pA, the remaining of the recording was discarded. No offline compensation was applied to recordings and no liquid junction potential correction was done. Analysis of electrophysiological recordings were performed with IgorPro (WaveMetrics).

During experiments in which the electrophysiological behaviour of neurons was analyzed, a series of 1 s hyperpolarizing and depolarizing current steps were injected in the soma. This allowed to extract passive properties from the hyperpolarizing steps while extracting active properties from the depolarizing steps. The analysis was performed with codes which were

kindly provided by Olexiy Kochubey and slightly modified by Ayah Khubieh for the needs of the recordings performed in this PhD project.

For passive properties, we extracted the membrane resistance and time constant for each neuron. Given that some neurons had a sag in response to hyperpolarizing currents, we only considered the peak value to avoid including the I_h current in the analysis. The same was done while fitting the decay with an exponential fit: if there was a sag, the fit was done until 95% of the minimum was reached, otherwise, the fit was done until the steady state. After extracting the values for all hyperpolarizing steps, an average was done for the membrane time constant, while a linear fit was done for the peak of the voltage responses.

As for the active properties of the neurons, the number of action potentials fired for each depolarizing step were extracted as well as the inter-spike intervals. These values allowed us to plot the frequency of events for each current step and fitting these data with a line provided the gain of the neuron (Hz/pA). Additionally, the inter-spike intervals were used to determine the frequency adaptation. Indeed, each inter-spike interval is the inverted instantaneous frequency ($freq$) between two action potentials. From the instantaneous frequencies we extracted an early frequency adaptation and a late frequency adaptation using these calculations: $freq_2/freq_1$ and $freq_{last}/freq_1$, respectively. With $freq_1$ being the frequency between the first pair of action potentials.

When applying optogenetic protocols, each stimulus was repeated for several sweeps and averaged. In general, single light pulse were applied every 5 s and averages are done over 12 consecutive sweeps. As for 10Hz train or pair pulses, they were applied every 12 to 20 s and averages are done for 10 consecutive sweeps. Average peak amplitude was calculated based on the peak of the average trace. Delay to the start of the response was calculated as the time at 10% of the maximal amplitude subtracted by the time of the light stimulus. Paired pulse ratios (PPR) were extracted by comparing the peak of the first event with the peak of the consecutive event. If the PPR was larger than one, it indicated a facilitation. On the contrary, if the PPR was smaller than one, then the synaptic connection was depressing.

All data reported in this PhD thesis is expressed as mean ± standard deviation. Number of

recordings are reported as "n=" whereas the number of mice are reported as "N=".

Acquired images were treated with Fiji (Schindelin et al., 2012) with macros provided by the BioImaging and Optics Platform (BIOP) at EPFL, which allowed extraction of the slide scanner images. Cell counting was performed using a macro for cell counting in Fiji.

3 | Results

When this project started, we were interested in investigating the connectivity between the pInsCx, as a potential source of nociceptive input during fear conditioning, and the input region of the LA, where the coincidence of CS and US is thought to induce plasticity. Previous work has identified this input region to be located in the dorsal part of the LA (Romanski et al., 1993). Coincidentally, we found in the ISH atlas of the Allen Brain Institute, that neurons which expressed VGluT2 seemed to be located specifically in the dorsal part of the LA (Fig 1.4). This led us to hypothesize that VGluT2 expression might be a marker for the input region of the LA and we wanted to investigate the input these neurons received from the pInsCx.

3.1   Anatomical characterization of LA VGluT2$^{\text{Cre}}$+ neurons

To identify VGluT2-expressing neurons in the brain, which would allow us to characterize them, we used the genetically-modified Cre-mouse line VGluT2$^{\text{Cre}}$. When this strain was crossed with the R26_LSL_tdTomato reporter mouse, we experienced an issue in the offspring due to a high background fluorescence in the amygdala, which made it difficult to identify fluorescent somata with confidence. Given that VGluT2 is highly expressed in the thalamus and that the LA receives a lot of thalamic projections, we believe that this was the reason for the high background. To avoid this issue, we chose to inject an AAV vector expressing a Cre-dependent tdTomato fluorescent protein (AAV8:CAG:DIO:tdTomato) in the LA. Another option was to cross the VGluT2$^{\text{Cre}}$ mouse with a R26_LSL_H2B_mCherry reporter mouse, in

which the fluorescent expression is restricted to the nucleus of the neuron expressing Cre. Using either of these methods reduced the overall neuropil fluorescence, simplifying the differentiation of fluorescent neurons from the background.

A Wild type mouse (C57BL/6J)

B VGluT2^{Cre} x R26_LSL_H2B_mCherry mouse
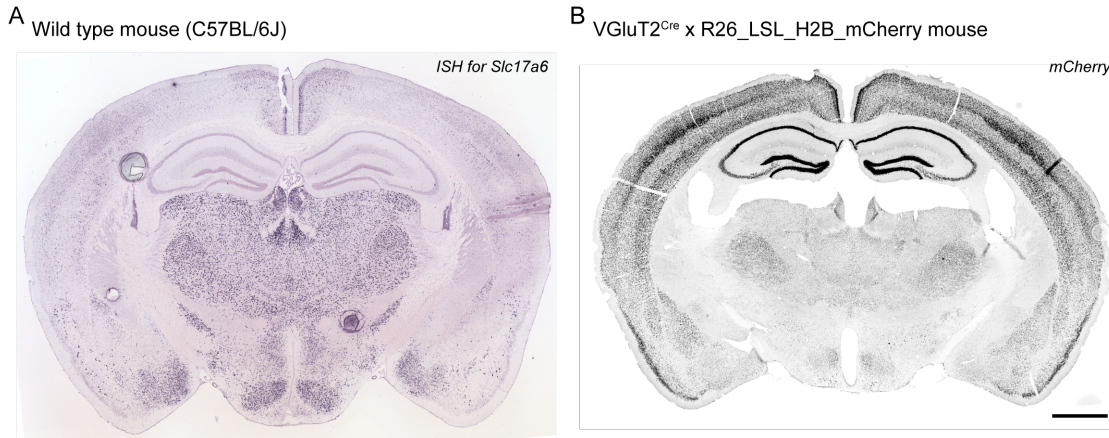
Figure 3.1 – Comparison of Allen Brain Institute ISH with the VGluT2^{Cre} histology. **(A)** Expression of *Slc17a6* shown with this chromogenic ISH in a wild type animal. This image is from the publicly available Allen Brain Institute database. **(B)** Widefield image of a slice from a VGluT2^{Cre} x R26_LSL_H2B_mCherry mouse brain. This image was inverted to have mCherry fluorescent cells appear dark for better comparison with (A). Scale bar: 1 mm.

First, we wanted to gain a better understanding of the anatomical localization of VGluT2^{Cre}+ neurons in the amygdala. We also wanted to investigate the overlap of fluorescent cells with CamKIIa-expressing neurons using the approach described in Methods 2.4.3: we performed an IHC on slices from a VGluT2^{Cre} x R26_LSL_H2B_mCherry mouse brain. Given the ISH images from the Allen Brain Institute (Fig. 3.1.A), we expected fluorescent cells to be mainly located in key areas, such as the thalamus or the LA. However, on our images, the distribution of fluorescent cells appeared to be more generalized, in particular in the cortex (Fig. 3.1.B).

The colocalization of VGluT2^{Cre}+ and CamKIIa+ neurons was easily discernible given that the Cre-dependent mCherry fluorescence is nucleus-targeted, while the CamKIIa IHC tends to only stain the cytoplasm of the neurons while leaving the nucleus empty (Fig. 3.2). Our observations were confirmed in the confocal images where we found that the Cre-reporter expression was not limited to the LAdl, but rather to the whole BLA (see widespread red cells in Fig. 3.2.A). This expression was also found in adjacent regions, such as the claustrum or the cortex, but not in the Astria. As for the CamKIIa IHC, we could see a very broad population of neurons stained, except for a low staining in the claustrum, especially in the VEn (Ventral

Endopiriform claustrum) for example. Regarding the amygdala, there were many neurons which expressed Cre-dependent mCherry and were, at the same time, stained for CamKIIa.
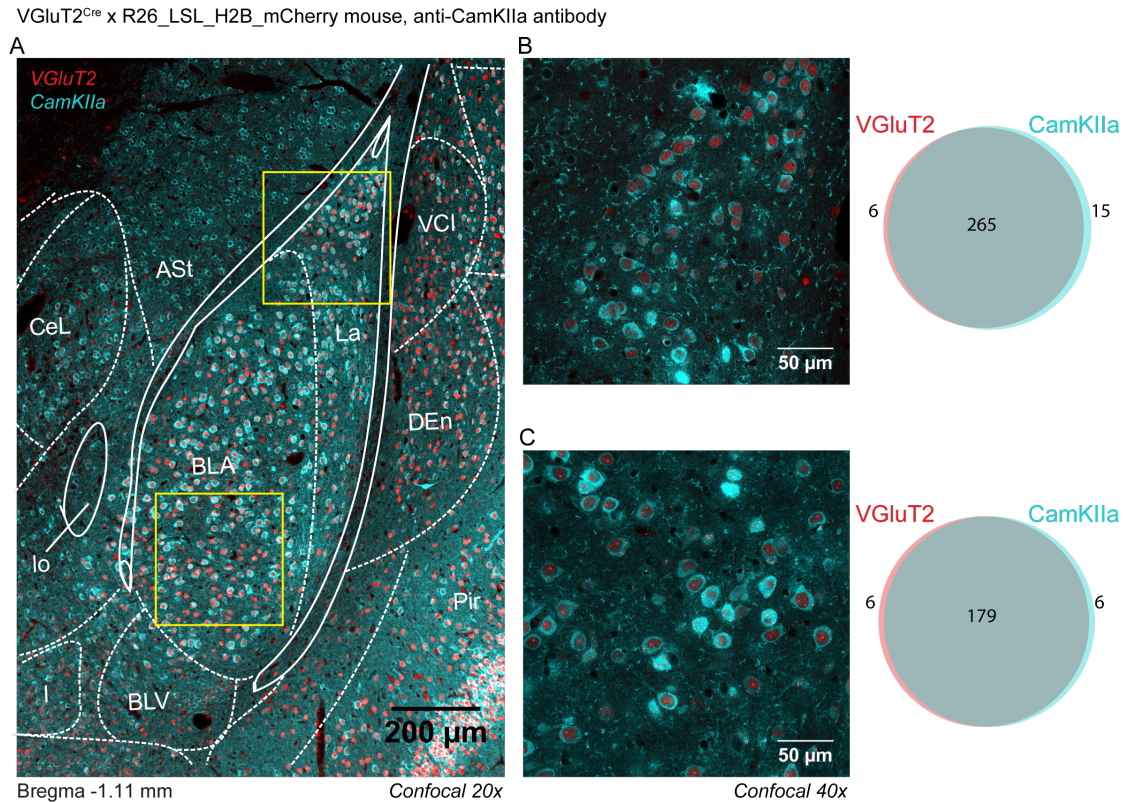
Figure 3.2 – VGluT2^{Cre}+ neurons colocalize with CamKIIa+ neurons in the BLA. (A) Confocal image of the basolateral complex of the amygdala in a histological slice of a VGluT2^{Cre} x R26_LSL_H2B_mCherry mouse which was immunohistochemically stained with an antibody against CamKIIa. This image was taken with an objective of magnification 20x. Yellow boxes indicate the regions which were then later imaged with a higher magnification of 40x. Brain atlas overlay is from Paxinos and Franklin, 2012. Scalebar: 200 µm. **(B - C)** Example z-section from the Lateral Amygdala and Basal Amygdala (respectively top and bottom panel), which were used to count the number of VGluT2^{Cre}+ and CamKIIa+ neurons. The Venn Diagrams on the right indicate the number of counted cells for each population and shows the amount of overlap. Scalebars: 50 µm.
ASt, amygdalostriatal transition area; BLA, basolateral amygdaloid nucleus, anterior part; BLV, basolateral amygdaloid nucleus, ventral part; CeL, central amygdaloid nucleus, lateral division; DEn, dorsal endopiriform claustrum; I, intercalated nuclei of the amygdala; Io, inferior olivary nucleus; La, lateral amygdaloid nucleus; VCl, ventral part of claustrum; VEn, ventral endopiriform claustrum.

To precisely evaluate the level of overlap of these two populations, we acquired z-stacks with a higher magnification in a subregion of the LA and a subregion of the BA (yellow boxes in Fig. 3.2.A and enlargements in Fig. 3.2.B-C). With these images, we were able to count the number of cell nuclei which expressed Cre-dependent mCherry and the number of neuron cytoplasms which were stained with CamKIIa antibodies. On the 286 cells which were

counted in the LA sample (Fig. 3.2.B), we found that 265 co-expressed mCherry and CamKIIa (92.7% of the counted cells), whereas we counted only 6 cells which were fluorescent with mCherry only (2.1% of the counted cells) and 15 cells which were CamKIIa+ only (5.2% of the counted cells). On the 191 cells which were counted in the BA sample (Fig. 3.2.C), we found that 179 co-expressed mCherry and CamKIIa (93.7% of the counted cells), whereas we counted only 6 cells which were only VGluT2^{Cre}+ or CamKIIa+ (3.1% of the counted cells each). Thus, essentially every CamKIIa-expressing neuron also has the VGluT2 gene locus active, at least to a small degree.

Given this unexpected broad expression of VGluT2 and the high overlap with CamKIIa+ cell population, we remained conservative and chose to consider VGluT2^{Cre}+ neurons to be principal neurons. We think the leaky fluorescence might be due to early developmental expression of VGluT2 or because of a low VGluT2 expression in neurons (see Discussion 4.1).

3.2 AP-firing properties of the LA VGluT2^{Cre}+ neurons

We wanted to learn more about the electrophysiological behaviour of the VGluT2^{Cre}+ neurons. As mentioned earlier, in order to be able to identify fluorescent cells, we chose to either inject AAV8:CAG:DIO:tdTomato in the LA of VGluT2^{Cre} mice, or simply use VGluT2^{Cre} x R26_LSL_H2B_mCherry mice. This prevented a high background fluorescence in the LA and helped detecting fluorescent neurons to perform current-clamp experiments on them.

For each recorded neuron, we measured the voltage response to injected current steps of 1 s and of different amplitudes (Fig. 3.3.A-B). From the hyperpolarizing steps, we were able to extract the passive properties of these neurons, such as their input resistance or the cell membrane time constant. From the depolarizing steps, we were able to analyze the active properties of these neurons, such as their AP-firing dynamics or their gain.
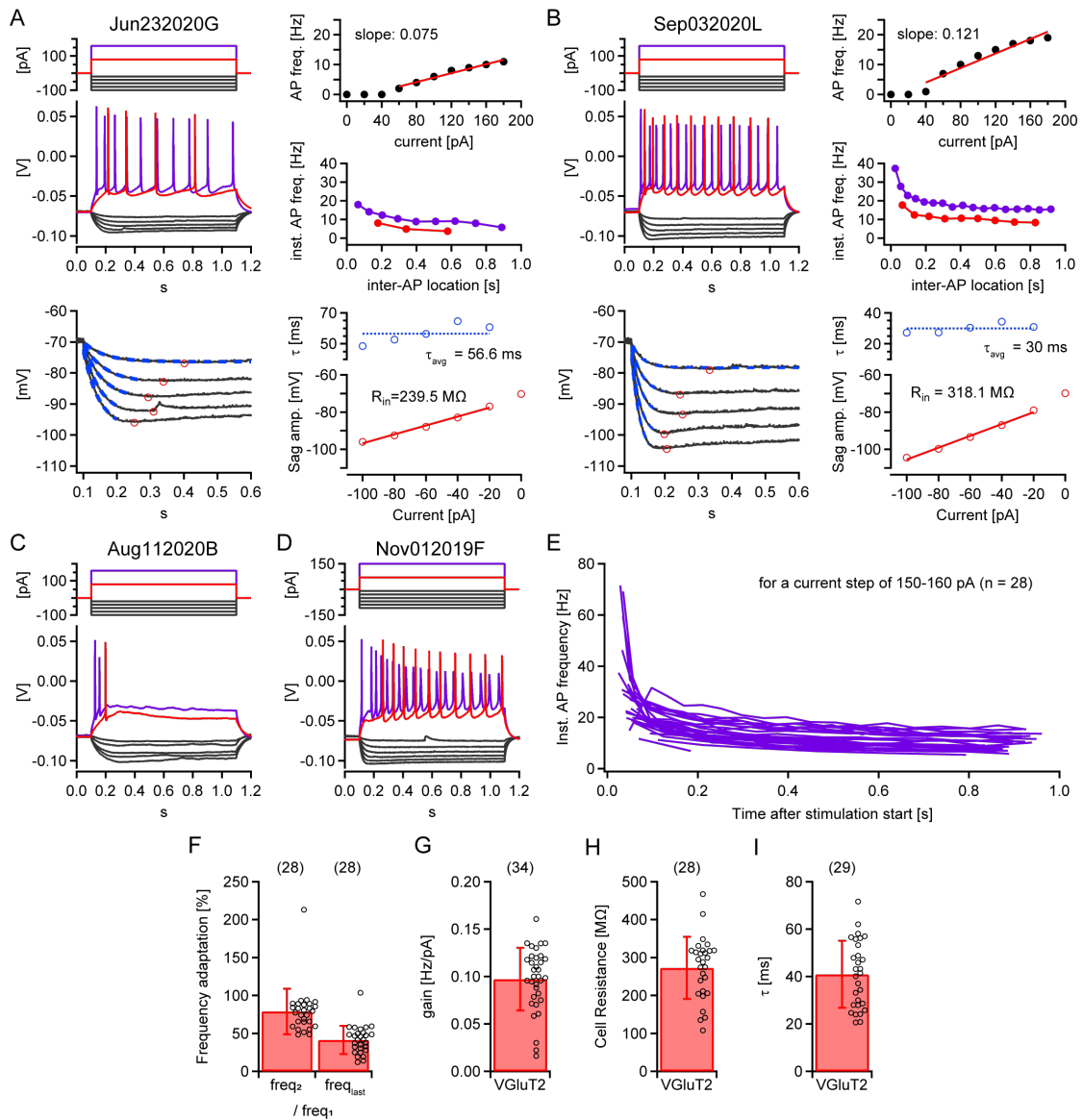
Figure 3.3 – Electrophysiological behaviour of VGluT2^Cre+ cells in the LA. **(A)** Example of a VGluT2^Cre+ neuron responding to 1 s depolarizing and hyperpolarizing current steps (*top left*). *Bottom left*: Exponential fit (dashed blue line) of the membrane deflection to hyperpolarizing currents and peak detection (red circles). *Bottom right*: plot of the extracted values from the bottom left panel. *Top right*: plot of AP frequency in function of injection current with a fit of the slope. *Top middle*: plot of instantaneous frequency depending for the two traces in the top left panel. **(B)** Same as (A) but for another VGluT2^Cre+ neuron. **(C-D)** Example of 2 neurons which had a different AP-firing than the typical responses seen in (A) and (B). These occurrences remained sparse. **(E)** Instantaneous frequency comparison of all recorded neurons (n=28) in response to a current step between +150 and +160 pA over the 1 s stimulation. **(F)** Average early (*left bar*) and late (*right bar*) frequency adaptation (n=28). Extracted from the curves in (E). **(G)** Average firing gain extracted from the slopes of AP frequency in function of current for each cell (n=34). **(H)** Average input resistance (n=28). Method of measuring the resistance is shown in bottom panels of (A) and (B). **(I)** Average membrane time constant τ (n=29). The time constant was extracted from exponential fits of the passive responses as shown on bottom panels of (A) and (B). Mean ± standard deviation.
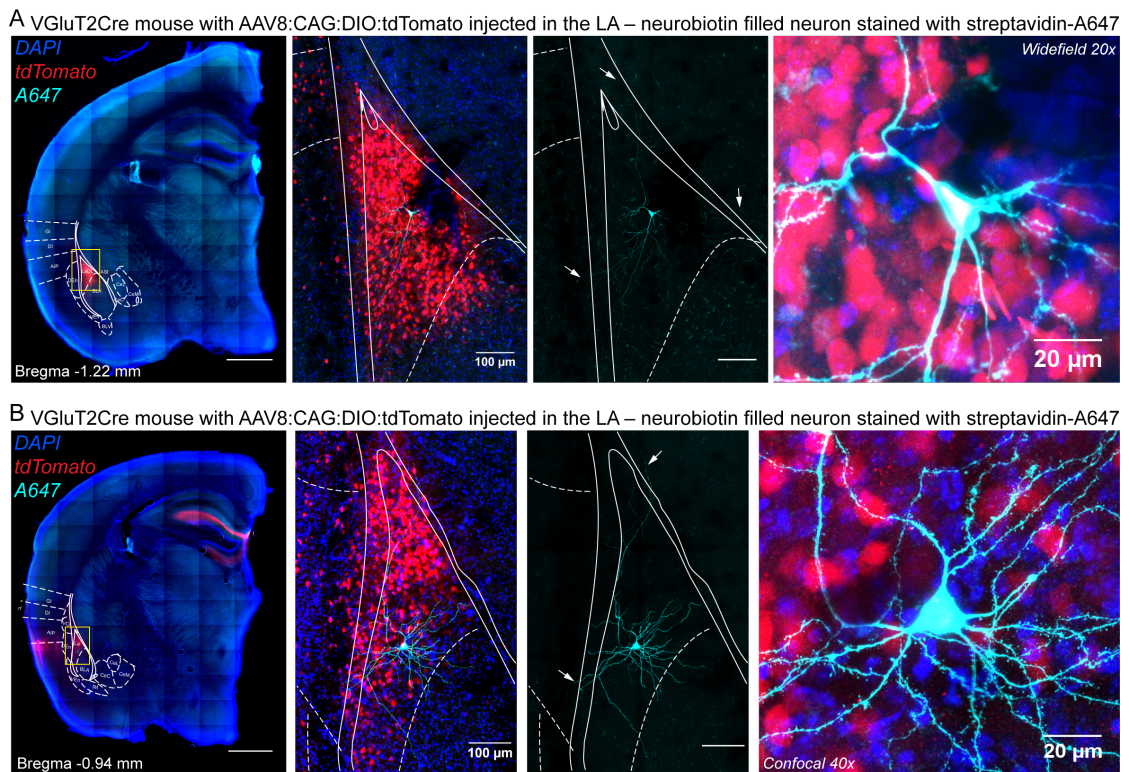
Most neurons had a similar AP-firing profile, except for a few neurons which behaved differently (2 examples in Fig. 3.3.C-D). In general, as the amplitude of the current step increases the response was characterized by a double-spike (2 APs with a short delay and almost no afterhyperpolarization) followed by a train of APs with increased inter-spike-intervals (ISIs), hence decreased instantaneous frequency. This was common to most neurons and could be best observed when comparing the instantaneous frequencies ($freq$), which were decaying curves, for an injected step current in the range of 150-160 pA (Fig. 3.3.E). When looking at the frequency adaptation for a 150-160 pA injected current, we found that early adaptation ($freq_2/freq_1$) was 78.9 ± 30 %, and late adaptation ($freq_{last}/freq_1$) was 41.4 ± 18.5 % (n=28 recordings from N=15 mice; Fig. 3.3.F). This shows a rather continuous decrease in instantaneous frequency over the time of the stimulation, and is proof of an accommodation occurring. We also extracted the firing rate gain from the slope of the AP frequency induced at different injected currents, and found that on average, the gain was of around 0.1 ± 0.03 Hz/pA (n=34 recordings from N=17 mice; Fig. 3.3.G).

As for the passive properties of these excitatory neurons, we observed that most neurons showed an I_h-current mediated sag during large hyperpolarizing steps. Hence, in these instances, we measured the input resistance and the time constant from, respectively, the sag amplitude and the curve decay before the sag. We found that on average, the input resistance was 273 ± 82 MΩ (n=28 recordings from N=14 mice; Fig. 3.3.H) and the average membrane time constant τ was 40.9 ± 14.1 ms (n=29 recordings from N=14 mice; Fig. 3.3.I).

Additionally, as mentioned in the methods, we took advantage of the whole-cell patch-clamp experiments to fill single VGluT2^{Cre}+ neurons in the LA with neurobiotin, an intracellular tracer, which was then made visible by binding it with streptavidin-conjugated Alexa-647 (see more detail in Methods 2.3.3). In general, the cells appeared to have a slight pyramidal shape. In a few cells, the projections of the neurons were successfully stained and we could see the projection extending beyond the BLA, especially towards the Astria or the external capsule (Fig. 3.4).

The electrophysiological and morphological data is consistent with the view that VGluT2^{Cre}+ neurons are principal cells of the LA.

A VGluT2Cre mouse with AAV8:CAG:DIO:tdTomato injected in the LA – neurobiotin filled neuron stained with streptavidin-A647

B VGluT2Cre mouse with AAV8:CAG:DIO:tdTomato injected in the LA – neurobiotin filled neuron stained with streptavidin-A647

Figure 3.4 – Morphologies VGluT2^{Cre}+ neurons. **(A)** Image of the slice which was used for patch-clamp and in which a VGluT2^{Cre}+ neuron was filled with neurobiotin (*left*). Scale bar: 1 mm. *Middle panels*: Widefield image from the region indicated on the left panel. One of the images shows the stained neuron alone to show processes. White arrows indicate processes which are beyond the BLA. Scale bar: 100 µm. *Right*: High magnification image of the cell body of the stained neuron in a widefield microscope. Scale bar: 20 µm. **(B)** Same as (A) for another neuron filled with neurobiotin except higher magnification images were acquired with a confocal microscope.
The overlays are from Paxinos and Franklin, 2012

3.3 pInsCx inputs to LA principal neurons

The LA is considered to be the input region of the amygdala, due to the numerous multimodal sensory afferents which terminate in the region (LeDoux, 2000). During fear conditioning, the US and CS signal converge to the LAdl (Fig. 1.2; Romanski et al., 1993). Although the CS input has been extensively studied, a lot less is known about the US signal, especially which region is the source of the US input to the LA. As mentioned previously (see Introduction 1.3), there is reasonable evidence to believe the pInsCx might be the source of aversive input to the LA. Hence, we were interested to investigate how this putative US input recruits the LA principal neurons.

In order to measure the pInsCx input onto principal neurons of the LA, we injected an AAV vector driving the expression of the opsin Chronos (AAV8:hsyn:Chronos-GFP) in the pInsCx of a VGluT2^{Cre} mouse and we also injected an AAV vector driving the Cre-dependent expression of tdTomato (AAV8:CAG:DIO:tdTomato) in the LA (Fig. 3.5.A). An example of such an injection is shown in Fig. 3.5.B for both the left (top panels) and the right (bottom panels) hemispheres. In a very few animals (N = 2 for a total of N = 14), we didn't inject the second AAV vector (AAV8:CAG:DIO:tdTomato) as we used a VGluT2^{Cre} x R26_LSL_H2B_mCherry mouse.
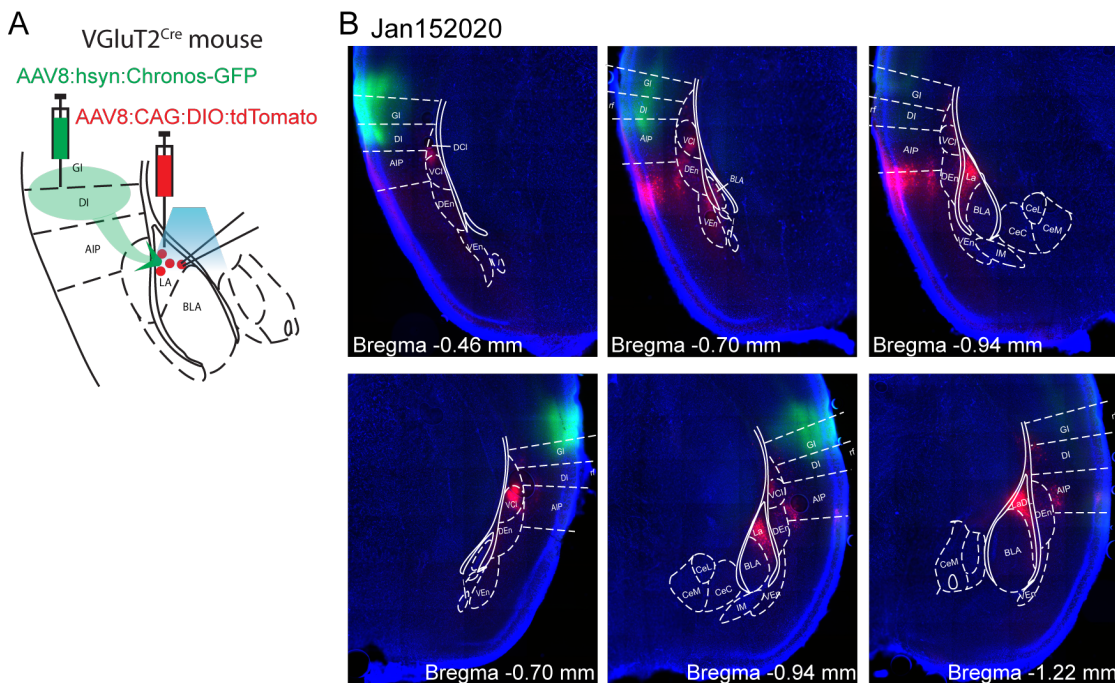
Figure 3.5 – Example of injection in a VGluT2^{Cre} mouse. **(A)** Scheme of the experimental design, injections were done in VGluT2^{Cre} mice to record long-range inputs from the pInsCx to LA VGluT2^{Cre}+ neurons by applying blue light locally. **(B)** Widefield images of thick slices, from a single animal, which were used for a patch-clamp experiment. Images are shown caudal to rostral (from left to right) for both hemispheres (top panels are for the left hemisphere and bottom panels are for the right hemisphere). Bregma coordinates are the ones associated with the overlays from the atlas by Paxinos and Franklin, 2012.

AIP, agranular insular cortex, posterior part; BLA, basolateral amygdaloid nucleus, anterior part; CeC, central amygdaloid nucleus, capsular part; CeL, central amygdaloid nucleus, lateral division; CeM, central amygdaloid nucleus, medial division; DCl, dorsal part of claustrum; DEn, dorsal endopiriform claustrum; DI, dysgranular insular cortex; GI, granular insular cortex; I, intercalated nuclei of the amygdala; IM, intercalated amygdaloid nucleus, main part; La, lateral amygdaloid nucleus; LaDL, lateral amygdaloid nucleus, dorsolateral part; rf, rhinal fissure; VCl, ventral part of claustrum; VEn, ventral endopiriformclaustrum.

After at least 4 weeks following the injections, we performed voltage-clamp recordings of fluorescent cells in the LA, and stimulated a pInsCx input by shining blue light on the slice, which should activate the opsins on the axons originating from the pInsCx and induce synaptic release. To differentiate excitatory from inhibitory inputs, we clamped the voltage of the neurons at different values and recorded the optogenetically-evoked postsynaptic currents (PSC). To measure excitation, we set the neuron voltage at -70 mV, close to the resting potential of the neuron and the reversal potential of chloride (at -71.8 mV, see Methods 2.3.2). For these experiments, we used cesium in the intracellular solution.

We first measured the amplitude of the optogenetically-evoked excitatory PSC (oEPSC) in response to a 1 ms light pulse at different intensities. We observed that the oEPSC amplitude increased as the light intensity increased, without reaching saturation, suggesting a high number of synaptic inputs (Fig. 3.6.A-B). In the remaining recordings of VGluT2^{Cre}+ neurons which will be discussed afterwards, all light stimulations were done at maximal intensity.

We next wished to learn more about the nature of the pInsCx input, i.e. whether the connection was glutamatergic and mono- or poly-synaptic. When adding NBQX to the recording solution, we observed that the oEPSCs were blocked (Fig. 3.6.C). This suggests that the synapses from the pInsCx onto principal neurons of the LA are glutamatergic. Additionally, we observed that adding TTX (1 μM) to the recording solution blocked the oEPSCs, which was predictable given that TTX prevents the AP-firing in afferent axons by blocking voltage-gated sodium channels. However, the evoked response was partly recovered (81.5% of the initial amplitude) when 4-AP (1 mM) was added to the recording solution. This suggests that the oEPSC evoked by stimulating the pInsCx axons is in part, mono-synaptic. Indeed, 4-AP allows the direct depolarization by the opsin-induced currents, which in turn recovers the neurotransmitter release (see Fig. 1.3; Petreanu et al., 2009). TTX and 4-AP were also used in an another experiment, but the recovery was of only 13.5% of the initial oEPSC amplitude (data not shown here). In that particular experiment, the delay to the oEPSC was of 4.3 ms which was on the higher end of recorded values, but would be too short for a poly-synaptic event.
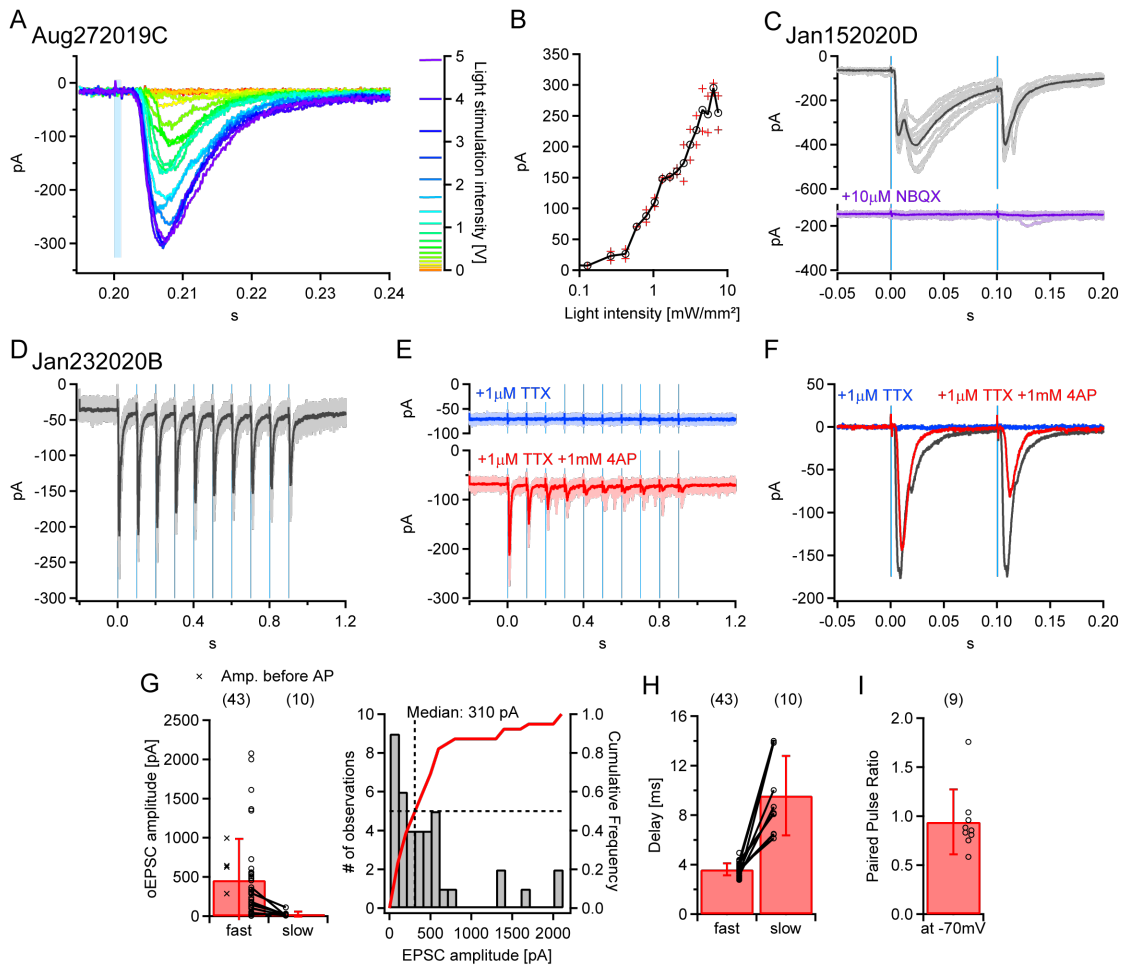
Figure 3.6 – Excitatory response of LA VGluT2^{Cre}+ neurons to a pInsCx stimulation. **(A)** Traces of an LA VGluT2^{Cre}+ neuron response to different intensities (scale bar on the right) of 1 ms light pulse. **(B)** Input-output curve for the same experiment as in (A). **(C)** oEPSC of an LA VGluT2^{Cre}+ neuron in response to a pair of maximal light intensity 1 ms pulses before (grey) and after (purple) bath application of NBQX. **(D)** oEPSC of an LA VGluT2^{Cre}+ neuron in response to a 10-Hz train of light stimulations at maximal intensity. **(E)** oEPSC of the same neuron and stimulation as in (D) when TTX (blue) and the combination of TTX and 4-AP (red) are applied to the bath. **(F)** Average traces of (D) and (E) superimposed for comparison. **(G)** Average and individual amplitudes for the fast (n=39, left bar) and slow (n=10, right bar) components of oEPSC in response to a single light stimulation. Some neurons had escape currents for the maximal intensity of light stimulation, so the crosses indicate their highest amplitude at a light intensity which did not induce an escape current, these data points were not included in the average (n=4). *Right panel*: histogram of the fast component of oEPSC in response to light stimulation, with the corresponding cumulative frequency. **(H)** Average and individual time delays between the start of the light pulse and the 10% of the amplitude of the oEPSC for both the fast (n=43, left bar) and slow (n=10, right bar) component in response to light stimulation. **(I)** Average and individual values of paired pulse ratio of recorded neurons in response to a pair of light pulses with a 100 ms delay (n=9).

In panels (C-E), darker traces represent the averages of the single traces. Mean ± standard deviation.

On average, oEPSCs in VGluT2^{Cre}+ cells located in the LA had an amplitude of 460 ± 525 pA after bi-lateral injection of Chronos in pInsCx (n=39 recordings from N=13 mice). In n=4 cells (N=2), the highest light intensity induced a response with an escape current (due to a failure of a complete clamping of the cell voltage). For these neurons, we extracted the maximal amplitude, for a lower light intensity, before the escape current appeared, but we did not include these amplitudes in the average calculation (Fig. 3.6.G, cross symbols). In 10 cells out of 32, we could differentiate a fast and a slow component in the oEPSCs (Fig. 3.6.C). In the remaining 11 cells, we could not analyse for a slow component for various reasons. These two components would likely correspond to a mono-synaptic response followed by a poly-synaptic response. Indeed, it would be highly unlikely for this slow component to be an optogenetically-evoked inhibitory PSC (IPSC) given that the potential at which the neurons were clamped (V_m = -70 mV) was too close to the reversal potential of chloride (E_{Cl} = -71.8 mV). The amplitude of this secondary component was on average of 24.4 ± 31.9 pA (n=10 recordings from N=8 mice; Fig. 3.6.G right bar).

We were also interested in the delay between the light stimulation and the start of the oEPSC response. This delay was measured by quantifying the difference between the start time of the light pulse and the time at which the EPSC reached 10% of its amplitude. We found that the delay to the fast and slow responses were, respectively, 3.6 ± 0.5 ms and 9.6 ± 3.2 ms (n=43 recordings from N=13 mice for the fast component; n=10 recordings from N=8 mice for the slow component; Fig. 3.6.H). This is consistent with the hypothesis that the fast component results from a direct synaptic release of the pInsCx projection, whereas the slow component would rather be the result of a poly-synaptic response.

As for the short-term dynamics of the oEPSC, we found that when stimulating the synaptic connection from the pInsCx onto principal neurons of the LA with two light-pulses with a 100 ms interval, the paired pulse ratio (PPR) was on average of 0.94 ± 0.33 (n=9 recordings from N=4 mice; Fig. 3.6.I).
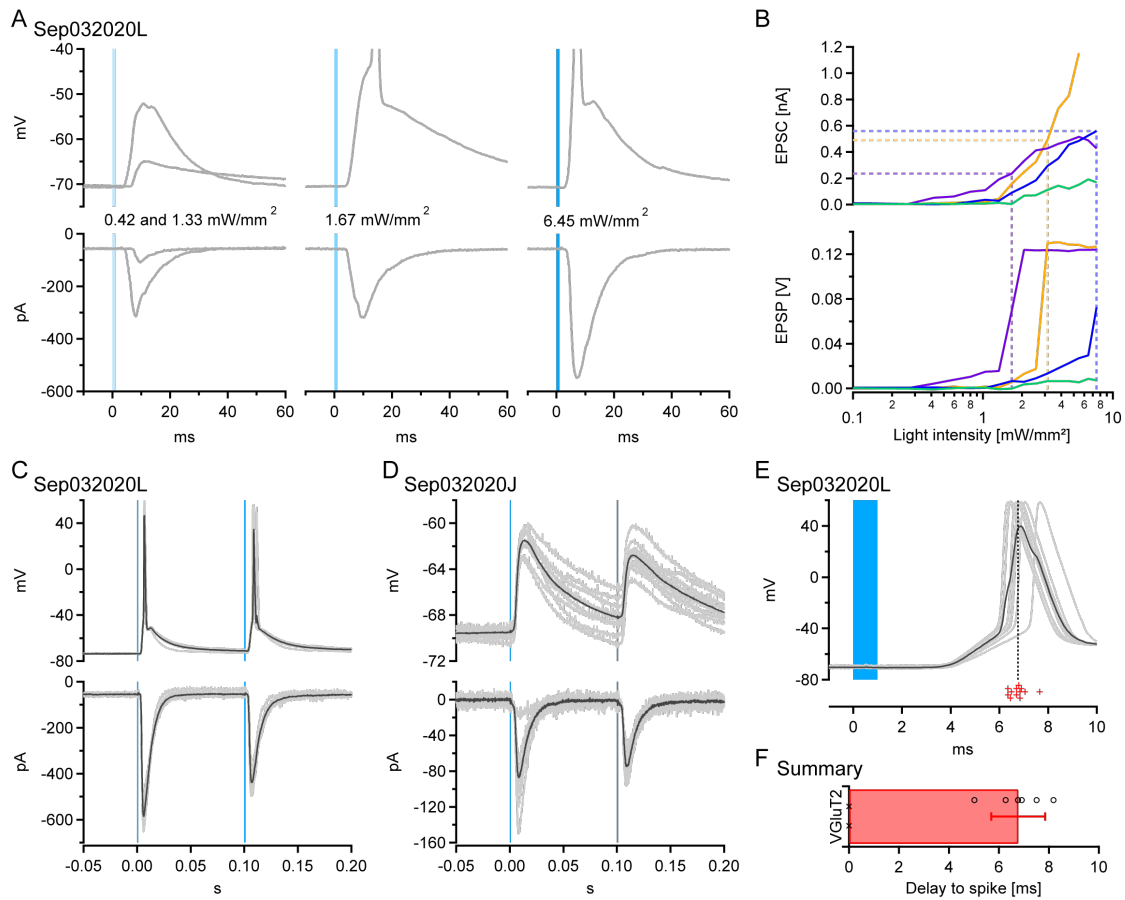
Figure 3.7 – pInsCx input activates VGluT2^{Cre}+ neurons. **(A)** Trace examples of a VGluT2^{Cre}+ neuron, in response to a 1 ms blue light pulse at different light intensities, during current- (top) and voltage-clamp (panels). **(B)** Input-output curves of oEPSC (top) and oEPSP for n=4 neurons (for 1 or 2 repetitions). Dotted lines indicate the current and light intensity at which a neuron had an AP evoked during one of the repetitions. Cell in (A) is represented in purple here. **(C)** oEPSP (top) and oEPSC (bottom) of a VGluT2^{Cre}+ neuron which had evoked APs in response to a pair of 1 ms light pulses at maximal intensity. **(D)** oEPSP (top) and oEPSC (bottom) of another VGluT2^{Cre}+ neuron which did not reach AP-threshold in response to a pair of 1 ms light pulses at maximal intensity. **(E)** Expanded response of the neurons shown in (C) following a single light pulse with extracted times of AP maximum (red crosses). The dotted line indicates the average time of AP maximum. **(F)** Average and individual data points of the time to AP maximum for different VGluT2^{Cre}+ neurons (n=5, circles). Cells which did not have AP evoked are displayed as crosses and were not included in the average (n=2, crosses).
In panels (C-E), darker traces represent the averages of the single traces. Mean ± standard deviation.

To evaluate whether the excitatory input from the pInsCx can drive AP firing of VGluT2^{Cre}+ neurons in the LA, we performed current-clamp recordings with a potassium intracellular solution (same method as Fig. 3.5). For these experiments, we wanted to compare the evoked oEPSC to the evoked membrane potential responses (oEPSP) and thereby assess the EPSC amplitude at which the threshold for AP firing was crossed (as done by Gjoni et al., 2018).

For example, in the cell shown in Fig. 3.7.A, for a small change in the intensity of the light pulse (from 1.33 to 1.67 mW/mm^2), although the oEPSC didn't seem to increase a lot it was enough for the membrane potential to cross the threshold (purple curve in Fig. 3.7.B). We were able to compare the voltage and current responses of neurons to increasing light intensities in n=4 recordings (N=3 mice), in which 3 cells showed AP firing. These neurons reached the AP-threshold at a light intensity in a range between 1.7 and 7.5 mW/mm^2 for an oEPSC in the range between 235 and 559 pA (Fig. 3.7.B).

In the n=3 recordings mentioned above and in another n=3 recordings (total N=5 mice), maximal intensity stimulation evoked an AP (Fig. 3.7.C). In n=2 recordings, maximal intensity stimulation did not evoke an AP (Fig. 3.7.D). In general, the delay to the AP was 6.8 ± 1.1 ms after light stimulation (n=6 recordings from N=5 mice; Fig. 3.7.E-F).

The pInsCx appears to robustly project to excitatory neurons of the LA with many fibres, forming direct synaptic connections onto these principal neurons. Inputs from the pInsCx are likely to evoke AP firing in these neurons. These APs would then evoke an EPSC in the neurons they project to around 10 ms following the light pulse.

3.4   Feedforward inhibition onto principal neurons of the LA

Previous studies showed, through the electrical stimulation of thalamic and cortical afferents, that additionally to glutamatergic inputs, sensory input in the LA seem to induce feedforward inhibition onto principal neurons (see Introduction 1.5). Additionally, given the importance of feedforward inhibition on behaviour (Wolff et al., 2014; Krabbe et al., 2019), we wanted to investigate whether pInsCx input also induced feedforward inhibition onto the principal neurons of the LA.

To measure inhibitory inputs onto VGluT2^{Cre}+ neurons, we used the same methodology as described in Results 3.3 (see Fig. 3.5.A). To perform these voltage-clamp experiments, we used an intracellular solution containing cesium, and clamped the neurons at a voltage of +15 mV which was close to the excitatory signal reversal potential.
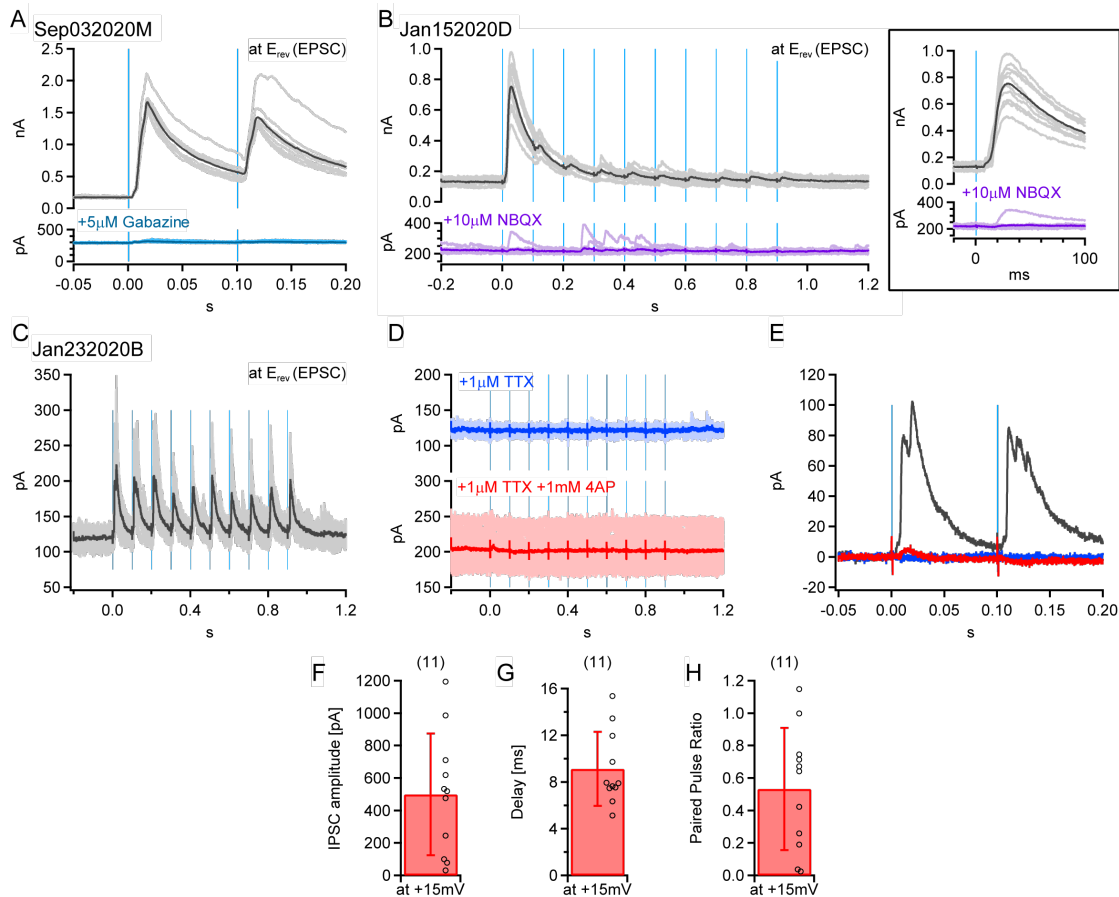
Figure 3.8 – Feedforward inhibitory input onto LA VGluT2^{Cre}+ neurons following light stimulation of pInsCx afferents. **(A)** oIPSCs of an LA VGluT2^{Cre}+ neuron in response to a pair of 1 ms light pulses before (grey) and after (cyan) bath application of Gabazine. **(B)** oIPSCs of an LA VGluT2^{Cre}+ neuron in response to a 10-Hz train of 1 ms light pulses before (grey) and after (purple) bath application of NBQX. Expansion of the first stimulation of the train on the right panel. **(C)** oIPSC of an LA VGluT2^{Cre}+ neuron in response to a 10-Hz train of light pulses at maximal intensity. **(D)** oEPSC of the same neuron and stimulation as in (C) when TTX (blue) and the combination of TTX and 4-AP (red) are applied to the bath. **(E)** Average traces of (C) and (D) superimposed for comparison. **(F)** Average and individual data points of the oIPSC amplitudes (n=11). **(G)** Average and individual data points of the delay between the light pulse and the 10% of the amplitude of the oIPSC in response to light stimulation (n=11). **(H)** Average and individual data points of the paired pulse ratio of recorded neurons in response to a pair of light pulses with 100 ms delay (n=11).
In panels (A-E), darker traces represent the averages of the single traces, for neurons voltage-clamped at the reversal potential of EPSC. Mean ± standard deviation.

When principal neurons were voltage-clamped at +15 mV, we observed an optogenetically-evoked outward PSC (Fig. 3.8.A). Given that the chloride reversal potential was -71.8 mV (see Methods 2.3.2), it was likely that this signal was inhibitory. To verify this, we added Gabazine to the recording solution and found that the outward PSC disappeared, confirming that this PSC is a GABAergic inhibitory PSC (IPSC) (Fig. 3.8.A).

If this optogenetically-evoked IPSC (oIPSC) is the result of feedforward inhibition, it would require glutamatergic axons from the pInsCx to connect to local inhibitory interneurons in the LA and evoke APs, which in turn would cause the inhibition of the principal cells. Thus, such a feedforward inhibitory connection would be sensitive to NBQX. Indeed, when adding NBQX to the recording solution, the inhibitory signal was blocked (Fig. 3.8.B), supporting the view of a local poly-synaptic relay in the LA.

Another way to determine the feedforward nature of the inhibitory signal is to first block the signal with TTX. If the pathway is indeed poly-synaptic, then adding 4-AP in the continued presence of TTX should not recover the oIPSC. Indeed, 4-AP only allows synaptic release of axons containing channelrhodopsin, which would not be the case of local interneurons (Fig 1.3). The finding in our experiment that oIPSC was not rescued by 4-AP (Fig. 3.8.C-E) is consistent with the view of a feedforward inhibition induced by pInsCx stimulation (see Introduction 1.4, Fig. 1.3).

We found that the amplitude of the oIPSC was 498.8 ± 374.6 pA (n=11 recordings from N=5 mice; Fig. 3.8.F), with a delay of 9.1 ± 3.2 ms (n=11 recordings from N=5 mice; Fig. 3.8.G). The delay of the oIPSC was larger than the one of the fast component of the oEPSC, which would again support the idea of the poly-synaptic nature of the connection. Regarding short term dynamics, the inhibitory signal appeared to be depressing for a pair of light pulses with a 100 ms delay. Indeed, we observed an average PPR of 0.53 ± 0.38 (n=11 recordings from N=5 mice; Fig. 3.8.H).

3.5   pInsCx inputs to VIP interneurons located in the LA

After investigating the responses of VGluT2$^{\text{Cre}}$+ neurons, and given the important role of VIP-INs in the disinhibition of the LA principal neurons, we wished to investigate whether VIP$^{\text{Cre}}$+ INs received a direct long-range excitatory input from the pInsCx. In terms of distribution, as expected, there are a few VIP$^{\text{Cre}}$+ INs, however they are evenly spread across the LA, making them a potential target of pInsCx projections (Fig. 3.9). Interestingly, the lateral CEA (CeL on the Fig. 3.9) appears bright, however this fluorescence is the result of VIP$^{\text{Cre}}$+ INs projections.

VIP^{Cre} x R26_LSL_tdTomato
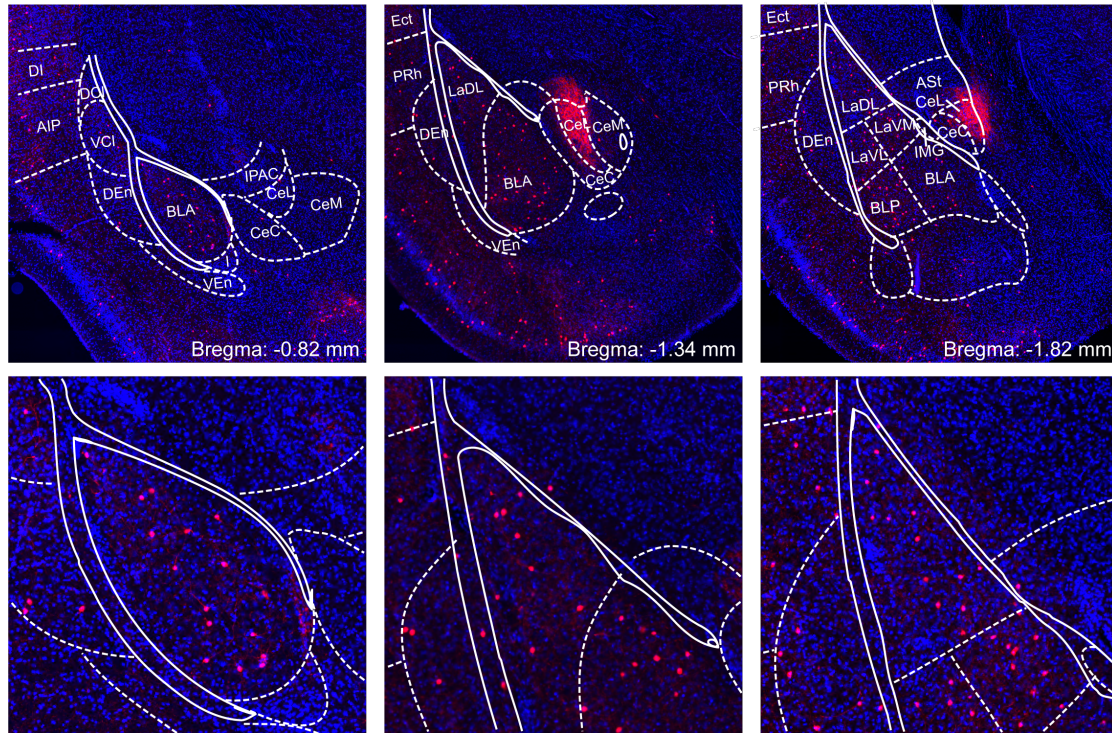
Figure 3.9 – Distribution of VIP^{Cre}+ INs in the LA. Images of thin slices from a VIP^{Cre} x R26_LSL_tdTomato mouse shown rostral to caudal (left to right) prepared and acquired by Palchaudhuri. Bottom pannels are an expansion of the top pannels focused on the LA regions for better clarity. Overlays are from Paxinos and Franklin, 2012.
AIP, agranular insular cortex, posterior part; ASt, amygdalostriatal transition area; BLA, basolateral amygdaloid nucleus, anterior part; BLP, basolateral amygdaloid nucleus, posterior part; CeC, central amygdaloid nucleus, capsular part; CeL, central amygdaloid nucleus, lateral division; CeM, central amygdaloid nucleus, medial division; DCl, dorsal part of claustrum; DEn, dorsal endopiriform claustrum; DI, dysgranular insular cortex; Ect, ectorhinal cortex; I, intercalated nuclei of the amygdala; IMG, amygdaloid intramedullary gray; IPAC, interstitial nucleus of the posterior limb of the anterior commissure; LaDL, lateral amygdaloid nucleus, dorsolateral part; LaVL, lateral amygdaloid nucleus, ventrolateral part; LaVM, lateral amygdaloid nucleus, ventromedial part; PRh, perirhinal cortex; VCl, ventral part of claustrum; VEn, ventral endopiriformclaustrum.

In order to test whether VIP-INs receive excitatory inputs from the pInsCx, we performed injections in VIP^{Cre} mice of an AAV vector driving the expression of the opsin Chronos (AAV8:hsyn:Chronos-GFP) in the pInsCx, and we injected an AAV vector driving the Cre-dependent expression of tdTomato (AAV8:CAG:DIO:tdTomato) in the LA to visualize the VIP^{Cre}+ neurons as fluorescent cells (Fig. 3.10). In most experiments (4 mice for a total of 7 mice), we used VIP^{Cre} x R26_LSL_tdTomato mice to visualise VIP^{Cre}+ neurons and only injected the AAV8 driving the expression of Chronos into the pInsCx.
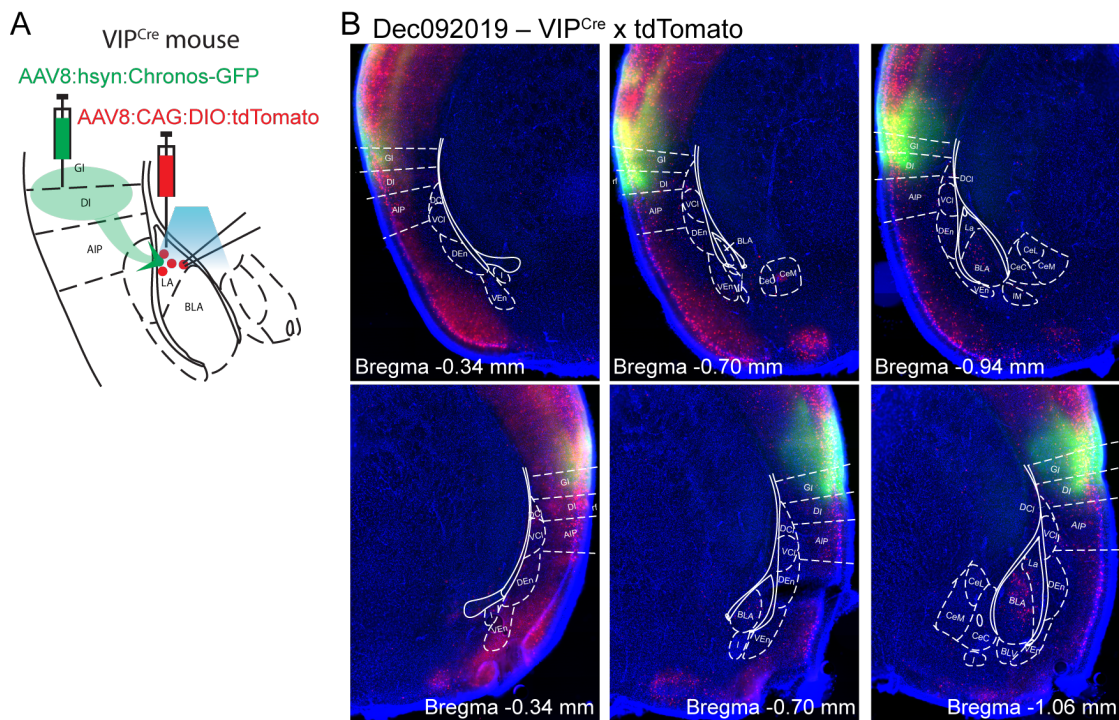
Figure 3.10 – Example of injection in a VIP^Cre mouse. **(A)** Scheme of the experimental design, injections were done in VIP^Cre mice to record long-range inputs from the pInsCx to LA VIP^Cre+ INs by applying blue light locally. **(B)** Widefield images of thick slices, from a single VIP^Cre x R26_LSL_tdTomato mouse, which were used for a patch-clamp experiment. Images are shown caudal to rostral (from left to right) for both hemispheres (top panels are for the left hemisphere and bottom panels are for the right hemisphere). Bregma coordinates are the ones associated with the overlays from the atlas by Paxinos and Franklin, 2012.

AIP, agranular insular cortex, posterior part; BLA, basolateral amygdaloid nucleus, anterior part; BLV, basolateral amygdaloid nucleus, ventral part; CeC, central amygdaloid nucleus, capsular part; CeL, central amygdaloid nucleus, lateral division; CeM, central amygdaloid nucleus, medial division; DCl, dorsal part of claustrum; DEn, dorsal endopiriform claustrum; DI, dysgranular insular cortex; GI, granular insular cortex; I, intercalated nuclei of the amygdala; IM, intercalated amygdaloid nucleus, main part; La, lateral amygdaloid nucleus; LaDL, lateral amygdaloid nucleus, dorsolateral part; rf, rhinal fissure; VCl, ventral part of claustrum; VEn, ventral endopiriformclaustrum.

At first, we performed voltage-clamp experiments at -70 mV, close to the resting potential of neurons and the reversal potential of chloride (E_{Cl} = -71.8 mV), with an intracellular solution containing cesium rather than potassium. To first evaluate the effect of the maximal light intensity, we recorded the oEPSC amplitude as the light intensity increased. We found that similarly to the principal neurons, the amplitude of the oEPSC increased without reaching a clear saturation (Fig. 3.11.A-B). This suggests that the VIP^Cre+ neurons are targeted by many fibers and maximal light intensity does not stimulate all pInsCx axons.
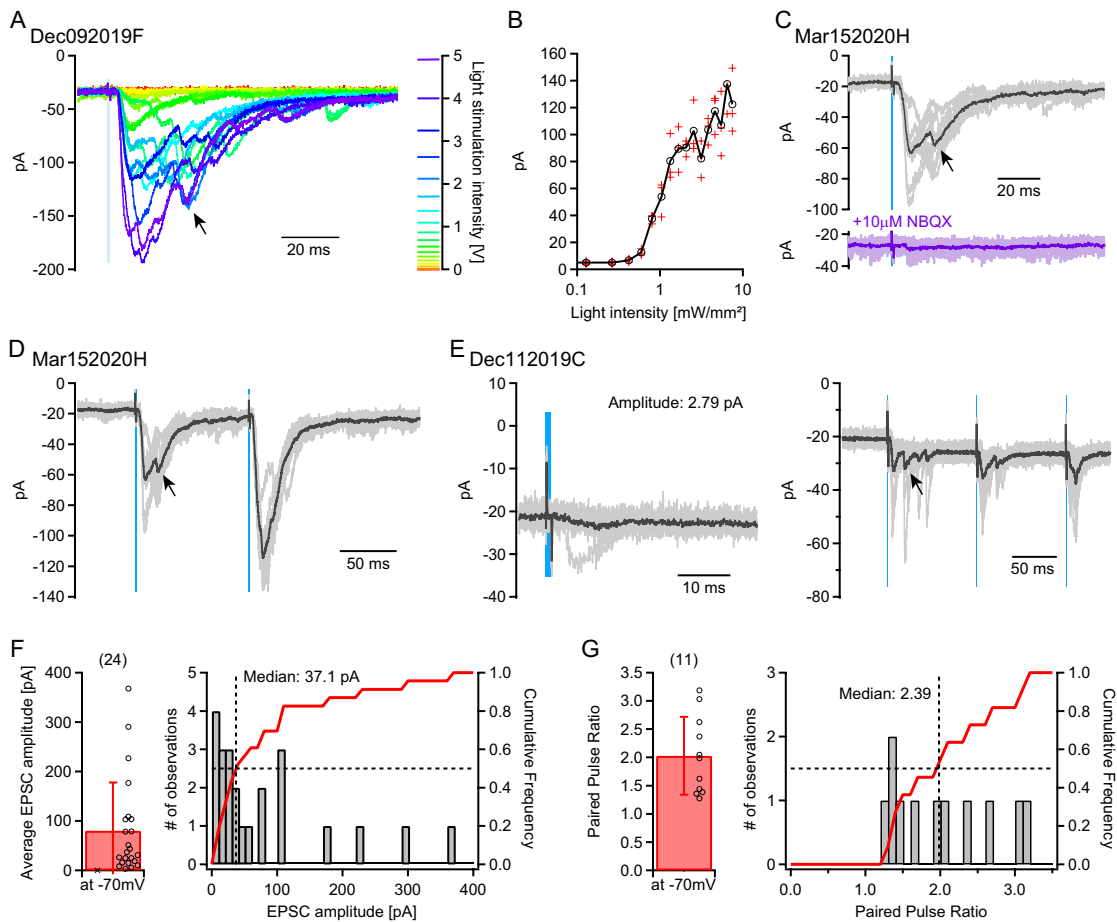
Figure 3.11 – LA VIP^{Cre}+ INs receive excitatory inputs following pInsCx afferents optogenetic stimulation. **(A)** Traces of an LA VIP^{Cre}+ IN response to different intensities (scale bar on the right) of 1 ms light pulse. **(B)** Input-output curve for the same experiment as in (A). **(C)** oEPSC of an LA VIP^{Cre}+ IN in response to a 1 ms pulse at maximal light intensity before (grey) and after (purple) bath application of NBQX. **(D)** oEPSCs of the same neuron as in (C) in response to a pair (100 ms delay) of light stimulations at maximal intensity. **(E)** Small oEPSC of an LA VIP^{Cre}+ IN in response to a 1 ms light pulse (left pannel) and increased response (right pannel) when afferents are stimulated at a higher frequency (10 Hz). **(F)** Average and individual amplitudes of oEPSC in response to a single light stimulation, one neuron did not receive an excitatory input (cross, n=1) and was excluded from the average calculation (n=23). *Right panel*: histogram of the amplitudes of oEPSC in response to a light stimulation, with the corresponding cumulative frequency. **(G)** Average and individual values of paired pulse ratio of recorded neurons in response to a pair of light pulses with a 100 ms delay (n=11). *Right panel*: histogram of the paired pulse ratio of recorded neurons, with the corresponding cumulative frequency.

In panels (C-E), darker traces represent the averages of the single traces. Arrows indicate slow components of the response. Mean ± standard deviation.

To verify the glutamatergic nature of this synaptic connection, we added NBQX to the bath solution during one recording. We found that the inward current was reduced by 95.1% by NBQX, which confirms that the EPSC is indeed glutamatergic (Fig. 3.11.C).

All 24 recorded cells showed a response to the light stimulation, except for 1 cell which didn't show any response. This suggests a high connectivity level of around 95.8%. Some neurons had an oEPSC with a very small amplitude (<5 pA) upon signle stimulation. In these recordings, repeated stimuli (10 pulses at 10 Hz) nevertheless evoked well-resolved EPSC (from 2.79 pA to 12.2 pA in Fig. 3.11.E). The general oEPSC amplitude in VIP^{Cre}+ INs was quite moderate, with an average 80.3 ± 97.5 pA, and most amplitudes smaller than 40 pA (n=23 recordings from N=7 mice; Fig. 3.11.F).

As for the short-term dynamics, when stimulating the pInsCx afferent fibers with a 10-Hz train or pair of light stimulation, we found that VIP^{Cre}+ INs received facilitating synaptic input from the pInsCx, with an average 2-fold increase of the EPSC response (PPR of 2 ± 0.7; n=11 recordings from N=3 mice; Fig. 3.11.D,G).

We noticed in several recordings that a slower peak appeared in response to a light stimulation (see arrows in Fig. 3.11). This prompted us to analyze more closely this secondary input which would most likely be the result of a poly-synaptic input (Fig. 3.12).

First we wanted to investigate the dynamics and amplitude of the fast and slow response for different light intensities. In the example shown in Fig. 3.12.A-C, we observed that the fast input appeared for a light intensity of around 0.8 mW/mm^2 whereas the slower input appeared for a light intensity of around 2 mW/mm^2, which suggests that the secondary input requires more light. Additionally, the total oEPSC amplitude appeared to saturate for a stronger light than the first component amplitude (50% of maximal amplitude reached at a light intensity of 1.6 mW/mm^2 compared with 1 mW/mm^2, for respectively the total and first components; Fig. 3.12.B). As for the delay to the start of oEPSC, the delay to the slow component appeared to be almost double of that of the fast component (Fig. 3.12.C), while both delays became shorter with more intense stimulation as shown before (Gjoni et al., 2018). Taken together, these observations suggest that the secondary component of the input would rather be the result of a poly-synaptic connection, given that such a feedforward connection would be dependent on the presynaptic neurons reaching the threshold, which would vary in time and robustness as the light intensity would increase.
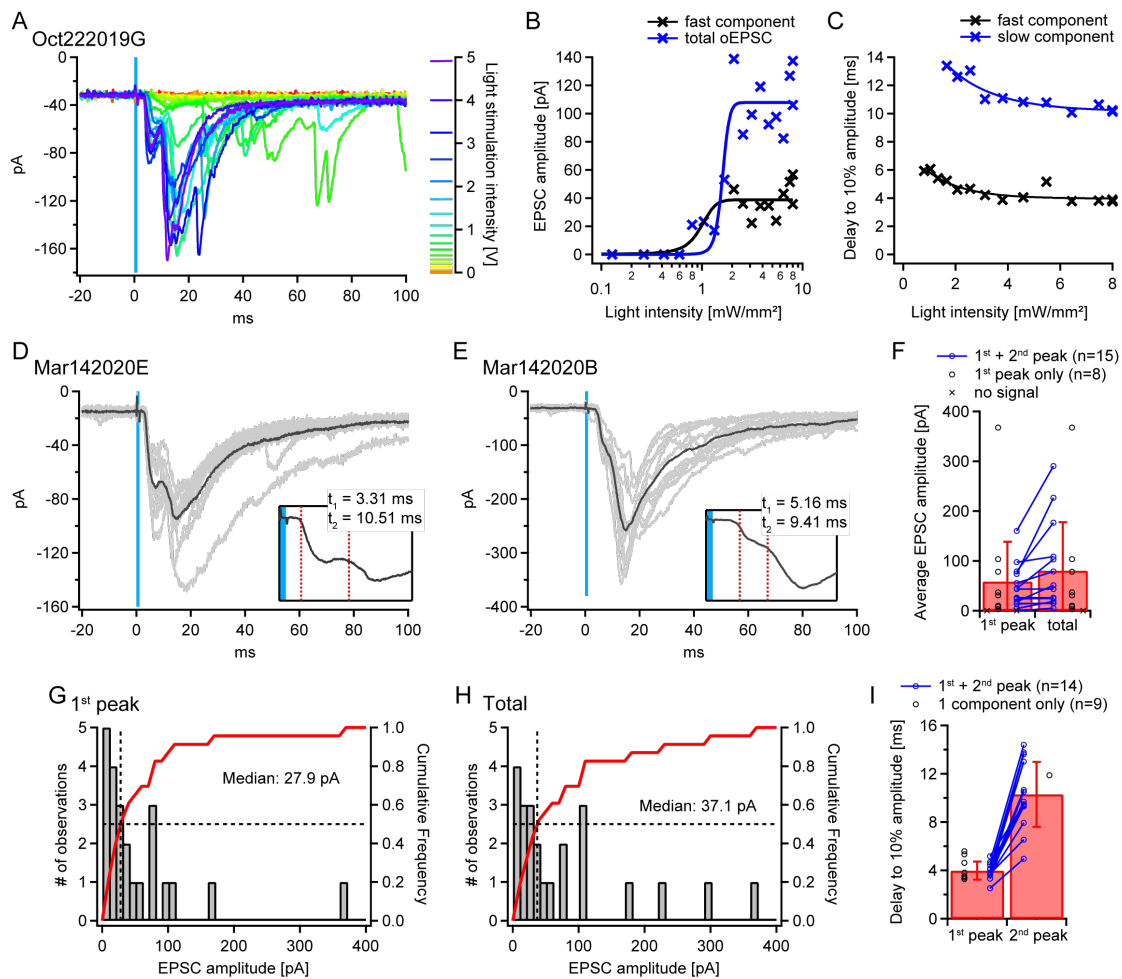
Figure 3.12 – Evoked excitatory response in LA VIP^{Cre}+ INs contains a fast and a slow component. **(A)** Traces of an LA VIP^{Cre}+ IN response to different intensities (scale bar on the right) of 1 ms light pulse. **(B)** Input-output curve for the amplitudes of the fast (black) and total (blue) evoked currents in (A). **(C)** Input-output curve for the delay to the fast (black) and slow (blue) components of the oEPSC in (A). **(D-E)** oEPSC of two VIP^{Cre}+ INs in response to a single 1 ms light pulse at maximal intensity. The inset shows an expansion of the risetime of the response and indicates the delays (red dotted line) to the fast and slow components. **(F)** Average and individual amplitudes for the fast component of oEPSC (left bar) and total oEPSC (right bar) in response to a single light stimulation (n=22). One neuron (n=1) didn't receive an excitatory input (cross) and another (n=1) had only a slow component. Some neurons had their total oEPSC amplitude equal to the amplitude of the fast component. **(G)** Histogram of the fast component of the oEPSCs in response to light stimulation shown in the left bar in (F). **(H)** Histogram of the total amplitude of the oEPSCs in response to light stimulation shown in the right bar in (F). **(I)** Average and individual values of delay to 10% amplitude of the oEPSC for the fast (left bar) and slow (right bar) components in response to a light pulse (n=23).
In panels (D-E), darker traces represent the averages of the single traces. Mean ± standard deviation.

Interestingly, in the cell showed in Fig. 3.12.A, the oEPSC amplitude appears to saturate as

the light intensity increases, compared to the example showed in Fig. 3.11.A. This could be

linked to the limited number of pInsCx afferents projecting to the neurons. This VIP^{Cre}+ IN

might have less synaptic connections with pInsCx afferents, which leads to smaller EPSC amplitudes which saturates before maximal intensity. However, if a neuron has a lot of synaptic connections from pInsCx afferents, there is a higher chance of these fibers not being activated at the same level of light intensity. Indeed, the cell in Fig. 3.12.A has a smaller amplitude than the one shown in Fig. 3.11.A.

Of the cells which received an excitatory input from the pInsCx (n=23), 65.2% had a slow component to the oEPSC (n=15). We show here 2 examples of VIP^{Cre}+ INs, in Fig. 3.12.D-E, which had different dynamics of a secondary component. In 11 of these 15 VIP^{Cre}+ INs, the total amplitude of the oEPSC was increased by the slow component with a stimulation at maximal light intensity (n=11 recordings from N=6 mice; blue in Fig. 3.12.F). More precisely, the fast component of the oEPSC alone had an amplitude of 58.6 ± 79.8 pA (n=22 recordings from N=6 mice), which is lower than the total amplitude of 80.3 ± 97.5 pA (n=23 recordings from N=6 mice). Note that in one case, a VIP^{Cre}+ IN didn't show a fast response but only a slow response (traces not shown), which explains the difference in the number of cells reported.

In terms of delays to the response, the slow component appeared at around 10.3 ± 2.7 ms compared to around 4 ± 0.7 ms for the fast component (n=23 recordings from N=6 mice; Fig. 3.12.I). The large delay of the slow response is consistent with the hypothesis of this secondary signal resulting from a poly-synaptic connection. Such a response could result from local activity of the principal neurons, which are activated by the light stimulation (Fig. 3.7).

Would the excitatory input resulting from pInsCx fiber stimulation be enough to trigger AP-firing in VIP cells? To answer this question, we performed current and voltage clamp recordings with VIP^{Cre}+ INs' membrane potential set at around -70 mV and using an intracellular solution containing potassium, while applying 10-Hz trains of light stimulation (Fig. 3.13). Of the 4 recordings we did, 2 neurons didn't spike in response to light stimulation (Fig. 3.13.A), 1 neuron had only a few inconsistent APs triggered, and another neuron had an AP triggered for each light stimulation (Fig. 3.13.B). These recordings would suggest that an oEPSC amplitude should be larger than 33 pA to activate a VIP^{Cre}+ IN, but this experiment

should be repeated to confirm this observation, ideally with dose-response measurements as were done in Fig. 3.7.B for VGluT2^{Cre}+ neurons.

When the VIP^{Cre}+ IN spiked in response to the first light stimulation of the train, we looked at the timing of the AP peak and we found that the average time was 12.6 ± 1.2 ms which shows that, at least in this neuron, the AP occured with a large delay, but also that the timing of the AP had a lot of jitter (Fig. 3.13.B). However, more recordings should be done to verify if this was not specific to this neuron.
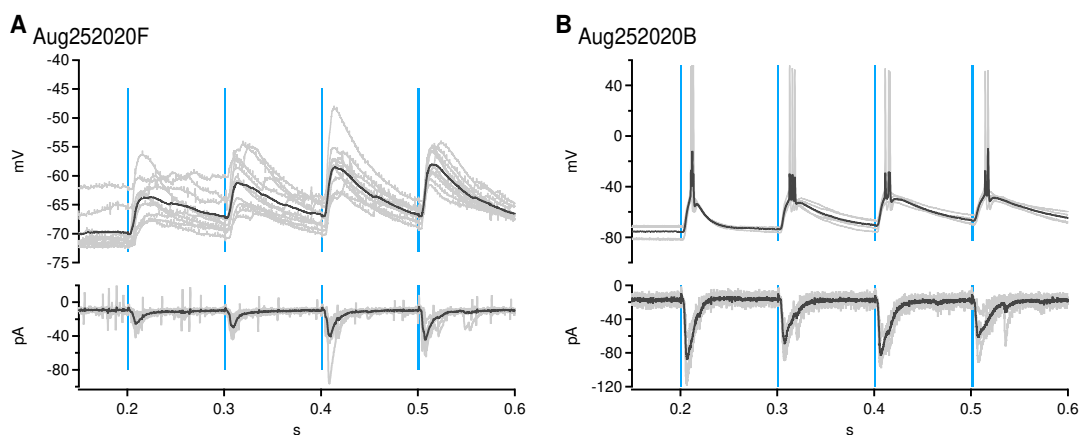
Figure 3.13 – Evoked postsynaptic potentials in LA VIP^{Cre}+ INs in response to pInsCx afferents light stimulation. **(A)** Example of an LA VIP^{Cre}+ IN which did not have APs elicited following a 10 Hz train of light stimulation. **(B)** Example of an LA VIP^{Cre}+ IN which had APs elicited by a 10 Hz train of light stimulation.

We then wanted to investigate whether VIP^{Cre}+ INs also received a feedforward inhibitory input from a pInsCx stimulation. In order to observe a purely inhibitory signal, we set the membrane potential to +15 mV, which is close to the reversal potential of EPSCs, and used an intracellular solution with cesium. When depolarized, we found that there was an outward current in VIP^{Cre}+ INs in response to optogenetic stimulation of pInsCx afferents. This current was blocked when Gabazine was added to the recording solution, hence proving that this signal is in fact a GABAergic inhibition (Fig. 3.14.A).
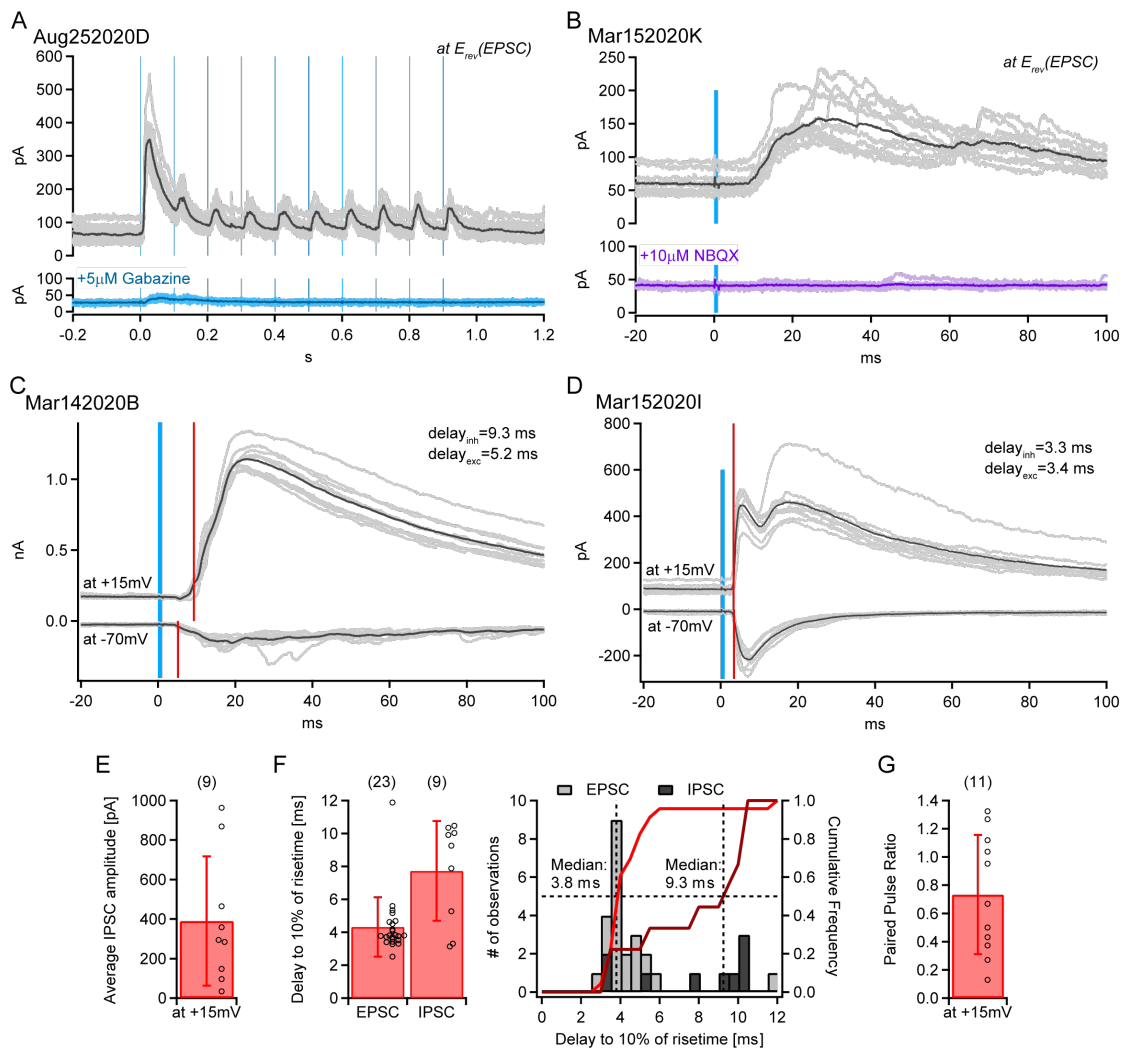
Figure 3.14 – Feedforward inhibiton input onto LA VIP^{Cre}+ INs following pInsCx stimulation. **(A)** oIPSCs of an LA VIP^{Cre}+ IN in response to a 10 Hz train of light stimulations before (grey) and after (cyan) bath application of Gabazine. **(B)** oIPSC of an LA VIP^{Cre}+ IN in response to a 1 ms light stimulation before (grey) and after (purple) bath application of NBQX. **(C-D)** oIPSC and oEPSC of two LA VIP^{Cre}+ INs in response to a 1 ms light stimulation. Red lines indicate the time at which 10% of the PSC amplitude is reached. In these examples, the inhibition is delayed in comparison with the excitation in (C) whereas both excitation and inhibition have the same delay in (D). **(E)** Average and individual data points of the oIPSC amplitudes (n=9). **(G)** Average and individual data points of the delay between the light pulse and the 10% amplitude of the oEPSC (n=23; left bar) and oIPSC (n=9; right bar) in response to light stimulation. *Right panel*: histograms of both the delays to oEPSC (light grey) and oIPSC (dark grey) and their associated cumulative frequencies. **(H)** Average and individual data points of the paired pulse ratio of recorded neurons in response to a pair of light pulses with 100 ms delay (n=11).

In panels (A-D), darker traces represent the averages of the single traces. (A-E) inhibitory responses were recorded in voltage-clamp at the reversal potential of EPSC. Mean ± standard deviation.

Additionally, in one experiment in which the oIPSC was delayed (10.5 ms), adding NBQX to the recording solution reduced the oIPSC by 97.8%, suggesting that the delayed inhibition is the result of feedforward inhibition (Fig. 3.14.B). This was confirmed in another recording with a reduction of 93.1%. Indeed, the NBQX blockage proves that this evoked response relies on a glutamatergic transmission, which is evidence to a disynaptic connection such as feedforward inhibition.

Most of the cells appeared to have a delayed inhibition compared to the excitatory response (n=7 recordings from N=3 mice; Fig. 3.14.C and F). In a few cells (n=2 recordings from N=2 mice), the oIPSC appeared to have a similar delay than the oEPSC as shown in Fig. 3.14.D (n=2 with a delay around 3.2 ms). For these 2 VIP^{Cre}+ INs, it could be possible that the neurons actually received a direct synaptic inhibition from pInsCx fibers, but no NBQX had been added during these experiments to verify the mono-synaptic nature of these connections. In the example in Fig. 3.14.D, despite the fast component of the oIPSC, a slower component could be observed, suggesting this neuron received mono- and poly-synaptic inhibitory inputs from pInsCx fiber stimulation.

On average, the oIPSC amplitude was 390.3 ± 327 pA, which was smaller than the oIPSC amplitude observed in principal neurons (n=9 recordings from N=3 mice; Fig. 3.14.E). As for the time of the start of the PSC after the light stimulation, we found that the delay was 7.7 ± 3 ms for the oIPSC compared to 4.3 ± 1.8 ms for the oEPSC, including the neuron which only received the slow response as mentioned earlier (n=9 recordings from N=3 mice; Fig. 3.14.F).

Regarding the short term dynamics, we found the the inhibitory input onto VIP^{Cre}+ INs resulting from pInsCx stimulation was depressing, with a 0.7-fold decrease of the oIPSC amplitude for a second light pulse a 100 ms after a light pulse (PPR of 0.7 ± 0.4; n=11 recordings from N=4 mice; Fig. 3.12.G).

We found that the VIP^{Cre}+ INs receive an excitatory input with a fast and a slow component, the latter being of poly-synaptic nature. We also found that the VIP^{Cre}+ INs receive a strong feedforward inhibitory input.

## 3.6   pInsCx inputs to SOM interneurons located in the LA

So far we have seen that principal neurons and VIP$^{\text{Cre}}$+ INs receive excitatory synapses from pInsCx afferent fibers. Additionally, most VIP$^{\text{Cre}}$+ INs also receive a poly-synaptic excitation from the pInsCx stimulation. We have also seen that both VGluT2$^{\text{Cre}}$+ neurons and VIP$^{\text{Cre}}$+ INs receive feedforward inhibition in response to the pInsCx stimulation. One candidate cell type which could be responsible for this local inhibitory signal is the SOM interneuron (SOM-IN) population, hence we wished to investigate the connectivity between the pInsCx and SOM$^{\text{Cre}}$+ INs.

In terms of their distribution, SOM$^{\text{Cre}}$+ INs were fewer than VIP$^{\text{Cre}}$+ INs (Fig. 3.15). Although they appeared to be distributed through the antero-posterior axis, the SOM$^{\text{Cre}}$+ INs were grouped into small clusters rather than evenly spread in the LA. Interestingly, we observed a high fluorescence in the central amygdala nuclei, as we did for the VIP$^{\text{Cre}}$+ INs (see CeL in Fig. 3.15). Although in the case of VIP$^{\text{Cre}}$+ INs this fluorescence was only due to a high density of projections, for the SOM$^{\text{Cre}}$+ INs, the lateral CEA is known to contain a lot of these cell-types (Li et al., 2013).

To measure pInsCx inputs onto SOM$^{\text{Cre}}$+ INs, we injected an AAV vector driving the expression of the opsin Chronos (AAV8:hsyn:Chronos-GFP) in the pInsCx, and we injected an AAV vector driving the Cre-dependent expression of tdTomato (AAV8:CAG:DIO:tdTomato) in the LA to visualize the SOM$^{\text{Cre}}$+ INs as fluorescent cells (Fig. 3.16.A). In some experiments (2 mice out of a total of 4 mice), we used SOM$^{\text{Cre}}$ x R26_LSL_tdTomato mice to visualize SOM$^{\text{Cre}}$+ INs and only injected the AAV driving the expression of Chronos into the pInsCx. An example of an injected brain is shown in Fig. 3.16.B for both hemispheres.

After 4 weeks or more following the injections, we performed voltage-clamp recordings of fluorescent cells while clamping their membrane potential to -70 mV, which is close to the reversal potential of chloride (E_{Cl} = -71.8 mV) and would allow to isolate excitatory inputs onto SOM$^{\text{Cre}}$+ INs. We recorded these neurons while using an intracellular solution containing cesium (see Methods 2.3.2).

SOM^{Cre} x R26_LSL_tdTomato
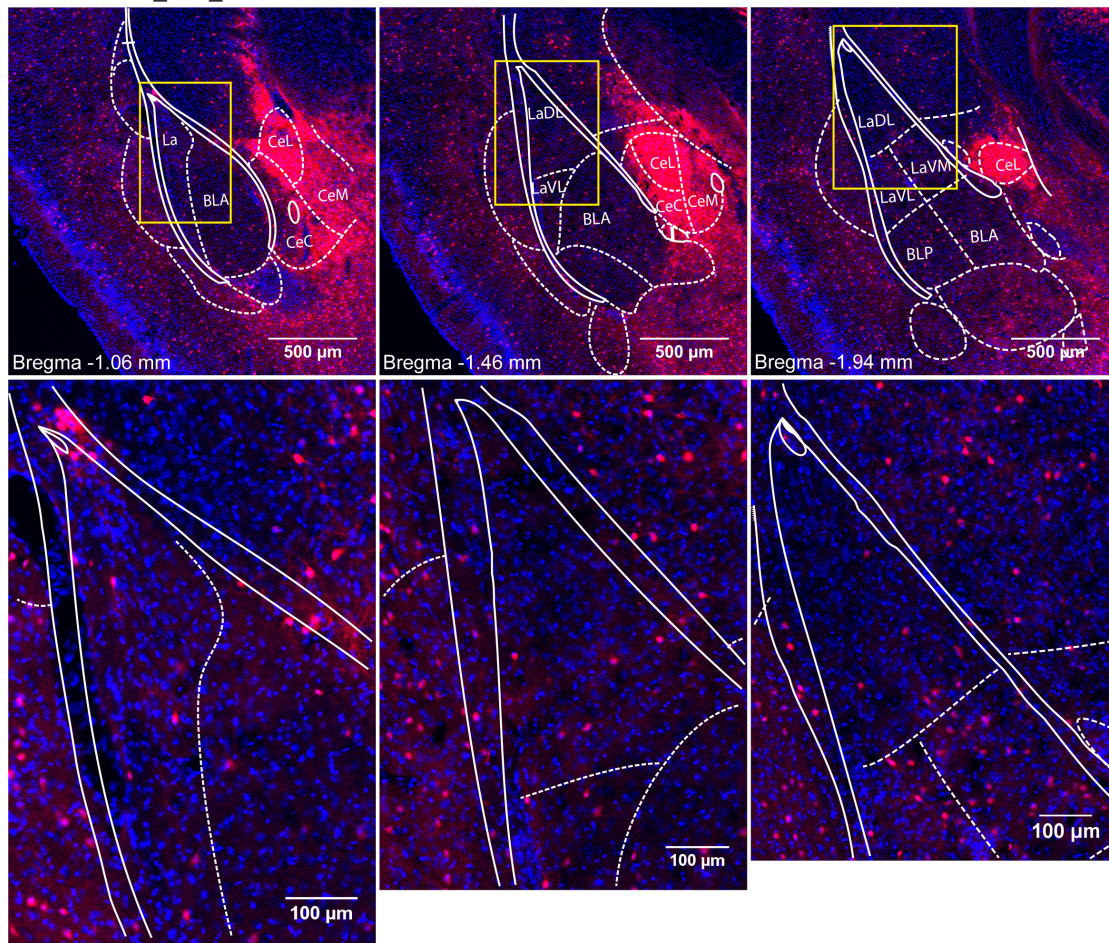
Figure 3.15 – Distribution of SOM^{Cre}+ INs in the LA. Images of thin slices from a SOM^{Cre} x R26_LSL_tdTomato mouse shown rostral to caudal (left to right). Bottom panels are an expansion of the yellow boxes in the top panels to focus on the LA regions for better clarity. Overlays are from Paxinos and Franklin, 2012.

BLA, basolateral amygdaloid nucleus, anterior part; BLP, basolateral amygdaloid nucleus, posterior part; CeC, central amygdaloid nucleus, capsular part; CeL, central amygdaloid nucleus, lateral division; CeM, central amygdaloid nucleus, medial division; LaDL, lateral amygdaloid nucleus, dorsolateral part; LaVL, lateral amygdaloid nucleus, ventrolateral part; LaVM, lateral amygdaloid nucleus, ventromedial part.

When stimulating the pInsCx afferents with an increasing light intensity, we noticed that the SOM^{Cre}+ INs response was less stable than for VGluT2^{Cre}+ neurons and VIP^{Cre}+ INs. Some of the variations were due to the spontaneous activity. Similarly to the VIP^{Cre}+ INs, we noticed that SOM^{Cre}+ INs also received a fast and slow component, but with increasing light intensities, as the slow component appeared, it also seemed to be quite unstable (Fig. 3.17.A-B). In the cortex, SOM-INs are often associated to low-threshold neurons with facilitatory
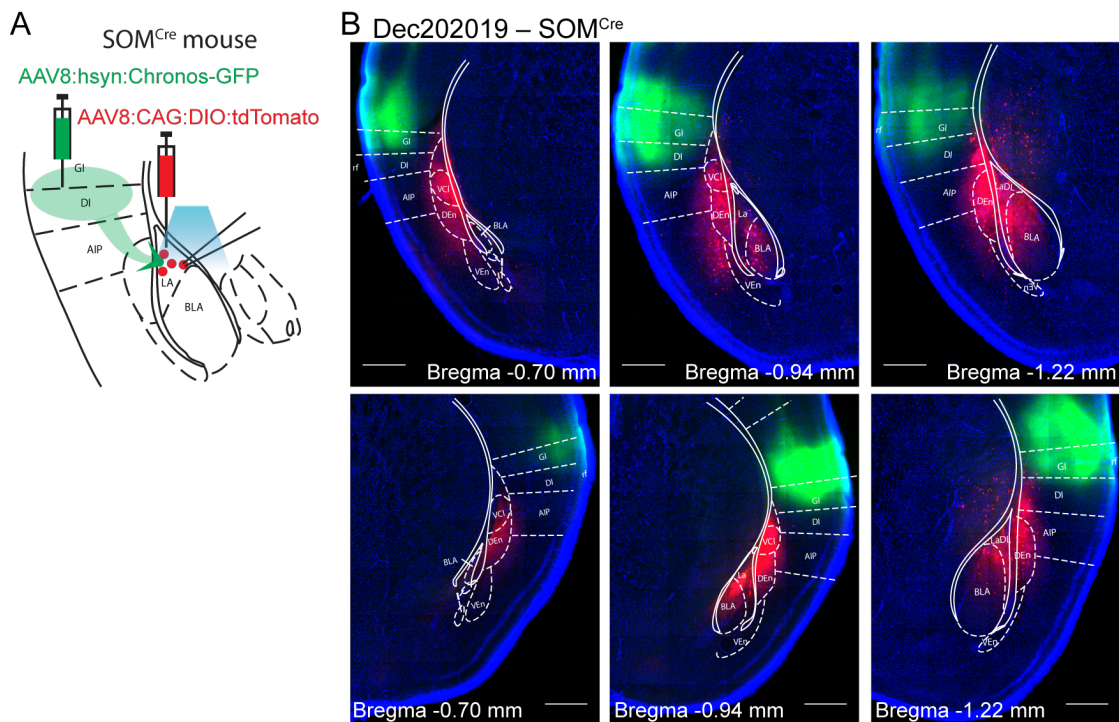
Figure 3.16 – Example of an injection in a SOM^{Cre} mouse. **(A)** Scheme of the experimental design, injections were done in SOM^{Cre} mice to record long-range inputs from the pInsCx to LA VIP^{Cre}+ INs by applying blue light locally. **(B)** Widefield images of thick slices, from a single SOM^{Cre} mouse previously injected as shown in (A), which were used for a patch-clamp experiment. Images are shown caudal to rostral (from left to right) for both hemispheres (top panels are for the left hemisphere and bottom panels are for the right hemisphere). Bregma coordinates are the ones associated with the overlays from the atlas by Paxinos and Franklin, 2012.

AIP, agranular insular cortex, posterior part; BLA, basolateral amygdaloid nucleus, anterior part; DEn, dorsal endopiriform claustrum; DI, dysgranular insular cortex; GI, granular insular cortex; I, intercalated nuclei of the amygdala; La, lateral amygdaloid nucleus; LaDL, lateral amygdaloid nucleus, dorsolateral part; rf, rhinal fissure; VCl, ventral part of claustrum; VEn, ventral endopiriform-claustrum.

properties and many failures for first PSCs (Wang et al., 2004). SOM^{Cre}+ INs located in the LA might share some of these properties.

All the SOM^{Cre}+ INs we recorded from at -70 mV (n=12) responded to light stimulation of the pInsCx afferents with an inward current. During one recording, we applied NBQX to the bath which resulted in 96.1% reduction of the input. This suggests that the inward current is a glutamatergic EPSC (Fig. 3.17.C).

We observed that the excitatory input onto SOM^{Cre}+ INs was facilitatory, as shown in Fig. 3.17.D-G. Interestingly, in the two neurons shown in these figures, the facilitation ap-
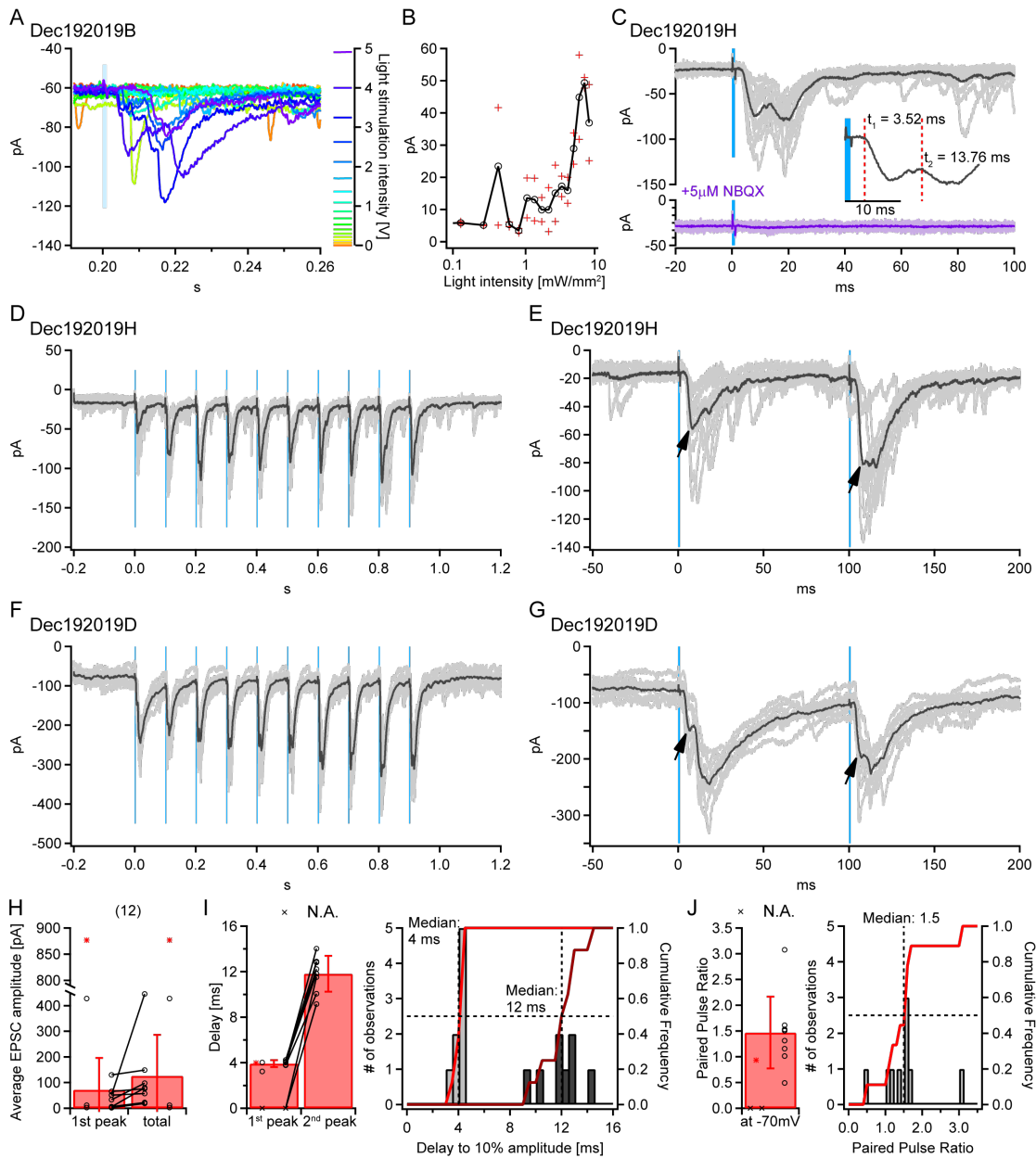
Figure 3.17 – pInsCx stimulation evokes an excitation in SOM^{Cre}+ INs composed of a fast and slow component. **(A)** Traces of an LA SOM^{Cre}+ IN response to different intensities (scale bar on the right) of 1 ms light pulse. **(B)** Input-output curve for the same experiment as in (A). **(C)** oEPSC of an LA SOM^{Cre}+ IN in response to a 1 ms pulse at maximal light intensity before (grey) and after (purple) bath application of NBQX. **(D)** oEPSCs of an LA SOM^{Cre}+ IN in response to a 10-Hz train of light stimulations at maximal intensity. **(E)** Expansion of the first two pulses of the train shown in (D). **(F)** Same as (D) but in a different neuron. **(G)** Expansion of the first two pulses of the train shown in (F). **(H)** Average and individual amplitudes of oEPSC in response to a single light stimulation for the fast component only (n=12; left bar) or the total amplitude (n=12; right bar). **(I)** Average and individual delays to 10% of oEPSC in response to a single light stimulation (n=8). In n=3 neurons the fast component was too small to extract a delay (crosses). The excluded data is plotted as the red star. *Right panel*: histogram of the amplitudes of oEPSC in response to a light stimulation, with the

peared to affect both the fast and slow components of the oEPSC (Fig. 3.17.D-E) or mainly the fast component of the oEPSC (Fig. 3.17.F-G).

Most SOM^{Cre}+ INs we recorded from (72.7%, with n=8 for a total of n=11) received a fast and slow component to the oEPSC in response to a 1 ms light pulse (n=12 recordings from N=4 mice; Fig. 3.17.H). For all these neurons, the slow component increased the total response amplitude of the signal. The amplitude of the fast oEPSC was 71.6 ± 124.2 pA whereas the total oEPSC (including the slow component) had an average amplitude of 126.1 ± 159.4 pA (n=11 recordings from N=4 mice; Fig. 3.17.H). Note that a cell was excluded from the averages given that it seemed to be an outlier, with a very large oEPSC amplitude (876.8 pA) and a response to train stimulation which was different from the other cells (red star in Fig. 3.17.H-J).

We also compared the delays to the start of the oEPSC for both the fast and the slow components (see example in small inset in Fig. 3.17.C) and found that the average delays were respectively 3.9 ± 0.3 ms (n=8 recordings from N=4 mice) and 11.8 ± 1.6 ms (n=8 recordings from N=4 mice). Note that some of the oEPSC amplitudes were too small to be able to extract the delay to the start of the signal (x marker on Fig. 3.17.I) and were excluded from the average measurement along the outlier (red star).

To analyze the short time dynamics, we compared the oEPSC amplitudes of the first and second stimulations in a 10 Hz train of light stimulation, only taking into account the fast component (see arrows in Fig. 3.17.D-G). We found that on average, most SOM^{Cre}+ INs received a facilitating input from the pInsCx with the second oEPSC 1.4-fold larger on average than the first oEPSC (PPR of 1.4 ± 0.7; n=9 recordings from N=4 mice; Fig. 3.17.J).

Similarly to the other cell types, we wished to know whether the excitatory input from the

Figure 3.17 – continued. corresponding cumulative frequency. **(J)** Average and individual values of paired pulse ratio of recorded neurons in response to a pair of light pulses with a 100 ms delay (n=11). *Right panel*: histogram of the paired pulse ratio of recorded neurons, with the corresponding cumulative frequency.
In panels (C-G), darker traces represent the averages of the single traces. Arrows indicate slow components of the response. Mean ± standard deviation.
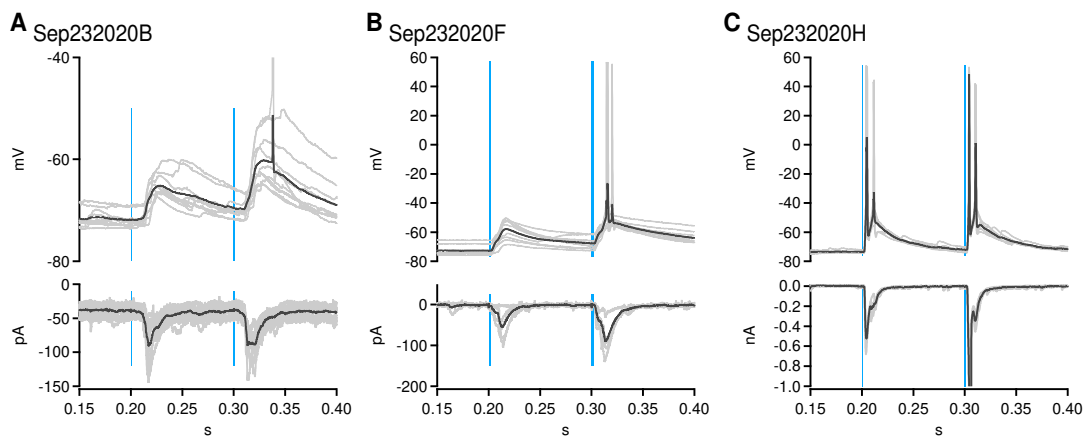
Figure 3.18 – pInsCx input onto SOM^{Cre}+ INs can evoke AP firing. Three examples of SOM^{Cre}+ INs recorded in current clamp. **(A)** This neuron seem to receive a delay input which crossed the AP threshold during one sweep only. **(B)** This neuron had a bigger oEPSC on the second stimulation, which induced an AP when recording in current-clamp. **(C)** This neuron had a strong oEPSC which induced a burst rather than a single AP in response to light stimulation in current-clamp.

pInsCx can drive AP firing in the LA SOM^{Cre}+ INs. Hence we did current and voltage-clamp recordings of SOM^{Cre}+ INs while stimulating the pInsCx fibers and using an intracellular solution containing potassium (Fig. 3.18). We successfully recorded from four different SOM-INs and found that 1 neuron didn't have any AP triggered, 1 neuron only had 1 elicited AP during 1 sweep (Fig. 3.18.A), 1 neuron had APs triggered but not for the first stimulation of the train (Fig. 3.18.B) and finally another neuron had 2 APs triggered by each light stimulation with each pair of AP seeming to correspond to the fast and slow component of the EPSCs (Fig. 3.18.C).

It seemed from these few recordings that the total amplitude of the EPSC should be larger than around 100 pA in order to elicit an AP in the SOM^{Cre}+ INs, however the median of the oEPSC amplitude is closer to 33 pA when considering only the fast component and 77 pA when considering the total amplitude of oEPSC. These values are below the apparent "threshold" we can deduce from these few experiments. This experiment should however be repeated for a more accurate interpretation of these results, with preferably a dose-response as we previously did for VGluT2^{Cre}+ neurons in Fig. 3.7.B. As for the delay to the peak of the AP following the first light stimulation of the train, the average time was 4.6 ± 0.4 ms for the neuron shown in Fig. 3.18.C, but the oEPSC was also quite large (526 pA) compared to the average oEPSC found in previous recording done with cesium-chloride intracellular solution

(Fig. 3.17.H). More experiments are necessary to check whether the delay to AP is indeed short in general for SOM[Cre]+ INs.
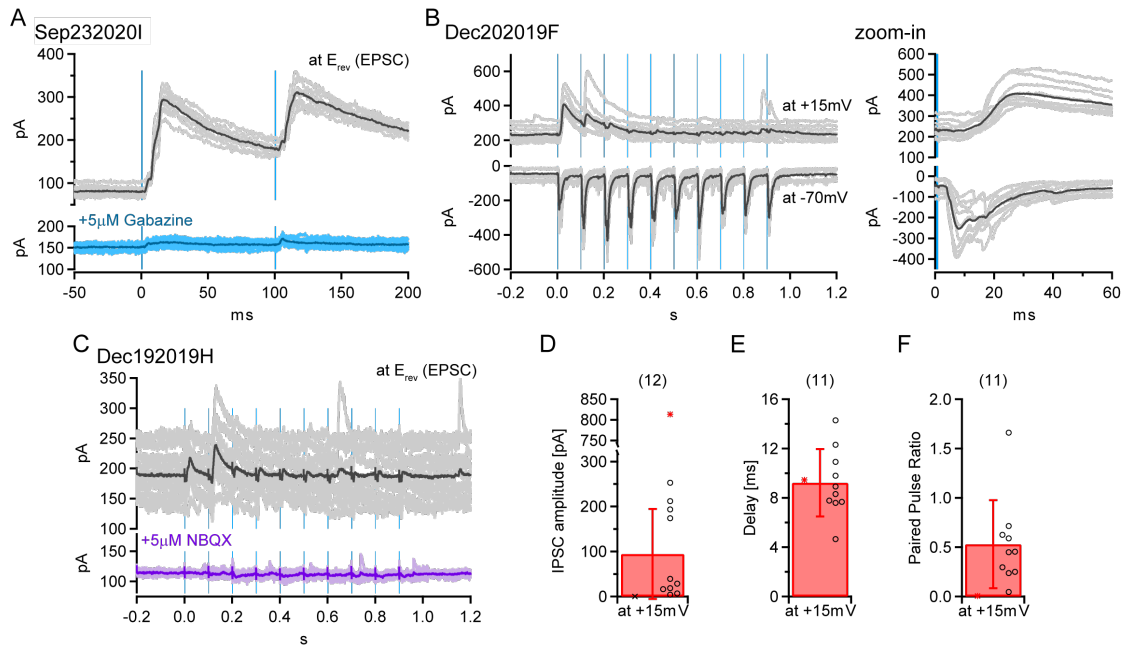
Figure 3.19 – pInsCx stimulation evokes a feedforward inhibitory input in SOM[Cre]+ INs. **(A)** oIP-SCs of an LA SOM[Cre]+ IN in response to a pair of 1 ms light pulses before (grey) and after (cyan) bath application of Gabazine. **(B)** oEPSCs and oIPSCs of an LA SOM[Cre]+ IN in response to a 10-Hz train of 1 ms light pulses. An expansion of the first stimulation is shown on the right panel to better show the delays of the PSCs. **(C)** oEPSCs and oIPSCs of an LA SOM[Cre]+ IN in response to a 10-Hz train of 1 ms light pulses before (grey) and after (purple) bath application of NBQX. **(D)** Average and individual data points of the oIPSC amplitudes (n=10). One neuron did not receive an oIPSC (cross), and another was considered an outlier (red star). **(E)** Average and individual data points of the delay between the light pulse and the 10% of the amplitude of the oIPSC in response to light stimulation (n=10). The outlier neuron (red star) was not included in the average. **(F)** Average and individual data points of the paired pulse ratio of recorded neurons in response to a pair of light pulses with 100 ms delay (n=10). The outlier (red star) was not included in the average.
In panels (A-C), darker traces represent the averages of the single traces. Neurons were voltage-clamped at the reversal potential of EPSC. Results reported are Mean ± standard deviation.

According to previous studies, we would expect SOM[Cre]+ INs to be inhibited during the aversive stimulus, in order for the dendrites of principal neurons to be disinhibited (Wolff et al., 2014; Krabbe et al., 2019). Hence, we wanted to verify whether slice recordings might reproduce this effect with a putative noxious stimulus from pInsCx.

To investigate inhibitory input onto SOM[Cre]+ INs, we voltage-clamped the neurons to +15 mV, close to the reversal potential of the EPSC, and used cesium intracellular solution. We found that following light stimulation of pInsCx afferents, an outward current appeared,

which was reduced by 94.4%, confirming that the signal was in fact GABAergic inhibition (Fig. 3.19.A).

When comparing the delays of the oEPSC and oIPSC, we could see that the inhibition appeared to be delayed compared to the excitation, which would suggest that similarly to VGluT2^{Cre}+ neurons and VIP^{Cre}+ INs, the inhibitory signal is a feedforward inhibitory signal (Fig. 3.19.B). This was supported by the fact the oIPSC was reduced by 93.8% supports the idea that the inhibitory input was dependent on a glutamatergic synaptic transmission (Fig. 3.19.C).

On 12 recorded cells, there was only 1 cell which did not receive any inhibition (91.6% of the neurons showed an oIPSC). On average, the oIPSC amplitude was 94.5 ± 100.1 pA (n=10; Fig. 3.19.D), however the SOM^{Cre}+ INs appeared to be divided into two groups which received small or strong inhibitory input. Note that the outlier mentioned previously was also not included in the averages reported for the inhibitory signal. After the light stimulation, we found that on average the delay to the start of oIPSC was 9.2 ± 2.7 ms which supports the idea that the oIPSC is the result of a feedforward inhibitory input (n=10; Fig. 3.19.E).

As for the short term dynamics, we found that most SOM^{Cre}+ INs received depressing inhibition as the fibers from pInsCx were stimulated with a 10-Hz train. Indeed, the second oIPSC was on average 2-fold smaller than the first oIPSC (PPR of 0.5 ± 0.4; n=10; Fig. 3.19.F).

Hence, we found that following the pInsCx afferent stimulation, the SOM^{Cre}+ INs received a moderate excitatory input, as well as a feedforward excitation and inhibition.

4 | Discussion

In this study, we have applied optogenetically-assisted circuit mapping to study which neuron types in the LA receive a direct excitatory input from the pInsCx, a cortical area with a documented role in pain processing (Rodgers et al., 2008). We found that pInsCx afferents robustly project to the three genetically identified cell types studied here, namely VGluT2^{Cre}+ neurons, VIP^{Cre}+ INs and SOM^{Cre}+ INs. The results show features expected from a "US-like" excitatory input, like a strong activation of LA principal neurons. However, other features of the pInsCx $\rightarrow$ LA connection, like a moderate excitation of SOM^{Cre}+ INs and the strong feedforward inhibition onto VIP^{Cre}+ INs, is less expected for a "US-like" input.

4.1 VGluT2-expressing neurons in the LA

As stated in the Introduction (Section 1.5), given the Allen Brain Institute images for ISH of the *Slc17a6* gene (which codes for VGluT2), we expected VGluT2 expression to be restricted to the dorsal tip of the LA, possibly corresponding to neurons which have been shown earlier to be responsive to both the CS and the US (see Fig. 1.2 and Fig. 3.1.A; Romanski et al., 1993). We were intrigued by the fact these neurons might have a specific molecular marker differentiating them from other principal neurons of the LA, which might be linked to their specific function. However, when we imaged histological sections from VGluT2^{Cre} x R26_LSL_H2B_mCherry mice (the latter is a Cre-dependent reporter line in which mCherry expression is directed to the cell's nucleus), we observed a broader mCherry expression than expected, notably with a lot of expression in the cortex, hippocampus, piriform cortex

and amygdala (Fig. 3.1.B). On the other hand, when Cre-dependent fluorescence resulted from the injection of an AAV vector in the LA of a VGluT2$^{\text{Cre}}$ mouse (see Fig. 3.5.A for the approach), the fluorescence within the BLA remained restricted to the LA (see Fig. 3.4 and Fig. 3.5.B). This is likely attributed to the properties of the viral serotype and injection spread.

The Allen Brain Institute provides a large database of ISH images. When we found an unexpected distribution of the fluorescence, we decided to look further in their database and found, in their transgenic mice characterization database, the images of ISH performed in a VGluT2$^{\text{Cre}}$ x R26_LSL_tdTomato mouse. In this animal, they performed an ISH for the expression of Cre (Fig. 4.1.A) and another ISH for the expression of tdTomato (Fig. 4.1.B). The distributions of the "VGluT2" neurons according to these two images are different, and is especially striking when comparing the cortex, hippocampus, piriform cortex and amygdala. In these structures, the distribution of the reporter gene (tdTomato) is very similar to the one of mCherry in our histology slices from VGluT2$^{\text{Cre}}$ x R26_LSL_H2B_mCherry mice (Fig. 3.1.B). On the other hand, the distribution of Cre expression is similar to the distribution of VGluT2 (*Slc17a6* ISH) from the Allen Brain Institute shown in Fig. 3.1.A.
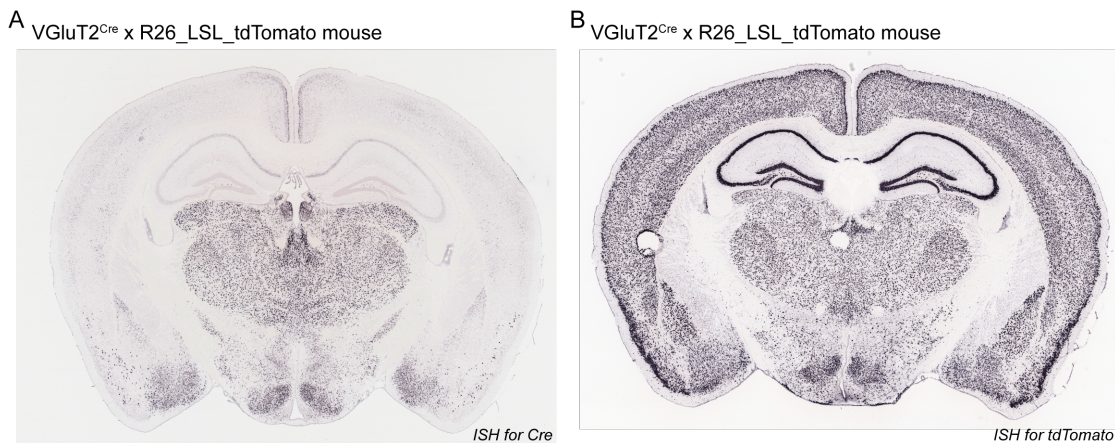
Figure 4.1 – VGluT2$^{\text{Cre}}$ x R26_LSL_tdTomato mouse characterization by the Allen Brain Institute. Publicly available images of the mouse transgenic line characterization as found on the website of the Allen Brain Institute. These images are for the characterization of the strain VGluT2$^{\text{Cre}}$ x R26_LSL_tdTomato. *In situ* hybridization (ISH) was done for Cre **(A)** and for tdTomato **(B)**.

We hypothesize that this difference might be due to the Cre/*loxP* mechanism. Indeed, the expression of Cre acts like a genetic switch that induces non-reversible recombination of the reporter gene in the Cre-dependent transgenic mouse, therefore permanently allowing

transcription of the Cre-dependent gene (Sauer, 1998). In different regions of the mouse brain, it was found that following birth, VGluT2 is transiently expressed in some neuronal populations before VGluT1 expression becomes upregulated. This was shown in the cerebellum by Miyazaki et al., 2003 and in the hippocampus by Fremeau et al., 2004a. This could also be the case in the amygdala and could explain the difference between the images from the ISH for Cre and for tdTomato (Fig. 4.1). Another possible reason for the difference might be that the *Slc17a6* gene is expressed at very low levels in some neurons, and that this expression might be sufficient to induce genome recombination, thereby inducing the expression of the fluorescent marker.

Even if this is indeed the case, it would not change our observation that the reporter gene mCherry, in the VGluT2Cre x R26_LSL_H2B_mCherry mouse strain, is co-expressed with CamKIIa. Indeed, in Fig. 3.2, only a few cells (2.1% of the counted neurons) expressed mCherry alone (mCherry being Cre-dependently expressed in a VGluT2^{Cre} mouse), which would be higher if the VGluT2 expressing neurons were a distinct population from CamKIIa neurons. The high overlap between the two populations reported in Fig. 3.2 is consistent with the view that the VGluT2 locus is active early in development in principal neurons of the LA (CamKIIa-expressing neurons).

In our experiments, although the injection of Cre-dependent tdTomato seemed to be restricted to the expected VGluT2-expressing population, we preferred remaining conservative and considered fluorescent cells to be simply excitatory, or principal neurons. This was consistent with the evidence from electrophysiological recordings (Fig. 3.3), which confirms that we could consider these neurons as principal neurons (class I neurons as in Sosulina et al., 2006).

One major difference with previous electrophysiological studies such as the work by Faber et al. (2001) was their observations of cells in the LA with a very strong accommodation resulting in a response to somatic current steps injection with only very few action potentials. In our experiments, we only reported one case of such a behaviour (see Fig. 3.3.C). The lack of similar neurons might be the result of species differences. Indeed, while we recorded from mice, Faber et al. (2001) recorded from rats.

4.2 The pInsCx makes a strong excitatory connection to LA principal neurons

One of the first questions we had when we started these experiments was whether the pInsCx provides equal inputs to various cell types in the LA. Hence we performed optogenetically-assisted circuit mapping in three different cell types: VGluT2^{Cre}+ neurons, VIP^{Cre}+ INs and SOM^{Cre}+ INs. We summarized the findings in Fig. 4.2.
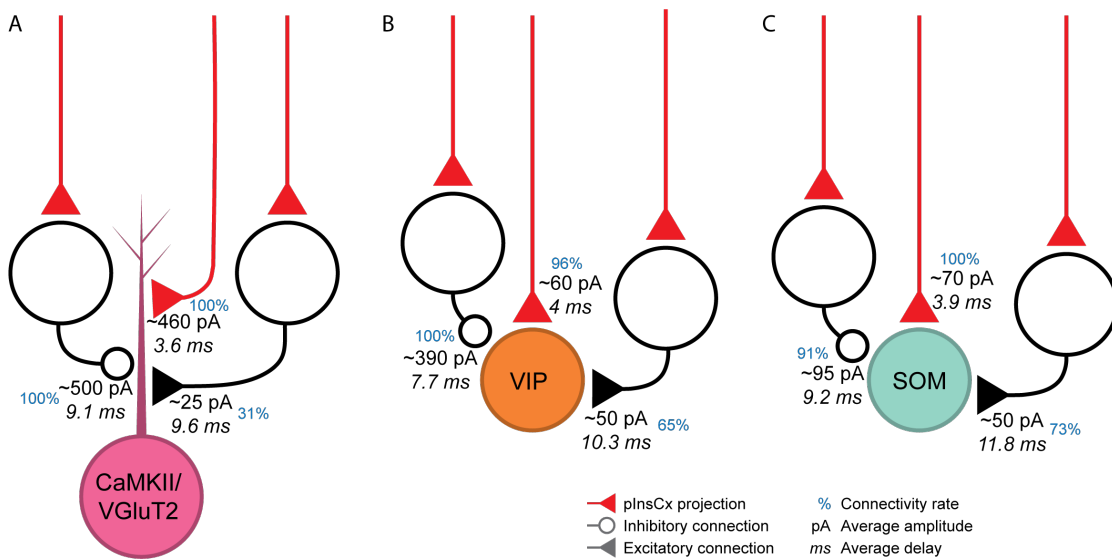
Figure 4.2 – Summary scheme of the inputs onto LA neurons following pInsCx stimulation. Summary of the postsynaptic currents and their delays evoked following the light stimulation of pInsCx afferents in **(A)** VGluT2^{Cre}+ neurons, **(B)** VIP^{Cre}+ INs and **(C)** SOM^{Cre}+ INs. Some of these inputs were concluded to be through a feedforward pathway, as represented here by open cells, given that *a priori* the cell type(s) mediating feedforward inhibition and feedforward excitation are not known (see Discussion for more details). Connectivity rates (blue text), signal amplitudes and delays were estimated from our recordings.

Using this method, we found that most of the neurons we recorded from within the LA received an excitatory input onto them when pInsCx afferents were stimulated with optogenetics. In our experiments, principal neurons received the strongest and fastest glutamatergic input from the pInsCx (Fig. 4.2.A), compared to the interneurons (Fig. 4.2.B-C); hence, we will first discuss the connection onto principal neurons.

We were first able to confirm the mono-synaptic nature of this connection given the short delay between the oEPSC and the light-stimulation (3.6 ms), and also through the use of

the drugs TTX and 4-AP (Fig. 1.3 and Fig. 3.6.D-F). This is what would be expected from a US input which should activate many neurons according to single-unit recordings during footshock done by Romanski et al. (1993) and Johansen et al. (2010a). Additionally, it is believed that for plasticity to occur, it is important that the US input activates local principal neurons (Blair et al., 2001).

In *in vivo* experiments, Johansen et al. (2010b) found that pairing an auditory stimulus with optogenetic excitation of LA principal neurons could induce fear learning in rats. Although this learning did not persist in the long-term, it showed that principal neuron excitation was sufficient to induce a transient learning. In our experiments, when we investigated whether the 1 ms light stimulation of the pInsCx afferents was sufficient to induce spiking, we found that 6 out of 8 neurons fired an evoked AP at maximal light intensity (Fig. 3.7). The optogenetical stimulation we used is quite strong and might not be representative of a natural activation of the pathway; however, we found that with increasing light intensity, the strength of the input varied continuously (Fig. 3.6.A-B), suggesting there are many independent synapses converging onto LA principal neurons (Gjoni et al., 2018). Hence, assuming that the pInsCx acts as an input for the US information, a strong activation of this region would be able to strongly depolarize the majority of LA principal neurons, with a part of the population having an AP evoked. Activation of principal neurons is a necessary condition for plasticity to occur (Quirk et al., 1997; Repa et al., 2001; LeDoux, 2000).

Given that most recorded neurons had an evoked AP in response to the pInsCx stimulation, if the principal neurons were highly interconnected in the LA, we would expect a feedforward excitatory response. However, only 10 out of 32 neurons had an oEPSC with a secondary component (Fig. 3.6.G-H), suggesting a low local connectivity between principal neurons within the LA. Additionally, the secondary input was very small compared to the pInsCx input. This is consistent with the view of an information flow through the amygdala complex as described by Pitkänen et al. (1997), in which the input enters the LA and is projected to many other subdivisions for parallel processing, while intra-divisional connections (for example within LAdl) remain sparse.

4.3 The pInsCx excitatory synapses onto VIP^{Cre}+ and SOM^{Cre}+ INs

Both SOM^{Cre}+ and VIP^{Cre}+ INs also received a glutamatergic input following pInsCx stimulation with a similarly short delay. All recorded neurons of these two populations received an input from the pInsCx, except one VIP^{Cre}+ IN (Fig. 3.11.F, Fig. 3.17.H). Although the connectivity rate is large, many of these inputs were small, with a median of 37 pA with full light intensity. In addition, the majority of these interneurons (65% of VIP^{Cre}+ INs and 72.7% of SOM^{Cre}+ INs; summarized in Fig. 4.2) received a delayed glutamatergic input which often increased the total amplitude of the oEPSC. As a result, VIP^{Cre}+ INs had a total oEPSC amplitude that was 137% the amplitude of the fast component (Fig. 3.12.F), and SOM^{Cre}+ INs had a total oEPSC amplitude that was 176% larger than the amplitude of the fast component (Fig. 3.17.H).

Given the delay of the oEPSC slow component of 10.3 ms for VIP^{Cre}+ INs and 11.8 ms for SOM^{Cre}+ INs (see Fig. 3.12.I and Fig 3.17.I), we determined that these inputs are most likely the result of a feedforward excitatory input. Principal neurons often might fire an AP following the stimulation of pInsCx axons (see above); hence, they are likely to be the source of this slow component. Indeed, when looking at the current-clamp response of the principal neurons following pInsCx afferents stimulation, we found that the average time of AP was 6.8 ms following the light pulse (Fig. 3.7). If we approximate a conduction time and synaptic delay of 4 ms, this would mean that the interneurons would receive a feedforward input at around 10.8 ms, which is close to the observed delays in both VIP^{Cre}+ INs and SOM^{Cre}+ INs (summarized in Fig. 4.2).

The oEPSC in the interneurons was smaller than in the principal neurons, however the AP threshold of the former would likely be lower than for principal neurons due to their smaller somata. In a few preliminary recordings, we found that 3 out of 4 VIP^{Cre}+ INs and 3 out of 4 SOM^{Cre}+ INs had an AP evoked by maximal light stimulation, although APs were not evoked in each trial or did not occur for the first stimulation in the train of light pulses (Fig. 3.13, Fig. 3.18). Additionally, Some of the oEPSCs recorded for these interneurons were not necessarily representative of the values observed in the populations. Hence, these

preliminary results do not allow us to conclude whether the strength of the EPSCs evoked by pInsCx inputs is sufficient to evoke AP firing in the interneurons; however, they indicate that some of them can.

In GAD67-GFP mice, the oEPSCs in LA interneurons reported by Polepalli et al. (2020) following auditory thalamic and cortical stimulations had an amplitude of, respectively, 191 pA and 167 pA, in almost 90% of recorded interneurons. These amplitudes appear to be larger than the total responses (including the slow components) to pInsCx stimulation reported in the current study (80 pA for VIP^{Cre}+ INs and 126 pA for SOM^{Cre}+ INs); however, it should be noted that the duration of the light stimulus was of 5 ms in the study by Polepalli et al., whereas it was 1 ms for our study. In the context of fear learning, there is a CS input before the US input, hence a prior activation of interneurons might affect their response upon arrival of the US input. Additional contributions from neuromodulatory systems could also be at play.

4.4 The pInsCx induces feedforward inhibition onto LA neurons

Given that many sensory inputs to the amygdala induce feedforward inhibition (Bissière et al., 2003; Wolff et al., 2014; Guthman et al., 2020), we wanted to investigate if that was also the case for the pInsCx input.

We found that all the recorded cell-types received an inhibitory input which was GABAergic and depended on glutamatergic synaptic transmission (Fig. 3.8, Fig. 3.14 and Fig. 3.19). Additionally, given the longer delays for these inhibitory responses compared with the excitatory responses evoked in these cell types by the pInsCx stimulation, we concluded that this inhibitory signal was indeed a feedforward input (summarized in Fig. 4.2).

We found feedforward inhibition in the large majority of the neurons we recorded from, at a membrane potential of +15 mV. Additionally, the feedforward inhibition was high in both the principal neurons and VIP^{Cre}+ INs, whereas it was considerably smaller in SOM^{Cre}+ INs (summarized in Fig. 4.2). This leads us to speculate that the pInsCx robustly and strongly

connects to an inhibitory neuron population which in turn inhibits these cell-types. Given the results reported in this study, we believe it is unlikely for this interneuron to be a VIP^{Cre}+ IN or a SOM^{Cre}+ IN (see Discussion 4.3). Indeed, these neurons receive a rather small excitatory input following the stimulation of pInsCx axons, which doesn't seem to induce AP-firing for small evoked EPSCs. The total oEPSC was larger when considering the slow component, but the delay to the poly-synaptic excitation appeared to be longer than the delay at which feedforward inhibition was induced (see Fig. 4.2). This would leave the possibility that this feedforward inhibitory signal might be caused by either PV-INs, or by the inhibitory neurons located in the intercalated cell cluster (ITC).

Lucas et al. (2016) showed in slice recordings that PV^{Cre}+ INs in the LA, which mediate feedforward inhibition onto principal neurons, receive strong inputs upon electrical stimulation of cortical and thalamic afferents (stimulation of the EC and IC, respectively). Although during the electrical stimulation of the EC and IC the upstream regions which are stimulated are unknown, it is possible that the pInsCx contributes to this strong input onto PV^{Cre}+ INs after EC stimulation. This would make PV^{Cre}+ INs a strong candidate for the observed feedforward inhibition in our experiments. However, this would conflict with the *in vivo* study by Wolff et al. (2014), who concluded that, during fear learning, PV-INs inhibit SOM-INs and principal neurons during the CS, while also disinhibiting the dendrites of principal neurons, whereas PV-INs are inhibited during the US. If the pInsCx is the source of nociceptive information, we would – in principle – expect PV-INs to be inhibited following pInsCx stimulation. Nevertheless, it is possible that we were limited by the *ex vivo* technique, which might not preserve the full circuitry. For example, neuromodulators might affect the activity of PV-INs following a noxious stimulus *in vivo*.

Another possibility would be that the pInsCx stimulation recruited interneurons within the ITC. We cannot exclude this possibility given that with our experimental setup, the optogenetic stimulation illuminated the slice in a radius of around 200 μm around the recorded neurons. In many studies, the GABAergic neurons in the ITC were found to induce feedforward inhibition in BLA neurons (Ehrlich et al., 2009). For example, Marowsky et al. (2005) showed that interneurons in the lateral ITC induced a feedforward inhibition onto BLA principal neurons which could be modulated by dopamine. Additionally, Bienvenu

et al. (2015) showed that large intercalated neurons were activated by noxious stimuli and projected to the BLA.

A surprising observation was also that in a few recordings, the evoked inhibition onto VIP^{Cre}+ INs had a short delay (Fig. 3.14.D), inconsistent with a feedforward nature. Although a direct inhibitory projection from the pInsCx would be unlikely, a study by Bertero et al. (2019) proved the existence of SOM long-range projection neurons from the auditory cortex to principal neurons of the LA. Some GABAergic long-range projection neurons were also found to project to other interneurons (Melzer et al., 2012). Given that the Chronos in our virus injection was not Cre-dependent, it is in principle possible that some long-range inhibitory interneurons were infected and projected to a few VIP^{Cre}+ INs. However, the study by Gehrlach et al. (2020) shows inhibitory projections from the insular cortex are highly unlikely. Hence, such an observation in our experiments could be explained by an imprecise injection, which would have infected another region of inhibitory neurons (in the ITC for example), but the 2 recordings in which we observed this were in 2 different mice, and images from the injections confirmed the correct target of the injections.

4.5 The pInsCx input onto the LA microcircuit

We found that principal neurons receive a strong and robust excitation from the pInsCx. However, the pInsCx appears to have unexpected properties as a noxious input to the LA in comparison to *in vivo* recordings of interneurons from Wolff et al. (2014) and Krabbe et al. (2019).

In vivo recordings showed that both PV-INs and SOM-INs appear to be inhibited during footshock, resulting in a disinhibition of principal neurons (Wolff et al., 2014). VIP-INs seem to be a good candidate to mediate this disinhibition as this neuron class is often reported to be involved in disinhibition in the cortex (Pi et al., 2013). Hence the US input should excite the VIP-IN population, which was indeed shown by Krabbe et al. (2019) using *in vivo* microendoscope Ca^{2+} imaging. However, we observed that following optogenetic stimulation of the pInsCx axons in the LA, VIP^{Cre}+ INs received a small excitation followed by

a large feedforward inhibition (summarized in Fig. 4.2.B). These results are not necessarily contradictory, as there might be factors which could explain this difference.

For example, during fear conditioning, prior to the US, the local interneurons might be activated by the CS, and depending on their activity, these interneurons might be in different states (inhibited, disinhibited or excited), which would modulate their response to the US. Indeed, Polepalli et al. (2020) showed that around half of the interneurons they recorded from in the LA of a GAD67-GFP mouse responded to an optogenetic stimulation of the auditory thalamus or cortex afferents. This prior activity might prime the interneurons to respond differently to a US input.

It is also possible that, *in vivo*, due to conserved neuromodulatory projections, the response of interneurons is modulated. Unfortunately, it is not possible to reproduce "natural" neuro-modulation in *in vitro* recordings, as it would be induced through different pathways. There is convincing evidence for a contribution of various neuromodulatory systems in fear learning (see Likhtik and Johansen, 2019 for a review), which makes this a possible explanation for the observed difference. For example, an *in vitro* study by Chu et al. (2012) showed that, in the BLA, dopamine suppressed GABA release specifically at inhibitory synapses between $PV^{Cre}+$ INs and principal neurons with no effect on the GABA release onto interneurons. Another study by Letzkus et al. (2011) showed that in the auditory cortex cholinergic modulation induced the activation of interneurons which inhibited PV-INs and resulted in the disinhibition of principal neurons. Acetylcholine could be a candidate neuromodulator to increase the response of LA VIP-INs to US input.

Finally, in the study by Krabbe et al. (2019), *in vivo* Ca^{2+} imaging of $VIP^{Cre}+$, $PV^{Cre}+$ and $SOM^{Cre}+$ interneurons during fear learning showed that during CS and US, different cell types within each groups can have heterogeneous responses (Supplementary Fig. 1 in Krabbe et al., 2019). This is most likely due to the fact that interneuron groups based on molecular markers are heterogeneous (see Introduction 1.5). Such a heterogeneity of cell-types within each genetically-identified interneuron class, might have contributed to some of the variability of input amplitudes, or mono- versus poly-synaptic inputs that we have observed in our experiments. Further experiments would be required to verify this.

Based on our observations, we hypothesize that the strong feedforward inhibitory input onto the VIP^{Cre}+ INs and principal neurons would be the result of PV-INs being activated by the pInsCx input. This hypothesis is supported by the study from Lucas et al. (2016). Additionally, in a very few experiments with PV^{Cre}+ INs, we found that they received a strong excitatory input from the pInsCx (ranging from 110 to 611 pA at a delay of 3.5 ± 0.4 ms in n=9 recordings); however, these recordings were not restricted to the LA but extended to the BA. Indeed, we observed that PV^{Cre}+ INs were of low density in the anterior LA; we targeted the anterior LA for our recordings, because this region receives a high density of pInsCx axons (S. Palchaudhuri, *unpublished observations*).
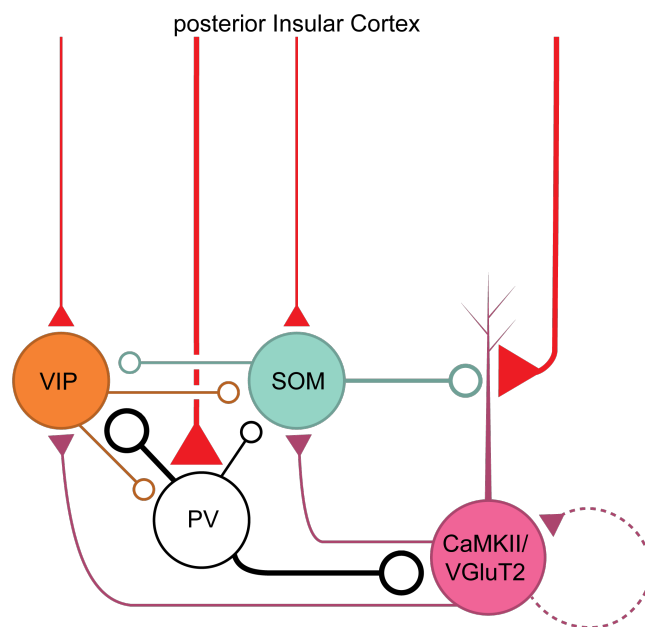
Figure 4.3 – Hypothesized local circuit response to pInsCx stimulation. This scheme represents the hypothesized local circuit response to pInsCx stimulation given the observed data. Sizes of lines indicate the strength of the signal. The dotted line represents a low probability connection. We hypothesize the large feedforward inhibition observed in both VIP^{Cre}+ INs and principal neurons is through the pInsCx activation of PV^{Cre}+ INs.

As for the slow component of the EPSCs observed in our experiments in VIP^{Cre}+ and SOM^{Cre}+ INs, they are most likely the result of a poly-synaptic input (Fig. 3.12 and Fig. 3.17). We hypothesize that this delayed input might be the result of the local activation of principal neurons following the stimulation of the pInsCx afferents. Our hypotheses are summarized in Fig. 4.3.

Although this proposed circuit seems to contradict the findings by Krabbe et al. (2019) for a role of VIP-INs in disinhibition, we believe it suggests the idea that there are additional factors which promote the activity of VIP-INs *in vivo*, which we could not control in our *in vitro* experiments. Indeed, additional regions might project to VIP-INs in the LA during a noxious stimulus and promote their activity, whether a neuromodulatory nucleus or another input region coding for US-information. Despite the high feedforward inhibitory input onto VIP^{Cre}+ INs we observed, a strong activation might allow an AP to be triggered before the inhibitory signal. There is also evidence that this inhibition could be specifically modulated by a neuromodulator, as was shown in the cortex through nicotinic activation of VIP-INs (Alitto and Dan, 2012; Fu et al., 2014).

4.6 Perspectives and future studies

There is a need to leverage new techniques to uncover the functional contributions of long-range inputs onto the neural coding of the LA, which would allow to better understand how fear learning occurs (Johansen et al., 2012). This is evidenced by two recent studies addressing the effect of long-range inputs onto different cell-types of the BLA (Guthman et al., 2020; Polepalli et al., 2020). However, there are no studies investigating the long-range inputs from a region involved in the US signal transmission. In this study, we have systematically studied the inputs from the pInsCx, a putative nociceptive input region, onto different cell-types of the LA.

One obvious element missing from this study is the investigation of the pInsCx signal onto PV^{Cre}+ INs. Performing these recordings would allow to verify our hypothesis that PV-INs receive a strong input from the pInsCx and are responsible for the feedforward inhibition observed in VIP neurons. Indeed, although we observed a low density of PV^{Cre}+ INs in the anterior LA, their role might be important in the circuit and might compensate for their low density (Lucas et al., 2016).

Other experiments which might yield further insights would be to perform the same experiments with neuromodulators (or agonists) added to the bath. This would allow to test

whether the local connectivity would be affected by neuromodulators and could explain the difference in our observations with the previous *in vivo* studies (Wolff et al., 2014; Krabbe et al., 2019).

Additional potential experiments include the injection of inhibitory opsins (such as Halorhodopsin or Archaerhodopsin) in the local circuit, and testing whether the observed inputs are modified when one of the cell-type is silenced. For example, the injection of an AAV expressing an excitatory channelrhodopsin in the pInsCx and the injection of an AAV expressing a Cre-dependent inhibitory channelrhodopsin (with a different excitation light) in the LA of a VIP^{Cre} animal would allow to measure whether the evoked feedforward inhibition is reduced when a specific interneuron type is silenced. We performed a few experiments with such a paradigm, but the choice of opsins did not allow for their independent optical stimulation.

To gain a better understanding of the specific nociceptive properties of the pInsCx input, it would be valuable to investigate the target cell specificity of a long range synaptic input for afferents originating from other regions. Such experiments could for example be done for projections from MGm/PIN, known to carry the auditory input to the LA (McDonald, 1998; LeDoux, 2000).

Slice recordings combined with optogenetically-assisted circuit mapping, such as performed in this PhD project, allow to understand how a long-range input differentially recruits different cell-types of the local microcircuit. This helps further understand how plasticity might be induced, and shines light on observed differences between *ex vivo* and *in vivo* studies.

Bibliography

Alitto, H. J. and Y. Dan (2012). "Cell-type-specific modulation of neocortical activity by basal forebrain input." In: *Frontiers in systems neuroscience* 6, p. 79. DOI: 10.3389/fnsys.2012. 00079.

Atallah, B., W. Bruns, M. Carandini, and M. Scanziani (2012). "Parvalbumin-Expressing Interneurons Linearly Transform Cortical Responses to Visual Stimuli". In: *Neuron* 73.1, pp. 159–170. DOI: 10.1016/j.neuron.2011.12.013.

Atasoy, D., Y. Aponte, H. H. Su, and S. M. Sternson (2008). "A FLEX Switch Targets Channelrhodopsin-2 to Multiple Cell Types for Imaging and Long-Range Circuit Mapping". In: *The Journal of Neuroscience* 28.28, pp. 7025–7030. DOI: 10.1523/jneurosci.1954-08.2008.

Barsy, B., K. Kocsis, A. Magyar, Babiczky, M. Szabó, J. M. Veres, D. Hillier, I. Ulbert, O. Yizhar, and F. Mátyás (2020). "Associative and plastic thalamic signaling to the lateral amygdala controls fear behavior". In: *Nature Neuroscience* 23.5, pp. 625–637. DOI: 10.1038/s41593-020-0620-z.

Bertero, A., P. L. C. Feyen, H. Zurita, and A. j. Apicella (2019). "A Non-Canonical Cortico-Amygdala Inhibitory Loop". In: *The Journal of Neuroscience* 39.43, pp. 8424–8438. DOI: 10.1523/jneurosci.1515-19.2019.

Bienvenu, T. C., D. Busti, B. R. Micklem, M. Mansouri, P. J. Magill, F. Ferraguti, and M. Capogna (2015). "Large Intercalated Neurons of Amygdala Relay Noxious Sensory Information". In: *The Journal of Neuroscience* 35.5, pp. 2044–2057. DOI: 10.1523/jneurosci.1323-14.2015.

Bissière, S., Y. Humeau, and A. Lüthi (2003). "Dopamine gates LTP induction in lateral amygdala by suppressing feedforward inhibition". In: *Nature Neuroscience* 6.6, pp. 587–92. DOI: 10.1038/nn1058.

Bibliography

Blair, H. T., G. E. Schafe, E. P. Bauer, S. M. Rodrigues, and J. E. LeDoux (2001). "Synaptic Plasticity in the Lateral Amygdala: A Cellular Hypothesis of Fear Conditioning". In: *Learning & Memory* 8.5, pp. 229–242. DOI: 10.1101/lm.30901.

Boyden, E. S., F. Zhang, E. Bamberg, G. Nagel, and K. Deisseroth (2005). "Millisecond-timescale, genetically targeted optical control of neural activity". In: *Nature Neuroscience* 8.9, pp. 1263–1268. DOI: 10.1038/nn1525.

Brooks, J., L. Zambreanu, A. Godinez, A. B. Craig, and I. Tracey (2005). "Somatotopic organisation of the human insula to painful heat studied with high resolution functional imaging". In: *NeuroImage* 27.1, pp. 201–209. DOI: 10.1016/j.neuroimage.2005.03.041.

Cho, J.-H., I. T. Bayazitov, E. G. Meloni, K. M. Myers, W. A. Carlezon, S. S. Zakharenko, and V. Y. Bolshakov (2012). "Coactivation of thalamic and cortical pathways induces input timing–dependent plasticity in amygdala". In: *Nature Neuroscience* 15.1, pp. 113–122. DOI: 10.1038/nn.2993.

Chu, H.-Y., W. Ito, J. Li, and A. Morozov (2012). "Target-Specific Suppression of GABA Release from Parvalbumin Interneurons in the Basolateral Amygdala by Dopamine". In: *The Journal of Neuroscience* 32.42, pp. 14815–14820. DOI: 10.1523/jneurosci.2997-12.2012.

Ehrlich, I., Y. Humeau, F. Grenier, S. Ciocchi, C. Herry, and A. Lüthi (2009). "Amygdala Inhibitory Circuits and the Control of Fear Memory". In: *Neuron* 62.6, pp. 757–771. DOI: 10.1016/j.neuron.2009.05.026.

Faber, E., R. J. Callister, and P. Sah (2001). "Morphological and Electrophysiological Properties of Principal Neurons in the Rat Lateral Amygdala In Vitro". In: *Journal of Neurophysiology* 85.2, pp. 714–723. DOI: 10.1152/jn.2001.85.2.714.

Fanselow, M. S. and A. M. Poulos (2005). "The Neuroscience of Mammalian Associative Learning". In: *Annual Review of Psychology* 56.1, pp. 207–234. DOI: 10.1146/annurev.psych.56.091103.070213.

Fremeau, R. T., K. Kam, T. Qureshi, J. Johnson, D. R. Copenhagen, J. Storm-Mathisen, F. A. Chaudhry, R. A. Nicoll, and R. H. Edwards (2004a). "Vesicular Glutamate Transporters 1 and 2 Target to Functionally Distinct Synaptic Release Sites". In: *Science* 304.5678, pp. 1815–1819. DOI: 10.1126/science.1097468.

Fremeau, R. T., S. Voglmaier, R. P. Seal, and R. H. Edwards (2004b). "VGLUTs define subsets of excitatory neurons and suggest novel roles for glutamate". In: *Trends in Neurosciences* 27.2, pp. 98–103. DOI: 10.1016/j.tins.2003.11.005.

Fu, Y., J. Tucciarone, J. Espinosa, N. Sheng, D. Darcy, R. Nicoll, Z. Huang, and M. Stryker (2014). "A Cortical Circuit for Gain Control by Behavioral State". In: *Cell* 156.6, pp. 1139–1152. DOI: 10.1016/j.cell.2014.01.050.

Gehrlach, D. A., T. N. Gaitanos, A. S. Klein, C. Weiand, A. A. Hennrich, K.-K. Conzelmann, and N. Gogolla (2020). "A whole-brain connectivity map of mouse insular cortex". In: *bioRxiv*, p. 2020.02.10.941518. DOI: 10.1101/2020.02.10.941518.

Gjoni, E., F. Zenke, B. Bouhours, and R. Schneggenburger (2018). "Specific synaptic input strengths determine the computational properties of excitation–inhibition integration in a sound localization circuit". In: *The Journal of Physiology* 596.20, pp. 4945–4967. DOI: 10.1113/jp276012.

Grewe, B. F., J. Gründemann, L. J. Kitch, J. A. Lecoq, J. G. Parker, J. D. Marshall, M. C. Larkin, P. E. Jercog, F. Grenier, J. Z. Li, A. Lüthi, and M. J. Schnitzer (2017). "Neural ensemble dynamics underlying a long-term associative memory". In: *Nature* 543.7647, pp. 670–675. DOI: 10.1038/nature21682.

Guthman, E. M., J. D. Garcia, M. Ma, P. Chu, S. M. Baca, K. R. Smith, D. Restrepo, and M. M. Huntsman (2020). "Cell type specific control of basolateral amygdala neuronal circuits via entorhinal cortex-driven feedforward inhibition". In: *eLife* 9, e50601. DOI: 10.7554/elife.50601.

Herry, C. and J. P. Johansen (2014). "Encoding of fear learning and memory in distributed neuronal circuits". In: *Nature Neuroscience* 17.12, pp. 1644–1654. DOI: 10.1038/nn.3869.

Huang, Y.-Y. and E. R. Kandel (1998). "Postsynaptic Induction and PKA-Dependent Expression of LTP in the Lateral Amygdala". In: *Neuron* 21.1, pp. 169–178. DOI: 10.1016/s0896-6273(00)80524-3.

Humeau, Y., C. Herry, N. Kemp, H. Shaban, E. Fourcaudot, S. Bissière, and A. Lüthi (2005). "Dendritic Spine Heterogeneity Determines Afferent-Specific Hebbian Plasticity in the Amygdala". In: *Neuron* 45.1, pp. 119–131. DOI: 10.1016/j.neuron.2004.12.019.

Janak, P. H. and K. M. Tye (2015). "From circuits to behaviour in the amygdala". In: *Nature* 517.7534, pp. 284–292. DOI: 10.1038/nature14188.

Bibliography

Johansen, J. P., H. Hamanaka, M. H. Monfils, R. Behnia, K. Deisseroth, H. T. Blair, and J. E. LeDoux (2010a). "Optical activation of lateral amygdala pyramidal cells instructs associative fear learning". In: *Proceedings of the National Academy of Sciences* 107.28, pp. 12692–12697. DOI: 10.1073/pnas.1002418107.

Johansen, J. P., J. W. Tarpley, J. E. LeDoux, and H. T. Blair (2010b). "Neural substrates for expectation-modulated fear learning in the amygdala and periaqueductal gray". In: *Nature Neuroscience* 13.8, pp. 979–986. DOI: 10.1038/nn.2594.

Johansen, J. P., S. B. Wolff, A. Lüthi, and J. E. LeDoux (2012). "Controlling the Elements: An Optogenetic Approach to Understanding the Neural Circuits of Fear". In: *Biological Psychiatry* 71.12, pp. 1053–1060. DOI: 10.1016/j.biopsych.2011.10.023.

Klapoetke, N. C., Y. Murata, S. S. Kim, S. R. Pulver, A. Birdsey-Benson, Y. K. Cho, T. K. Morimoto, A. S. Chuong, E. J. Carpenter, Z. Tian, J. Wang, Y. Xie, Z. Yan, Y. Zhang, B. Y. Chow, B. Surek, M. Melkonian, V. Jayaraman, M. Constantine-Paton, G. K.-S. Wong, and E. S. Boyden (2014). "Independent optical excitation of distinct neural populations". In: *Nature Methods* 11.3, pp. 338–346. DOI: 10.1038/nmeth.2836.

Krabbe, S., J. Gründemann, and A. Lüthi (2018). "Amygdala Inhibitory Circuits Regulate Associative Fear Conditioning". In: *Biological Psychiatry* 83.Nat Neurosci 17 2014, pp. 800–809. DOI: 10.1016/j.biopsych.2017.10.006.

Krabbe, S., E. Paradiso, S. d'Aquin, Y. Bitterman, J. Courtin, C. Xu, K. Yonehara, M. Markovic, C. Müller, T. Eichlisberger, J. Gründemann, F. Ferraguti, and A. Lüthi (2019). "Adaptive disinhibitory gating by VIP interneurons permits associative learning". In: *Nature Neuroscience* 22.11, pp. 1834–1843. DOI: 10.1038/s41593-019-0508-y.

Kuhlman, S. J. and Z. J. Huang (2008). "High-Resolution Labeling and Functional Manipulation of Specific Neuron Types in Mouse Brain by Cre-Activated Viral Gene Expression". In: *PLoS ONE* 3.4, e2005. DOI: 10.1371/journal.pone.0002005.

LeDoux, J., P Cicchetti, A Xagoraris, and L. Romanski (1990). "The lateral amygdaloid nucleus: sensory interface of the amygdala in fear conditioning". In: *Journal of Neuroscience* 10.4, pp. 1062–1069. DOI: 10.1523/jneurosci.10-04-01062.1990.

LeDoux, J., J Iwata, P Cicchetti, and D. Reis (1988). "Different projections of the central amygdaloid nucleus mediate autonomic and behavioral correlates of conditioned fear". In: *Journal of Neuroscience* 8.7, pp. 2517–2529. DOI: 10.1523/jneurosci.08-07-02517.1988.

LeDoux, J. E. (2000). "Emotion Circuits in the Brain". In: *Annual Review of Neuroscience* 23.1, pp. 155–184. DOI: 10.1146/annurev.neuro.23.1.155.

Letzkus, J. J., S. Wolff, and A. Lüthi (2015). "Disinhibition, a Circuit Mechanism for Associative Learning and Memory". In: *Neuron* 88.2, pp. 264–276. DOI: 10.1016/j.neuron.2015.09.024.

Letzkus, J. J., S. B. E. Wolff, E. M. M. Meyer, P. Tovote, J. Courtin, C. Herry, and A. Lüthi (2011). "A disinhibitory microcircuit for associative fear learning in the auditory cortex". In: *Nature* 480.7377, pp. 331–335. DOI: 10.1038/nature10674.

Li, H., M. A. Penzo, H. Taniguchi, C. D. Kopec, Z. J. Huang, and B. Li (2013). "Experience-dependent modification of a central amygdala fear circuit". In: *Nature Neuroscience* 16.3, pp. 332–339. DOI: 10.1038/nn.3322.

Likhtik, E. and J. P. Johansen (2019). "Neuromodulation in circuits of aversive emotional learning". In: *Nature Neuroscience* 22.10, pp. 1586–1597. DOI: 10.1038/s41593-019-0503-3.

Lucas, E., A. Jegarl, H. Morishita, and R. Clem (2016). "Multimodal and Site-Specific Plasticity of Amygdala Parvalbumin Interneurons after Fear Learning". In: *Neuron* 91.3, pp. 629–643. DOI: 10.1016/j.neuron.2016.06.032.

Madisen, L., T. A. Zwingman, S. M. Sunkin, S. W. Oh, H. A. Zariwala, H. Gu, L. L. Ng, R. D. Palmiter, M. J. Hawrylycz, A. R. Jones, E. S. Lein, and H. Zeng (2010). "A robust and high-throughput Cre reporting and characterization system for the whole mouse brain". In: *Nature Neuroscience* 13.1, pp. 133–140. DOI: 10.1038/nn.2467.

Mahanty, N. K. and P. Sah (1998). "Calcium-permeable AMPA receptors mediate long-term potentiation in interneurons in the amygdala". In: *Nature* 394.6694, pp. 683–687. DOI: 10.1038/29312.

Marowsky, A., Y. Yanagawa, K. Obata, and K. E. Vogt (2005). "A Specialized Subclass of Interneurons Mediates Dopaminergic Facilitation of Amygdala Function". In: *Neuron* 48.6, pp. 1025–1037. DOI: 10.1016/j.neuron.2005.10.029.

McDonald, A. J. (1992). "Cell types and intrinsic connections of the amygdala". In: *The amygdala: Neurobiological aspects of emotion, memory, and mental dysfunction*. Ed. by J. P. Aggleton. New York: Wiley-Liss, pp. 67–96.

McDonald, A. J. (1998). "Cortical pathways to the mammalian amygdala". In: *Progress in Neurobiology* 55.3, pp. 257–332. DOI: 10.1016/s0301-0082(98)00003-3.

Bibliography

Medina, J. F., J. C. Repa, M. D. Mauk, and J. E. LeDoux (2002). "Parallels between cerebellum- and amygdala-dependent conditioning". In: *Nature Reviews Neuroscience* 3.2, pp. 122–131. DOI: 10.1038/nrn728.

Melzer, S., M. Michael, A. Caputi, M. Eliava, E. C. Fuchs, M. A. Whittington, and H. Monyer (2012). "Long-Range–Projecting GABAergic Neurons Modulate Inhibition in Hippocampus and Entorhinal Cortex". In: *Science* 335.6075, pp. 1506–1510. DOI: 10.1126/science. 1217139.

Miyazaki, T., M. Fukaya, H. Shimizu, and M. Watanabe (2003). "Subtype switching of vesicular glutamate transporters at parallel fibre–Purkinje cell synapses in developing mouse cerebellum". In: *European Journal of Neuroscience* 17.12, pp. 2563–2572. DOI: 10.1046/j. 1460-9568.2003.02698.x.

Muller, J. F., F. Mascagni, and A. J. McDonald (2007). "Postsynaptic targets of somatostatin-containing interneurons in the rat basolateral amygdala". In: *Journal of Comparative Neurology* 500.3, pp. 513–529. DOI: 10.1002/cne.21185.

Muller, J. F., F. Mascagni, and A. J. Mcdonald (2003). "Synaptic connections of distinct interneuronal subpopulations in the rat basolateral amygdalar nucleus". In: *Journal of Comparative Neurology* 456.3, pp. 217–236. DOI: 10.1002/cne.10435.

Muller, J. F., F. Mascagni, and A. J. McDonald (2006). "Pyramidal cells of the rat basolateral amygdala: Synaptology and innervation by parvalbumin-immunoreactive interneurons". In: *Journal of Comparative Neurology* 494.4, pp. 635–650. DOI: 10.1002/cne.20832.

Muller, J., K. P. Corodimas, Z. Fridel, and J. E. LeDoux (1997). "Functional Inactivation of the Lateral and Basal Nuclei of the Amygdala by Muscimol Infusion Prevents Fear Conditioning to an Explicit Conditioned Stimulus and to Contextual Stimuli". In: *Behavioral Neuroscience* 111.4, pp. 683–691. DOI: 10.1037/0735-7044.111.4.683.

Nabavi, S., R. Fox, C. D. Proulx, J. Y. Lin, R. Y. Tsien, and R. Malinow (2014). "Engineering a memory with LTD and LTP." In: *Nature* 511.7509, pp. 348–52. DOI: 10.1038/nature13294.

Nagel, G., T. Szellas, W. Huhn, S. Kateriya, N. Adeishvili, P. Berthold, D. Ollig, P. Hegemann, and E. Bamberg (2003). "Channelrhodopsin-2, a directly light-gated cation-selective membrane channel". In: *Proceedings of the National Academy of Sciences* 100.24, pp. 13940–13945. DOI: 10.1073/pnas.1936192100.

Paxinos, G. and K. Franklin (2012). *Paxinos and Franklin's the Mouse Brain in Stereotaxic Coordinates*. Amsterdam: Academic Press.

Peron, S. P., J. Freeman, V. Iyer, C. Guo, and K. Svoboda (2015). "A Cellular Resolution Map of Barrel Cortex Activity during Tactile Behavior". In: *Neuron* 86.3, pp. 783 –799. DOI: https://doi.org/10.1016/j.neuron.2015.03.027.

Petreanu, L., D. Huber, A. Sobczyk, and K. Svoboda (2007). "Channelrhodopsin-2–assisted circuit mapping of long-range callosal projections". In: *Nature Neuroscience* 10.5, pp. 663–668. DOI: 10.1038/nn1891.

Petreanu, L., T. Mao, S. M. Sternson, and K. Svoboda (2009). "The subcellular organization of neocortical excitatory connections". In: *Nature* 457.7233, pp. 1142–1145. DOI: 10.1038/nature07709.

Pi, H.-J., B. Hangya, D. Kvitsiani, J. I. Sanders, Z. J. Huang, and A. Kepecs (2013). "Cortical interneurons that specialize in disinhibitory control". In: *Nature* 503.7477, pp. 521–524. DOI: 10.1038/nature12676.

Pitkänen, A., V. Savander, and J. E. LeDoux (1997). "Organization of intra-amygdaloid circuitries in the rat: an emerging framework for understanding functions of the amygdala". In: *Trends in Neurosciences* 20.11, pp. 517–523. DOI: 10.1016/s0166-2236(97)01125-9.

Polepalli, J. S., H. Gooch, and P. Sah (2020). "Diversity of interneurons in the lateral and basal amygdala". In: *npj Science of Learning* 5.1, p. 10. DOI: 10.1038/s41539-020-0071-z.

Quirk, G. J., J. L. Armony, and J. E. LeDoux (1997). "Fear Conditioning Enhances Different Temporal Components of Tone-Evoked Spike Trains in Auditory Cortex and Lateral Amygdala". In: *Neuron* 19.3, pp. 613–624. DOI: 10.1016/s0896-6273(00)80375-x.

Quirk, G. J., J. C. Repa, and J. E. LeDoux (1995). "Fear conditioning enhances short-latency auditory responses of lateral amygdala neurons: Parallel recordings in the freely behaving rat". In: *Neuron* 15.5, pp. 1029–1039. DOI: 10.1016/0896-6273(95)90092-6.

Rainnie, D. G., E. K. Asprodini, and P. Shinnick-Gallagher (1993). "Intracellular recordings from morphologically identified neurons of the basolateral amygdala". In: *Journal of Neurophysiology* 69.4, pp. 1350–1362. DOI: 10.1152/jn.1993.69.4.1350.

Repa, J. C., J. Muller, J. Apergis, T. M. Desrochers, Y. Zhou, and J. E. LeDoux (2001). "Two different lateral amygdala cell populations contribute to the initiation and storage of memory". In: *Nature Neuroscience* 4.7, pp. 724–731. DOI: 10.1038/89512.

Bibliography

Rhomberg, T., L. Rovira-Esteban, A. Vikór, E. Paradiso, C. Kremser, P. Nagy-Pál, O. I. Papp, R. Tasan, F. Erdélyi, G. Szabó, F. Ferraguti, and N. Hájos (2018). "VIP-immunoreactive interneurons within circuits of the mouse basolateral amygdala". In: *Journal of Neuroscience* 38.31, pp. 2063–17. DOI: 10.1523/jneurosci.2063-17.2018.

Rodgers, K. M., A. M. Benison, A. Klein, and D. S. Barth (2008). "Auditory, Somatosensory, and Multisensory Insular Cortex in the Rat". In: *Cerebral Cortex* 18.12, pp. 2941–2951. DOI: 10.1093/cercor/bhn054.

Rogan, M. T. and J. E. LeDoux (1995). "LTP is accompanied by commensurate enhancement of auditory-evoked responses in a fear conditioning circuit". In: *Neuron* 15.1, pp. 127–136. DOI: 10.1016/0896-6273(95)90070-5.

Romanski, L. M., M.-C. Clugnet, F. Bordi, and J. E. LeDoux (1993). "Somatosensory and auditory convergence in the lateral nucleus of the amygdala." In: *Behavioral Neuroscience* 107.3, p. 444. DOI: 10.1037/0735-7044.107.3.444.

Romanski, L. and J. LeDoux (1992). "Equipotentiality of thalamo-amygdala and thalamo-cortico-amygdala circuits in auditory fear conditioning". In: *Journal of Neuroscience* 12.11, pp. 4501–4509. DOI: 10.1523/jneurosci.12-11-04501.1992.

Rumpel, S., J. LeDoux, A. Zador, and R. Malinow (2005). "Postsynaptic Receptor Trafficking Underlying a Form of Associative Learning". In: *Science* 308.5718, pp. 83–88. DOI: 10.1126/science.1103944.

Sah, P., E. S. L. Faber, M. L. D. Armentia, and J. Power (2003). "The Amygdaloid Complex: Anatomy and Physiology". In: *Physiological Reviews* 83.3, pp. 803–834. DOI: 10.1152/physrev.00002.2003.

Samson, R. and D. Paré (2006). "A spatially structured network of inhibitory and excitatory connections directs impulse traffic within the lateral amygdala". In: *Neuroscience* 141.3, pp. 1599–1609. DOI: 10.1016/j.neuroscience.2006.04.077.

Sauer, B. (1998). "Inducible Gene Targeting in Mice Using the Cre/loxSystem". In: *Methods* 14.4, pp. 381–392. DOI: 10.1006/meth.1998.0593.

Schindelin, J., I. Arganda-Carreras, E. Frise, V. Kaynig, M. Longair, T. Pietzsch, S. Preibisch, C. Rueden, S. Saalfeld, B. Schmid, J.-Y. Tinevez, D. J. White, V. Hartenstein, K. Eliceiri, P. Tomancak, and A. Cardona (2012). "Fiji: an open-source platform for biological-image analysis". In: *Nature Methods* 9.7, pp. 676–682. DOI: 10.1038/nmeth.2019.

Shaban, H., Y. Humeau, C. Herry, G. Cassasus, R. Shigemoto, S. Ciocchi, S. Barbieri, H. v. d. Putten, K. Kaupmann, B. Bettler, and A. Lüthi (2006). "Generalization of amygdala LTP and conditioned fear in the absence of presynaptic inhibition". In: *Nature Neuroscience* 9.8, pp. 1028–1035. DOI: 10.1038/nn1732.

Sosulina, L., S. Meis, G. Seifert, C. Steinhäuser, and H.-C. Pape (2006). "Classification of projection neurons and interneurons in the rat lateral amygdala based upon cluster analysis". In: *Molecular and Cellular Neuroscience* 33.1, pp. 57–67. DOI: 10.1016/j.mcn. 2006.06.005.

Swanson, L. W. and G. D. Petrovich (1998). "What is the amygdala?" In: *Trends in Neurosciences* 21.8, pp. 323–331. DOI: 10.1016/s0166-2236(98)01265-x.

Szinyei, C., T. Heinbockel, J. Montagne, and H.-C. Pape (2000). "Putative Cortical and Thalamic Inputs Elicit Convergent Excitation in a Population of GABAergic Interneurons of the Lateral Amygdala". In: *Journal of Neuroscience* 20.23, pp. 8909–8915. DOI: 10.1523/ jneurosci.20-23-08909.2000.

Taniguchi, H., M. He, P. Wu, S. Kim, R. Paik, K. Sugino, D. Kvitsiani, D. Kvitsani, Y. Fu, J. Lu, Y. Lin, G. Miyoshi, Y. Shima, G. Fishell, S. B. Nelson, and Z. J. Huang (2011). "A Resource of Cre Driver Lines for Genetic Targeting of GABAergic Neurons in Cerebral Cortex". In: *Neuron* 71.6, pp. 995–1013. DOI: 10.1016/j.neuron.2011.07.026.

Taylor, J. A., M. Hasegawa, C. M. Benoit, J. A. Freire, M. Theodore, D. A. Ganea, T. Lu, and J. Gründemann (2020). "Single cell plasticity and population coding stability in auditory thalamus upon associative learning". In: *bioRxiv*, p. 2020.04.06.026401. DOI: 10.1101/ 2020.04.06.026401.

Tovote, P., M. S. Esposito, P. Botta, F. Chaudun, J. P. Fadok, M. Markovic, S. B. E. Wolff, C. Ramakrishnan, L. Fenno, K. Deisseroth, C. Herry, S. Arber, and A. Lüthi (2016). "Midbrain circuits for defensive behaviour". In: *Nature* 534.7606, pp. 206–212. DOI: 10.1038/ nature17996.

Tovote, P., J. P. Fadok, and A. Lüthi (2015). "Neuronal circuits for fear and anxiety". In: *Nature Reviews Neuroscience* 16.6, nrn3945. DOI: 10.1038/nrn3945.

Vong, L., C. Ye, Z. Yang, B. Choi, S. Chua, and B. B. Lowell (2011). "Leptin Action on GABAergic Neurons Prevents Obesity and Reduces Inhibitory Tone to POMC Neurons". In: *Neuron* 71.1, pp. 142 –154. DOI: https://doi.org/10.1016/j.neuron.2011.05.028.

Bibliography

Wang, Y., M. Toledo-Rodriguez, A. Gupta, C. Wu, G. Silberberg, J. Luo, and H. Markram (2004). "Anatomical, physiological and molecular properties of Martinotti cells in the somatosensory cortex of the juvenile rat". In: *The Journal of Physiology* 561.1, pp. 65–90. DOI: 10.1113/jphysiol.2004.073353.

Washburn, M. and H. Moises (1992). "Electrophysiological and morphological properties of rat basolateral amygdaloid neurons in vitro". In: *Journal of Neuroscience* 12.10, pp. 4066–4079. DOI: 10.1523/jneurosci.12-10-04066.1992.

Weinberger, N. M. (2007). "Associative representational plasticity in the auditory cortex: A synthesis of two disciplines". In: *Learning & Memory* 14.1-2, pp. 1–16. DOI: 10.1101/lm.421807.

Weinberger, N. M. (2011). "The medial geniculate, not the amygdala, as the root of auditory fear conditioning". In: *Hearing Research* 274.1-2, pp. 61–74. DOI: 10.1016/j.heares.2010.03.093.

Weisskopf, M., E. Bauer, and J. LeDoux (1999). "L-type voltage-gated calcium channels mediate NMDA-independent associative long-term potentiation at thalamic input synapses to the amygdala." In: *The Journal of neuroscience : the official journal of the Society for Neuroscience* 19.23, pp. 10512–9. DOI: 10.1523/jneurosci.19-23-10512.1999.

Wilensky, A. E., G. E. Schafe, and J. E. LeDoux (1999). "Functional Inactivation of the Amygdala before But Not after Auditory Fear Conditioning Prevents Memory Formation". In: *Journal of Neuroscience* 19.24, RC48–RC48. DOI: 10.1523/jneurosci.19-24-j0006.1999.

Wilson, N. R., C. A. Runyan, F. L. Wang, and M. Sur (2012). "Division and subtraction by distinct cortical inhibitory networks in vivo". In: *Nature* 488.7411, pp. 343–348. DOI: 10.1038/nature11347.

Wolff, S. B. E., J. Gründemann, P. Tovote, S. Krabbe, G. A. Jacobson, C. Müller, C. Herry, I. Ehrlich, R. W. Friedrich, J. J. Letzkus, and A. Lüthi (2014). "Amygdala interneuron subtypes control fear learning through disinhibition". In: *Nature* 509.7501, p. 453. DOI: 10.1038/nature13258.

Woodruff, A. R. and P. Sah (2007). "Networks of Parvalbumin-Positive Interneurons in the Basolateral Amygdala". In: *The Journal of Neuroscience* 27.3, pp. 553–563. DOI: 10.1523/jneurosci.3686-06.2007.

List of Abbreviations

4-AP	4-Aminopyridine
AAV	Adeno-associated virus
AMPA	α-amino-3-hydroxy-5-methyl-4-isoxazolepropionic acid
AP	Action potential
BA	Basal amygdala
BLA	Basolateral complex
BMA	Basal medial amygdala
BSA	Bovine serum albumin
Ca^{2+}	Calcium
CamKIIa	Ca^{2+}/calmodulin-dependent protein kinase II
CEA	Central amygdala
ChR2	Channelrhodopsin–2
CS	Conditioned stimulus
EC	External capsule
EPSC	Excitatory postsynaptic current
EPSP	Excitatory postsynaptic potential
GABA	γ-aminobutyric acid
IC	Internal capsule
IHC	Immunohistochemistry
IN	Interneuron
IPSC	Inhibitory postsynaptic current
IPSP	Inhibitory postsynaptic potential
ISH	*In situ* hybridization
ITC	Intercalated cell cluster
LA	Lateral amygdala
LAdl	Dorsolateral area of the lateral amygdala
LEC	Lateral entorhinal cortex
LTD	Long-term depression
LTP	Long-term potentiation
MGm	Medial geniculate nucleus
NBQX	2,3-dioxo-6-nitro-7-sulfamoyl-benzo[f]quinoxaline
oEPSC	Optogenetically-evoked excitatory postsynaptic current

oIPSC   Optogenetically-evoked inhibitory postsynaptic current
PAG   Periaqueductal gray
PBS   Phosphate-buffered saline
PFA   Paraformaldehyde
PIN   Posterior intralaminar nucleus
pInsCx   Posterior insular cortex
PSC   Postsynaptic current
PSP   Postsynaptic potential
PV   Parvalbumin
SOM   Somatostatin
TTX   Tetrodoxin
US   Unconditioned stimulus
VGluT2   Vesicular Glutamate Transporter 2
VIP   Vasoactive intestinal peptide

Ayah Khubieh

Contact: Chemin de l'Ochettaz, 16A
1025 St-Sulpice VD
ayah.khubieh@gmail.com
+41 79 138 77 74

Nationality: Swiss

Curriculum Vitae

Education	Sept 2020	**US and Europe regulation and quality compliance for drug/device product development course (CMC, ISO 60601, ISO 14971)** Jointly organized by the Federal Polytechnique School of Lausanne (EPFL) and the College of Sciences, San Diego State University
	2014 – 2021	**PhD in Neurosciences** Brain and Mind Institute, EPFL, Switzerland
	2008 – 2013	**Bachelor and Masters in Life Sciences and Technology Engineering** Specialization: Neuroscience Youngest master graduate award EPFL, Switzerland
Professional experiences	2014 – 2021	**Doctoral assistant** *Laboratory of Synaptic Mechanisms (LSYM), EPFL, Switzerland* Thesis' project title: Target cell-type specificity of a cortico-amygdala long range synaptic connection. • Data organization, documentation and analysis • Writing of a thesis (in English) • Laboratory techniques (genotyping, immunohistochemistry, …) • Presentation at an international conference (FENS) • Student supervision • Teaching experience in electronics and statistics
	2012 – 2013	**Research assistant** *Neurosciences & Mental Health, The Hospital for Sick Children, Toronto, Canada* Masters' project title: Effect of feedforward inhibition on synchrony transfer between neurons operating in a noisy environment.
	2011	**Summer internship** *MR Imaging and Spectroscopy (PCMD), F. Hoffmann-La Roche AG, Switzerland* • Creating database of preclinical data for meta-analysis
	2008 – 2012	**Multiple internships to learn laboratory techniques** *Pain Research Unit (CHUV), LCN (EPFL), LSYM (EPFL) and NMNF (EPFL)*
Other experiences		**Leader of an escape game team:** • Finalist in Romandie championship 2018 • Winner of the 2019 Swiss-German championship (Escape Together) **Vice-president in the association for Life Sciences PhD students** **Volunteering in Tech4Kids:** • Teaching children (4-14 years old) robotics and programming **Seminar organization in SV-industry:** • Expose students to career opportunities in Life Sciences **Sponsoring and travelling modalities in SV-Travel (for bachelor class)**
Skills		**Programming languages:** Python, Matlab, html, C/C++, Arduino **Software expertise:** Microsoft office, Adobe Illustrator **Techniques:** Microscopy, Laboratory safety, Genotyping, Electrophysiology **Soft skills:** Scientific writing, communication, project management, presentation
Languages		**French:** Native language **Arabic:** Mother language **English:** Fluent **German:** Basics

89